COMPACTED FLY ASH MIXTURES AS HIGHWAY SAFETY BARRIERS

by
Doruk MEHMETOĞLU
B.S. in C.E., Boğaziçi University, 1992

Submitted to the Institute for Graduate Studies in Science and Engineering in partial fulfillment of the requirements for the degree of
Master of Science
in
Civil Engineering

Boğaziçi University
1994

ACKNOWLEDGMENTS

I express my gratitude to my thesis supervisor, Associate Prof. Dr. Gökhan BAYKAL, who has motivated me to finish this work with his kind suggestions and comments.

I would like to thank the Boğaziçi University Soil Mechanics and Geotechnical Engineering Laboratory technician Erdal YILMAZ, who has helped me to complete the related experiments.

I would also like to express my sincere thanks to my parents, for their kind support and understanding.

ABSTRACT

During the past years, research had been carried on in the Boğaziçi University, Soil Mechanics and Foundation Engineering Laboratory to find a way of utilizing two wastes, namely fly ash and rubber chips from old tires. As a result, it had been determined that these wastes could successfully be used in waste liner construction. The purpose of this work is to find a new field of utilization for these materials.

The materials used for this purpose are self cementitious high-calcium fly ash from Soma TEK-B Thermal Power Plant, pulverized waste rubber, lime and spherical and crushed ice particles. As a result of the work undertaken a light-weight energy absorbing material which may be utilized in the construction of traffic barriers is developed and a new field of utilization for fly ash and waste rubber is provided.

For the laboratory experiments, a total number of 126 fly ash-rubber-ice and fly ash-lime-ice samples of different compositions were prepared using static compaction. Additional water in the form of crushed or spherical ice particles was provided for the hydration reaction of fly ash and to increase the energy absorbing capacity by introducing voids into the samples. All of the samples were cured for a period of 56 days. Ultra sound, compression and double punch tests were performed on them.

Laboratory studies indicated a maximum increase in compressive strength with added lime and crushed ice. Energy absorbing capacity and tensile strength were increased most after adding lime and spherical ice. It was concluded that this material could be used in crash-cushion construction.

ÖZET

Geçmiş senelerde Boğaziçi Üniversitesi Zemin Mekaniği ve Temel Mühendisliği Laboratuvarında atık malzemeler olan uçucu kül ve eski oto lastiklerinden elde edilen lastik parçacıkları üzerinde çalışmalar yapılmış ve bunların çöplük alanlarında tecrit malzemesi olarak kullanılabileceği kanıtlanmıştır. Bu çalışmanın amacı aynı atık malzemelerin değerlendirilebileceği yeni bir alan bulmaktır.

Bu çalışmada Soma TEK-B Termik Santralı'ndan alınan kalsiyum muhtevası yüksek uçucu kül, atık toz lastik, kireç ve küresel ve kırılmış buz parçacıkları kullanılmıştır. Çalışmalar sonucunda oto-korkuluk olarak kullanılabilecek hafif ve enerji emme kapasitesi yüksek bir malzeme üretilmiş ve uçucu kül ve kullanılmış oto lastiklerine yeni bir kullanım alanı daha sağlanmıştır.

Toplam 126 numune uçucu kül-lastik-buz ve uçucu kül-söndürülmüş kireç-buz karışımlarının statik olarak sıkıştırılmasıyla hazırlanmıştır. Numunelere külün hidratasyon reaksiyonuna ilave su sağlamak ve numune içinde boşluklar elde ederek enerji emme kapasitesini arttırmak amaçlarıyla küresel veya kırılmış buz parçacıkları katılmıştır. Bütün numuneler 56 gün küre tabi tutulmuşlardır. Numuneler üzerinde ultrases geçiş süresi, basınç dayanımı, ve çift taraflı delme (double punch test) deneyleri uygulanmıştır.

Deneyler sonunda, basınç mukavemetinin kireç ve kırılmış buz, enerji emme kapasitesi ve çekme mukavemetinin kireç ve küresel buz ilaveli numunelerde maksimum değerlere eriştiği görülmüştür. Elde edilen malzemenin enerji emici oto-korkuluk olarak kullanılabileceği sonucuna varılmıştır.

TABLE OF CONTENTS

LIST OF FIGURES

LIST OF TABLES

LIST OF SYMBOLS

δA_i	Infinitesimally small rectangular area
γ_{max}	Maximum dry unit weight
μ	Effective coefficient of friction
θ	Impact angle
ρ	Net density
σ_t	Simple tensile strength
υ	Poisson's ratio
$3CaO.Al_2O_3$	Tricalcium aluminate
4CaO.3Al2O3.SO4	Calcium sulfoaluminate
A	Total area under a curve
Al	Aluminum
Al_2O_3	Alumina
As	Arsenic
a	Radius of the double punch steel disk
a"	Deceleration in [m/sec^2] units
a'	Deceleration in [g] units
Be	Beryllium
b	Sample radius
Ca	Calcium
CaO	Calcium oxide
$CaSO_4$	Anhydrite
CBR	California Bearing Ratio
C_c	Coefficient of concavity
Cd	Cadmium
CE	Nominal compaction energy
C_m	Calibration constant of the CBR compession machine
CO_2	Carbon dioxide
C_u	Coefficient of uniformity
D	Stopping distance after impact
d	Total crash cushion deformation
dm	Mass of small stationary barrier
dm/ds_{max}	Maximum feasible module mass per unit length

ds	Small increment along barrier length
dt	Small increment of time
dV	Small loss of vehicle speed
dx	Small part of crash cushion deformation at the point of impact
E	Young's (dynamic elasticity) modulus
F	Crash cushion force
Fe	Iron
Fe_2O_3	Iron oxide
F_x	Crash cushion force acting on the car through a small deformation
G_A	Average deceleration
g	Acceleration due to gravity
H	Sample height
Hg	Mercury
K	Potassium
K_2O	Potassium oxide
KE	Kinetic energy
L	Load applied by the CBR machine piston
LOI	Loss on ignition value
M	Vehicle mass
Mg	Magnesium
MgO	Magnesium oxide
N	Nitrogen
Na	Sodium
Na_2O	Sodium oxide
O	Oxygen
P	Load applied in double punch test
S	Sulfur
Si	Silicon
SiO_3	Silica
SO_3	Sulphate
s	Stopping distance
s_f	Final value of stopping distance
s_i	Consecutive integers (module diameters)
s_u	Nearest distance between two probe surfaces
Ti	Titanium

t	Time of deceleration
t_p	Distance travelled by the CBR piston during compression
t_u	Time of transmission
U	Work
V	Impact speed
V_c	Volume of Standard Proctor compaction mold
V_p	Speed of vehicle when parallel to railing
v	Vehicle speed
v_{avg}	Average velocity
v_f	Final speed
v_o	Initial vehicle speed (speed of impact)
v_s	Sound velocity determined by the ultrasonic tester
W	Vehicle weight
w_{opt}	Optimum water content

1. INTRODUCTION

Fly ash is the particulate matter removed from the stack gas of power plants as a waste product and constitutes ecological and disposal problems. It is the resultant of the burning of clay, pyrite, and calcite in coal, lignite or like fuels under high temperatures in the combustion chamber. Two main groups of fly ash based on the source of coal, namely Class F and Class C have been identified by ASTM C618-80, Standard Specification for Fly Ash and Raw or Calcinated Natural Pozzolan for Use as a Mineral Admixture in Portland Cement Concrete[1].

Disposal of fly ash is a burden on the energy producers and increases the cost of power. In recent years, work has been carried on for the utilization of this waste product which is pozzolanic and is self-cementitious as well in the case of Type C fly ashes (since they have higher free lime content). Fly ash is being used in the fields of transportation and geotechnical engineering as an additive to cement and in the stabilization of both fine and coarse grained soils.

The increasing use of motor vehicle transportation all over the world has emphasized the problem of traffic safety. Highway accident losses can be reduced in many ways. Preventing crashes from occurring by taking certain measures is one solution to the problem, which might sometimes prove to be inefficient. Another attempt taken at decreasing the number of casualties is to focus on the "at-crash" phase of accidents by providing safety barriers and energy absorbing devices.

The objective of this study was to produce an energy absorbing, light weight, economical, easy to prepare material, which could be used as traffic safety barriers.

Mixtures of fly ash, rubber, lime and ice were prepared to obtain an energy absorbing material. Among these materials, fly ash and rubber from tire chips were wastes and using them in crash-cushion construction would provide an additional utilization area for them.

The compressive and double punch tensile strength of samples prepared using fly ash, lime, rubber and ice have been investigated in this study. Additional information about the samples has been obtained using non-destructive ultrasonic test. Other fields of application can easily be found for these mixtures with further investigation.

1.1. Fly Ash

1.1.1. General Description

Fly ash is basically a siliceous or siliceous and aluminous combustion waste product, occurring as a result of burning pulverized bituminous or lignite coal under high temperatures. It is a very fine particulate matter that is collected from the flue gasses[2]. ASTM identifies two classes of fly ash based on the coal source; Class F fly ash originating from bituminous coals and Class C from sub-bituminous and lignite origins[2]. Differences occurring during coal formation processes over geological time periods have brought forward vast variations among coal types.

1.1.2. The Origin of Coal

Coal is the end product of a sequence of biological and geological processes. It is an inhomogeneous organic

fuel, formed largely from partially decomposed and metamorphosed plant materials.

The bulk of all coal deposits were formed in a peat swamp environment where different types of vegetation flourished, reflecting primary conditions of climate, water level and water chemistry of the swamp[3]. Conditions for peat accumulation have been favorable at many different places and times during approximately the past 350 million years of the earth's history[4].

Once incorporated in the peat, the plant material undergoes drastic physical and chemical changes. Microbes within the peat attack it. The pressure and temperature increase, the woody and bark tissue is converted into a gel-like substance, which through hardening becomes vitrinite, the most common and valuable component of coal. Waxes, resin, natural charcoal, etc., are quite resistant to degradation and are preserved even in higher rank coals[4].

1.1.3. Coal Types

Increasing overburden pressure and rising temperature due to the increased depth of burial are the driving forces for the rank change from peat to lignite, sub bituminous, bituminous and anthracitic coals. The process of conversion of plant materials, such as peat, to coal is called "coalification". The basic coal types can be described as below :

(A) Lignite, the lowest rank of coal, was formed from compacted and altered peat. It is brown to black in color and is composed of woody materials embedded in pulverized and partially decomposed vegetable matter. It has a high moisture content (20 per cent) and low heating value, and displays jointing and bedding.

(B) Sub-bituminous coal is dull and black in color and is banded. It displays cleavage and usually splits parallel to bedding planes. It has lost some moisture content, but is still of low heating value[5].

(C) Bituminous coal is dense, compacted, banded, brittle, dark black in color and displays columnar cleavage. It is more resistant to disintegration in air; has low moisture content (one to two per cent) and high to medium volatile matter content. The heating values of bituminous coals are high. Most bituminous coals are reported to be deposited 300 to 100 million years ago.

(D) Anthracite is the highly metamorphosed coal, is jet black in color, is hard and brittle, breaks with a conchoidal fracture and displays a high luster[5]. Its carbon content is high and moisture content is low.

(E) Neither peat nor graphite are coal, but they are the initial and end products of the progressive coalification process[5].

1.1.4. Coal Composition

The composition of coal is determined by ASTM proximate and ASTM ultimate analysis. Proximate analysis determines the moisture content and per cent volatiles, ash and fixed carbon. Ultimate analysis gives elemental analysis for carbon, hydrogen, nitrogen, sulfur and oxygen. The residual mineral matter is shown as ash. Proximate and ultimate analysis for a selected variety of coals from the United States is shown in TABLE 1.1. In TABLE 1.2 proximate and ultimate analysis of some Turkish lignites from Manisa, Soma are given.

TABLE 1.1. Typical proximate and ultimate analysis of coals and char[5].

Coal I.D. rank	Utah Church Mine bit.	Pittsburgh bit.(high volatile)	Pittsburgh bituminous	Sewell bit. (medium volatile)	Pocahantas bit. (low volatile)
MOIST.(%)	2.5-2.7	2.0	1.0	-	1.9
PROX.(%)					
Volatiles	44.1-45.5	36.6	28.9	29.2	16.3
Fixed Carbon	42.6-44.2	55.4	63.2	63.9	75.6
Ash	9.2-9.5	6.0	6.9	6.9	6.2
ULT.(%)					
Carbon	69.8-71.5	77.5	80.6	81.4	84.2
Hydrogen	5.5-5.6	5.3	4.9	4.8	4.3
Nitrogen	1.4-1.5	1.5	1.5	1.6	1.2
Sulfur	0.4-0.7	1.2	0.7	0.7	0.7
Oxygen	11.2-13.2	8.5	5.4	4.6	3.4
Ash	9.2-9.5	6.0	6.9	6.9	6.2

Coal I.D. rank	Anthracite (low volatile)	Illinois coal bit.	Illinois coal char	North Dakota lignite	Wyoming sub-bit.	Kentucky bit.
MOIST.(%)	1.3	10.1	0.9	29.9	27.8	8.6
PROX.(%)						
Volatiles	8.8	35.9	2.4	29.5	32.9	35.2
Fixed carbon	71.8	46.7	76.1	33.4	34.3	41.5
Ash	18.1	7.3	20.6	7.2	5.0	23.3
ULT.(%)						
Carbon	73.2	68.3	74.0	69.7	76.3	61.0
Hydrogen	3.1	5.0	0.7	3.8	4.4	4.4
Nitrogen	0.9	1.3	1.0	1.9	1.1	1.4
Sulfur	0.9	3.5	3.3	1.1	0.5	4.3
Oxygen	3.8	13.8	0.2	13.2	10.8	5.6
Ash	18.1	8.1	20.8	10.3	6.9	23.3

TABLE 1.2. Proximate and ultimate analysis of lignites from Manisa, Soma[6].

Coal I.D. rank	Sample Number				
	-	2	70	71	72
Moisture (%)	12.14	23.65	14.57	10.11	11.57
Proximate (%)					
Volatiles	32.81	37.47	31.55	35.28	30.80
Fixed Carbon	27.77	32.33	38.20	35.78	29.59
Ash	27.28	6.55	15.68	18.83	28.04
Ultimate (%)					
Carbon	43.44	-	-	-	-
Hydrogen	3.25	-	-	-	-
Sulfur	1.46	-	-	-	-
ASTM values (%)					
Volatiles	56.59	54.59	46.21	50.90	53.21
Fixed Carbon	43.41	45.41	53.79	49.10	46.79

Coal I.D. rank	Sample Number			
	73	74	75	108
Moisture (%)	12.46	14.68	11.49	12.14
Proximate (%)				
Volatiles	29.36	29.28	35.62	29.22
Fixed Carbon	37.69	35.08	39.05	31.79
Ash	20.49	20.96	13.84	26.85
Ultimate (%)				
Carbon	-	-	-	43.43
Hydrogen	-	-	-	3.24
Sulfur	-	-	-	1.46
ASTM values (%)				
Volatiles	45.02	46.87	48.57	49.95
Fixed Carbon	54.98	53.13	51.43	50.05

Typical compositions (mass per centages) of coal include 65 to 95 per cent carbon, two to seven per cent hydrogen, up to 25 per cent oxygen, 10 per cent sulfur and one to two per cent nitrogen[5]. Inorganic mineral matter (ash) as high as 50 per cent has been observed, but five to 15 per cent is more typical[5].

Mineral matter enters the coal deposit at various times of its formation history. Some minerals (mostly detrital clay minerals and quartz) are brought by moving water (e.g. rivers); others (pyrite) are precipitated from waters circulating through the peat with or without the help of specialized bacteria. The most common mineral impurities deposited in coal are clay minerals, namely silicates of aluminum, iron and magnesium. Pyrite, kaolinite, calcite and cleat fillings of carbonates and sulfides are also found in coal. Quartz, garnets, shale and feldspars are common too.

The concentration of ash-forming elements (excluding O, S and N) in whole coal may range arbitrarily between greater than 0.5 per cent for major elements such as Al, Ca, Fe and Si; 0.02 per cent to 0.5 per cent for minor elements such as K, Mg, Na, Ti and others; and less than 0.02 per cent for trace elements which include such elements as As, Be, Hg, Cd and the remaining majority of elements in the Periodic Table[4].

1.1.5. Fly Ash Formation

Most of the coal presently being consumed is by direct combustion of finely pulverized coal in large scale utility furnaces for generation of electric power[5]. As coal passes through the high temperature zone in the furnace, the volatile matter and carbon are burned off whereas most of the mineral impurities deposited in coal during its formation, such as clays, shale, quartz and feldspar generally fuse and

remain in suspension in the flue gas[7]. The fused matter is quickly transported to lower temperature zones where it solidifies as spherical particles. Some of the mineral matter agglomerates to form bottom ash, but most of it flies out with the flue gas stream and hence is called "fly ash". This ash is subsequently removed from the flue gas by mechanical separators, electrostatic precipitators or bag filters[7].

Pulverized coal combusters, which burn coal crushed and ground to a fineness of 70 to 80 per cent passing the No.200 (75 μm) sieve, produce the smallest fly ash particles. Fluidized bed combusters generate medium sized , and fixed bed (stokers) combusters generate coarser sized fly ash.

1.1.6. Types of Fly Ash

The ASTM Standard Specification for Mineral Admixtures-C618[1] defines two classes of fly ash - Class F and Class C. Class F fly ash is usually produced by burning anthracite or bituminous coals, which very rarely contain high calcium mineral matter in significant proportion, while the Class C fly ash is normally produced by burning sub-bituminous coals and lignite[8]. Sub-bituminous coals and lignites may contain a high amount of calcium. ASTM C618[1] does not differentiate fly ash on the basis of calcium content, although this objective is achieved indirectly by requiring a minimum of 70 per cent of major non-calcium oxides (silica+alumina+iron oxide) for Class F fly ash and 50 per cent for Class C fly ash, since the latter is high in calcium[7]. The separation of fly ash into two classes reflects differences in composition which affect cementitious and pozzolanic properties[8]. Both classes are pozzolanic, that is their fine glass (mullite) particles react with lime in the presence of water to form various cementing compounds. Class C fly ash usually has cementitious properties in addition to pozzolanic ones.

1.1.7. Chemical and Mineral Composition

Rapid cooling of the ash from the molten state as it leaves the flame causes fly ash to be predominantly non-crystalline (glassy - 50 to 90 per cent or even more) with minor amounts of crystalline constituents, such as mullite, quartz, magnetite (or ferrite spinel) an hematite[8].

Wide ranges exist in the amounts of the three principle constituents of fly ash, namely silica (SiO_3 - 25 to 60 per cent), alumina (Al_2O_3 - zero to 30 per cent), and iron oxide (Fe_2O_3 - five to 25 per cent). The magnesium (MgO) content of fly ash is generally not greater than five per cent[8]. Class F fly ashes usually contain less than five per cent where as Class C ones contain 15 to 35 per cent analytical calcium oxide (CaO). The level of alkali oxides expressed as Na_2O equivalent is generally less than five per cent in Class F fly ashes, but it may range up to about 10 per cent in Class C fly ashes[8]. For the purpose of comparison, the typical range of chemical composition for most fly ashes has been reported in TABLE 1.3.

Minor elements that may be present in varying amounts, depending on the origin of the coal include titanium, iron, magnesium, phosphorus, sulfur, oxygen, potassium, sodium, carbon and others as traces. Some fly ashes also have trace amounts of organic compounds other than unburned coal[8].

Class C fly ashes have loss on ignition values less than one per cent but for Class F ashes this value may range from one to more than 10 per cent. Loss on ignition value (LOI) is determined by heating one gram of oven-dried fly ash up to 700-800°C until it reaches a final fixed weight. The per cent change in weight is the LOI value for that specific fly ash. Carbon content of fly ash is theoretically assumed to be equal to the LOI, but in practice LOI also includes the

TABLE 1.3. Typical range of chemical composition for most fly ashes[10].

Chemical Composition	Maximum (%)	Minimum (%)	Typical (%)
Silica as (SiO_2)	58	38	48
Alumina as (Al_2O_3)	40	20	26
Iron oxide as(Fe_2O_3)	16	6	10
Calcium as (CaO)	10	2	4
Magnesium as (MgO)	3.5	1	2
Total sulfate as (SO_3)	2.5	0.5	1.2
Water Soluble Alkalis as (Na_2O, K_2O)	5.5	2	3

combined water and carbon dioxide lost by the decomposition of hydrates and carbonates present in coal. The differences in mineral and chemical compositions of Class C and F fly ashes are such as the following:

(A) The active compounds in Class C fly ashes, besides the basic calcium aluminosilicate glass, are free lime (CaO), anhydrite ($CaSO_4$), tricalcium aluminate ($3CaO.Al_2O_3$), calcium sulfoaluminate ($4CaO.3Al_2O_3.SO_4$) and rarely calcium silicate. The lime in Class C fly ashes is most of the time not in a free state, but is combined with the silicates and aluminates of the ash as a result of the intense heat in the furnace. Class C ashes react directly with water to form cementitious phases such as calcium-silicate-hydrate, calcium hydroxide and etringite by the influence of the cementitious calcium alumino-silicate glass and the presence of crystalline phases.

(B) Low calcium (Class F) fly ashes characteristically contain a large portion of alumino-silicate glass of high silica content plus crystalline phases of low reactivity, typically mullite, magnetite and quartz[8]. In the furnace very large spheres of molten glass may not cool rapidly and uniformly, thus crystallization of aluminosilicates, such as sillimanite and mullite as slender needles takes place in the interior of the glassy sphere[7]. Also, remnants of quartz in the original crystalline state are likely to be present.

High-silica glass is less reactive with water than the other glasses. The glassy phase in Class F fly ashes is more abundant but less reactive than Class C fly ashes for this reason. Therefore, the former requires higher glass contents to be as effective as the latter.

1.1.8. Physical Properties

Shape, fineness, grain-size distribution, density and composition of fly ash particles affect the properties of the mixtures prepared. The color of fly ash produced at different power plants or from different coal sources differs, which is an indication of the changed properties due to changes in coal source, loss on ignition, iron content or burning conditions.

(A) Particle size and shape characteristics of fly ash are dependent upon the source and uniformity of the coal, the degree of pulverization prior to burning, the combustion environment (temperature level and oxygen supply), uniformity of combustion and the type of collection system used (mechanical separators, bag filters or electrostatic precipitators)[8].

Most particles are glassy, transparent, solid and spherical in shape, but small quantities of imperfectly rounded ellipsoids are also present. Sometimes Class F fly ashes contain minor amounts (up to five per cent by weight) of hollow spheres which are either completely empty (cenospheres) or packed inside with smaller spheres (plerospheres). On the other hand, a small per cent of the particles are large size agglomerates of small silicate glass spheres or porous particles of incompletely burnt carbonaceous matter. Magnetite and hematite occur as opaque spheres in iron rich fly ashes.

(B) The grain sizes of individual particles of fly ash range from less than one μm to greater than one mm. Plants using mechanical separators produce coarser fly ash than those using bag collectors and electrostatic precipitators. Typical grain size distributions of Class C and Class F fly ashes is presented in FIGURE 1.1.

Abrasion resistance, freezing and thawing resistance and compressive strength are all direct functions of grain size and shape. Clean, glassy, spherical particles are good void fillers and reduce water requirement. But performance of fly ash may not be estimated by particle size alone, since rough-textured and porous glass spheres posses larger surface areas for reactivity than smooth spheres and may have higher strength as well.

(C) The specific gravity of solid fly ash particles ranges from 1.97 to 3.02 but is commonly in the range of 2.2 to 2.8[8]. High specific gravity indicates fine particles. Some cenospheres have a specific gravity less than one and can float on water. The specific gravities of Class C fly ashes, which are finer and contain less cenospheres compared to Class F fly ashes, are in the range of 2.4 to 2.8. Iron rich fly ashes have higher and carbon rich fly ashes lower specific gravities.

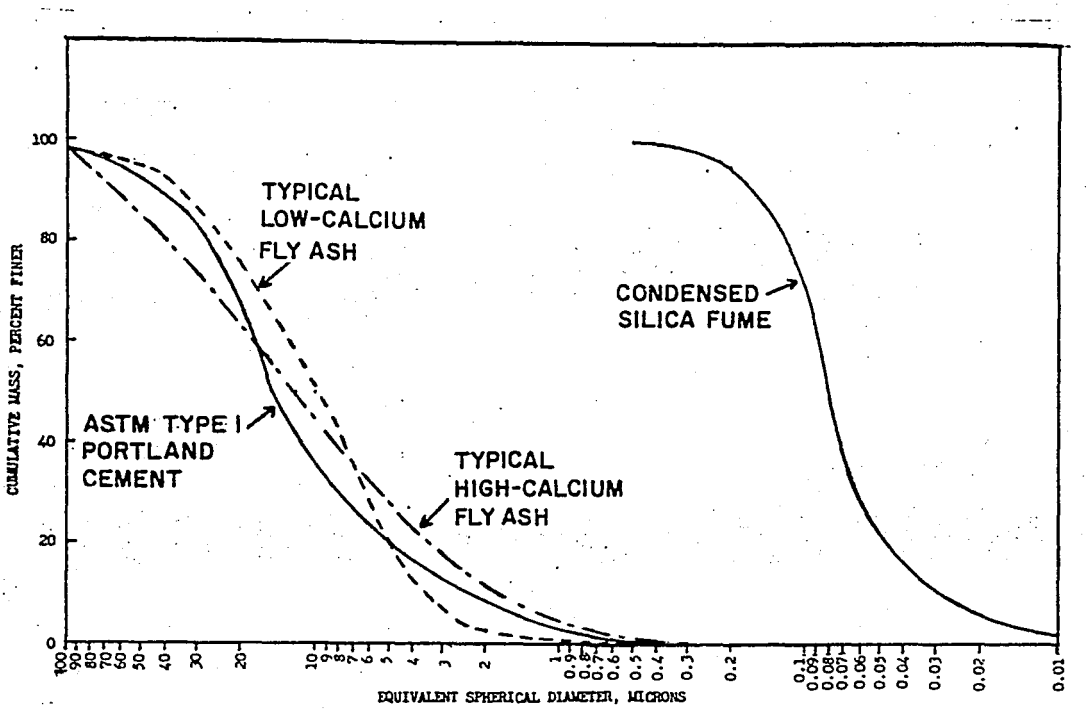

FIGURE 1.1. Particle size distribution of various materials[7].

(D) Specific surface area of fly ash is the ratio of the surface area of the material to its own mass. Fly ashes consisting of clean, glassy, fine spherical particles have high specific surface areas. The reactivity of fly ash increases with increased surface area. Rough-textured and porous glassy spheres which are sometimes seen in high calcium fly ashes possess larger surface area for reactivity than smooth spheres, hence particle size distribution alone may not reflect the potential reactivity of a fly ash. Specific surface area is determined by using air permeability and nitrogen adsorption tests. Some index properties of selected Michigan fly ashes are summarized in TABLE 1.4.

1.1.9. Factors Affecting Performance

The strength and durability of fly ash mixtures are influenced by a number of factors such as fly ash type,

moisture content and dry density, curing time or age and temperatures[2]. Behavior differences in relation to fly ash type have been discussed previously.

(A) The compressive strength of fly ash mixture increases with increasing density to a point near the maximum dry density, determined by the Standard Proctor Test[2]. Experiments show that, maximum compressive strength is obtained at a moisture content slightly less than the optimum moisture content required for maximum dry density[2].

TABLE 1.4. Index properties of some Michigan fly ashes[10].

Properties	Ash Source		
	Marysville	St. Clair	Trenton Channel
Specific gravity	2.61	2.48	2.36
Specific surface [cm^2/gr]	2620	3050	3050
Maximum dry density [lb/ft^3] (Modified Assho test)	74.2	90.5	92.8
Optimum water content [%]	32.0	23.0	19.5
Particle size distribution			
>2 mm (gravel size)	0	0	0
0.074 mm-2 mm (sand size)	12	6.5	10.5
0.002 mm-0.074 mm (silt size)	85	88.5	82.5
<0.002 mm (clay size)	3	5	7

(B) The rate of strength development is dependent on curing age and is much slower than in cement, however there is a gain of strength over a longer period of time in the former. The rate of the strength gain has been cited by Dumbleton, et al, as being 10 per cent of the ultimate strength occurring in seven days under normal curing conditions (moist cure at 21°C) and about 50 per cent at the end of 28 days[2]. The rate of strength gain can continue for a period of years. Rapid compaction immediately after mixing is absolutely necessary for strength development. Initial set times for fly ash are faster than Portland cement. A two hour delay before compaction reduces the strength by a factor of one-third, whereas a four hour delay reduces it by a factor of one-half.

(C) Cementation ceases at temperatures below 4°C, but higher temperatures will reactivate the pozzolanic reaction. At high temperatures cementation will proceed rapidly until the chemical compounds involved are depleted. ASTM C593-66T[9] (Tentative Specifications for Fly Ash and other Pozzolans for Use with Lime) specifications suggest a curing temperature of 38°C for seven days[2]. An accelerated curing period of seven days at 60°C has also been used as an approximation of the condition of the mixture cured at 21°C at the end of 28 days. However certain pozzolanic reactions may occur at higher temperatures and not occur at lower temperatures. It is always recommended that all testing be based on a 28-day curing period at 21+/-2°C and 100 per cent relative humidity[2].

1.1.10. Utilization of Fly Ash

Utilization of fly ash in engineering applications brings efficient solutions to many problems such as the disposal problem of a solid waste, provision of a needed construction material, energy and money consumption, etc.

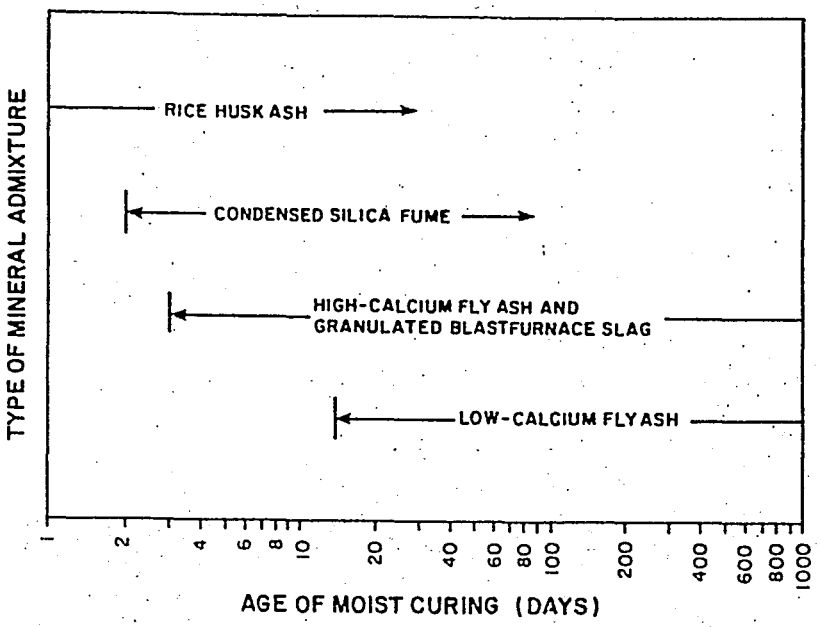

FIGURE 1.2. Effective period of strength gain for various combustion by-products[7].

Ecological problems associated with current fly ash disposal practices are air pollution in the case of stock-piling and the releasing of toxic metals into ponds and steams in the case of dumping. These toxic metal ions can be chemically bonded in calcium aluminate and sulfoaluminate hydrates , if fly ash is used as a concrete additive. Since fly ash does not require additional production energy input before use, it is clear that the energy and money saved from the replacement of cement or other materials will be in direct proportion to the amount of utilized ash.

Major uses for fly ash at present are as follows [10];

(a) mass concrete,

(b) ready mix concrete,

(c) stabilizer for road and highway subbases as an additive to lime stabilization treatment,

(d) asphalt paving filler,

(e) light-weight sintered aggregate,

(f) concrete blocks,

(g) auxiliary cementing material,

(h) oil well grouting,

(i) waste material stabilization,

(j) compacted, stabilized fly ash by itself in load bearing fills,

(k) structural fills,

(l) highway embankments,

(m) light-weight backfills[10],

(n) waste liner construction.

The study undertaken initiates a new field of application for fly ash, namely production of energy absorbing systems.

1.2. Rubber

There are two kinds of rubber, natural and synthetic. Natural rubber, which is used for many centuries, is obtained from different kinds of plants. Synthetic rubbers are derivatives of petrochemicals.

All rubbers are high polymers, possessing long, flexible molecules which are able to be "cross-linked" to form a three dimensional molecular network[11]. After cross linking, rubbers can not be reshaped by the application of heat and pressure.

The long, flexible, cross linked rubber molecules are responsible for the characteristic properties of rubber, among which the two most important ones are stiffness, and elasticity. A rubber must possess the requisite elasticity and stiffness at normal temperatures, to be of practical use.

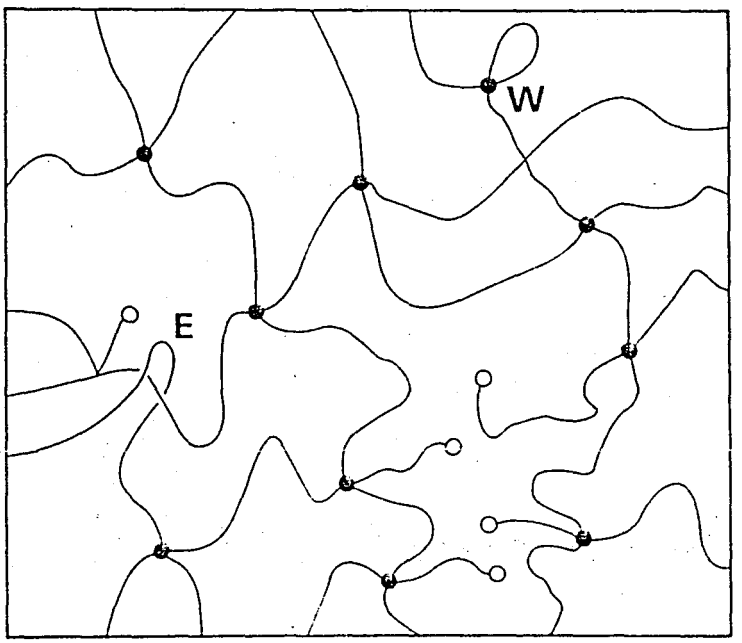

FIGURE 1.3. Representation of cross-linked rubber network. In addition to the cross links (solid circles) other features of the network include free polymer chain ends (open circles), entanglements (E) and 'wasted' cross-links (W)[11].

Stiffness and hardness relate to the Young's Modulus of rubber, which is much lower than that of steel. Young's Modulus is in the range of one to ten MN/m^2 for rubber, which is 2,000 to 200,000 times less stiff than mild steel[11].

Cross linked rubbers have tensile strengths in the range 10 - 30 MN/m^2; they are considerably weaker than steel (about 500 MN/m^2).

Rubber is a material which is capable of great extension and a quick return to its original length on releasing the stretching force. It must be able to return in one minute to within 20 per cent of its original length after being stretched to three times its original length at room temperature[11].

TABLE 1.5. Some basic properties of rubber compared with steel[11].

	Rubber	Mild Steel
Tensile strength (MN/m^2)	21	420
Elongation at break (%)	420	40
Young's Modulus (MN/m^2)	5.9	210,000
Shear modulus (MN/m^2)	1.4	81,000
Resilience (%)	60	100

Vulcanization is the traditional cross linking method; the industrial means of forming the cross linked network by heating raw (uncross linked) rubber with sulfur and certain other chemicals. Vulcanization produces a variety of cross link types and modifies the structure of the main polymer molecules.

Rubber is blended with other additives besides sulfur. Vulcanized unsaturated oils as softeners, zinc white and iron oxide as pigments, antioxidants, antiozonants, accelerators to increase the rate of vulcanization, carbon blacks as reinforcing fillers are being used in many products[12].

Rubber industry has become very dependent on the automotive industry with about 60 per cent of new rubber being consumed in tire production alone[12]. The rubbers widely used in tires are natural rubber, styrene-butadiene rubber and polybutadiene rubber.

In civil engineering, natural rubber and chloroprene rubbers are now widely accepted for bridge bearings whilst ethylene-propylene and butyl rubbers are important for reservoir lining.

In spite of the efforts to extend their operating life, rubber articles eventually become unusable, thus they constitute environmental and waste disposal problems. The physical and mechanical properties of the polymer base and of some other components of such articles, on the other hand, undergo only slight changes. The reuse of the polymeric base material of worn-out rubber articles is of particular value in such cases[13].

The rubber wastes can be ground down to one - two mm sized particles and re-introduced into commercial rubber stocks. In USSR such wastes are utilized in the production of roofings and tie plates, floor slabs for stock farms and as dispersed reinforcement in the manufacture of concretes. The tensile strength of concretes produced in this way are 25 - 50 per cent higher than those without rubber. Impact resistance of such concretes increases 2.5 to 4.5 folds and the cracking resistance increases by 25 - 50 per cent[13].

1.3. Roadside Traffic Safety

There are three basic elements in highway safety, the vehicle, the driver and the roadway. The highway engineer is

specifically concerned with the safety of the roadway and its adjacent development[14].

The physical and dynamic properties of the vehicles that will be using the roadway such as length, width, turning radius, braking ability, the driver eye height and the physical and mental capacities or limitations of drivers are the inputs for the roadway design.

Engineers can reduce highway accident losses in many ways. One approach is to attempt to prevent crashes from occurring by providing access control, suitable horizontal and vertical alignment, adequate lane widths and shoulders, appropriate signing and signaling and so forth. As a second approach the engineer focuses on the "at-crash" phase of accidents by providing clear roadsides, breakaway sign supports, redirecting barriers and energy attenuation devices[15]. In this work, measures to lessen the severity of the roadside hazards associated with out-of-control vehicles will be focused on.

1.3.1. Clear Roadsides

Many accidents on high speed roads involve out-of-control vehicles leaving the road and being in collision with hazardous obstacles. Providing a recovery area free of such physical obstructions will increase safety. This clear roadside area should be as wide, as flat, as rounded and as easy to traverse as it is feasible to construct for the conditions along each section of the highway[15].

The curve shown in FIGURE 1.4 is drawn using the data obtained from the General Motors Testing Site. The distance between the last stopping position of the vehicle after having left the road accidentally and the roadway has been recorded for many different vehicle types. It has been

determined that an area free of all obstacles and having a width of nine meters is sufficient to bring 80 per cent of the tested vehicles to a safe stop. The lower limit is nine meters, but it is recommended to provide a clear roadside 15 meters or more in width if it is at all possible within economical and practical limits. This way the per cent safety is increased.

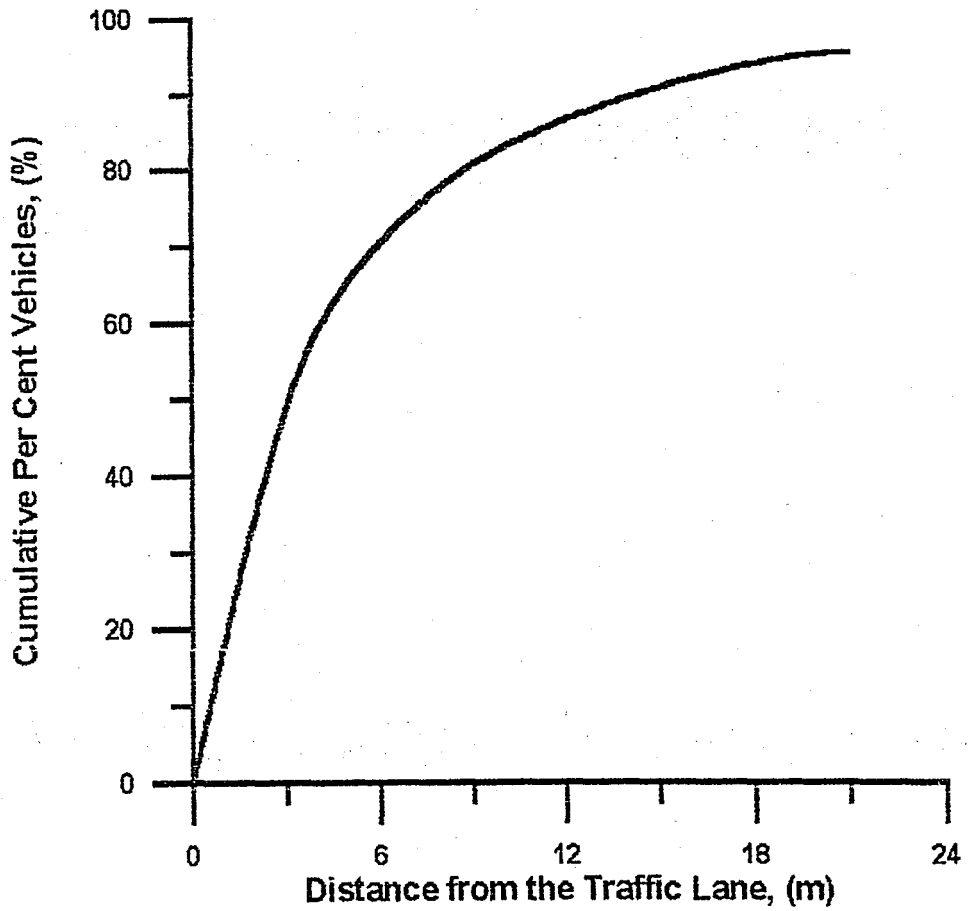

FIGURE 1.4. The stopping distance of out-of-way vehicles determined by General Motors Firm[16].

1.3.2. Breakaway Sign Supports

Breakaway poles and posts should be used in places where it is not possible to shield sign and lighting supports from traffic. New designs include frangible, shear, slip and sleeve bases for lighting supports and hinged joint and slip base sign supports[14]. Lower cost frangible posts can be made by drilling holes around normal solid base[17]. Breakaway supports should not be used in locations where a greater hazard is created by the pole falling on pedestrian areas, adjacent buildings or the roadway[14].

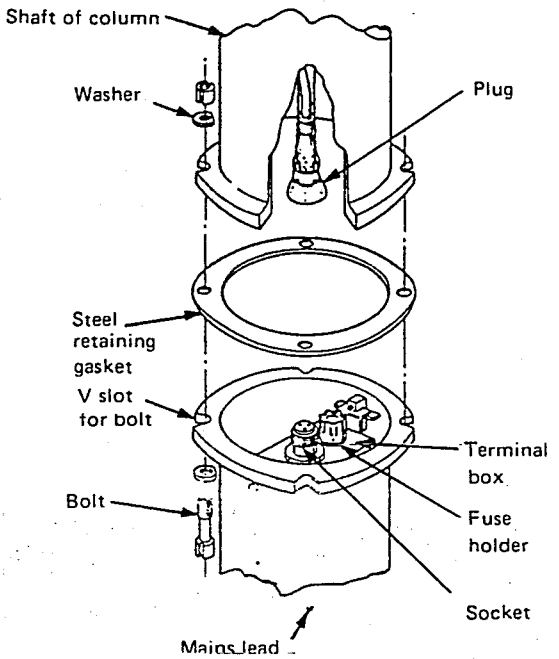

FIGURE 1.5. Diagram of breakaway joint (under impact) and pull-out electrical connection[17].

1.3.3. Barriers

At a number of locations on existing highways there are physical conditions that can not be readily modified to eliminate or minimize the hazard they present to out-of-control vehicles[14]. These hazardous locations include high

embankment slopes (see FIGURE 1.6), bridge piers, trees too close to the carriage way, abutments, non-breakaway sign supports and parapet noses. According to the Hand-Book of Barriers[16] prepared by the General Directorate of Turkish Highways, barriers should be used if the distance between such locations and the roadway is less than nine meters or if the road geometry is liable to lead to crashes.

Traffic barriers are highway appurtenances that provide a relative degree of protection to vehicle occupants from hazardous roadside features and from errant vehicles enroaching across a median[18]. They are not installed to protect or prevent damage to a sign or other highway appurte-

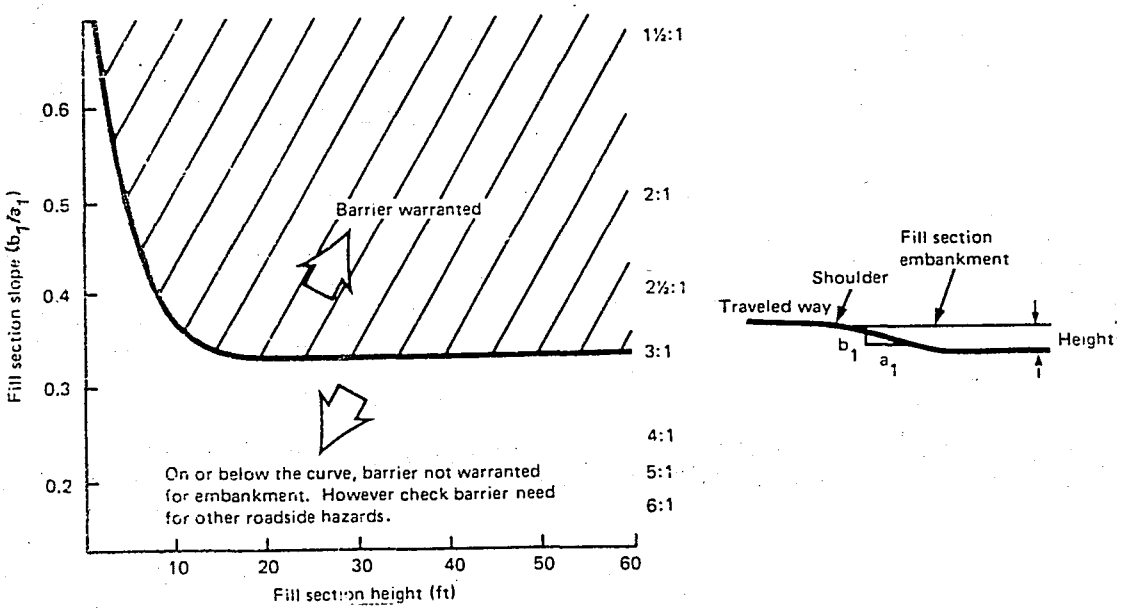

(1 ft = 0.305 m)

FIGURE 1.6. Barrier warrant for fill-section embankments as used in the USA[17].

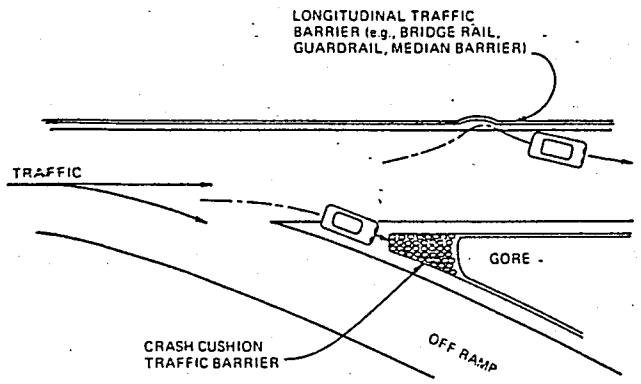

FIGURE 1.7. Traffic barrier definition[18].

nances. They should only be placed at locations where the hazardous feature can not be removed or relocated. Barriers should be amenable to quick repair of crash damage and must remain functional in all weather conditions. No matter how properly designed, the fact that barriers themselves can be sources of hazards, should be taken into consideration. They should never be used at locations where their necessity is not positively determined.

Traffic barriers are classified into two basic groups according to their function. Longitudinal barriers such as guardrails, bridge rails and median barriers perform by restraining and redirecting out-of-control vehicles away from roadside hazards. The second group consists of energy absorbing crash cushions which reduce the deceleration (G) forces that are developed upon impact of a vehicle on a fixed object, thus greatly minimize the severity of head-on collisions. Crash cushions must also function as a longitudinal barrier for glancing impacts along the barrier side.

Structural strength of the barrier and the safety of the occupants of impacting vehicles and other traffic must be the two factors considered in design. For instance, it may be necessary to reduce the rigidity of a system in order to

lessen the abruptness and severity of an impact, thereby improving safety[18].

Traffic barrier dynamic performance criteria are formulated for full scale vehicular crash testing where both strength and safety are simultaneously evaluated. These criteria are composed of

(a) vehicle impact characteristics,

(b) barrier response requirements, presented in the form of vehicle decelerations and trajectories[18].

Vehicle impact characteristics are presented in TABLE 1.6 for all traffic barrier systems. The values represent a severe crash of standard and light weight passenger vehicles. Vehicle weight, speed, approach angle and point of impact are the most significant characteristics affecting dynamic performance.

1.3.3.1. Longitudinal Barriers Longitudinal barriers should be designed to restrain and redirect a selected vehicle, which is representative of a large majority of the vehicle population using that roadway. The restraint provided by such barriers should not impose excessive deceleration forces on the vehicle occupants. They should be shaped such that the restraint action they provide will redirect the path of the vehicle parallel to the normal traffic flow and will not cause a multicar collision. Steel wires spun between steel posts, steel profiles attached to steel posts and prefabricated concrete elements can be used as longitudinal barriers.

TABLE 1.6. Vehicle impact characteristics[18].

Traffic Barrier Type	Vehicle Weight, kg(lb)	Impact Speed, km/h (mph)	Characteristics Angle (degree)	Barrier Impact Point
Longitudinal	2050(4500)	97(60)	25	A
Crash Cushion	910(2000)	97(60)	0	B
	2050(4500)	97(60)	0	B
	2050(4500)	97(60)	15	C
	2050(4500)	97(60)	25[a]	C

* A - midway between posts; B - barrier nose; C - along barrier side.

[a] For structural strength evaluation only.

In case of impact, the component parts of the barriers should not penetrate the passenger component. The smoothness of the vehicle-barrier interaction is assessed by the effective coefficient of friction, μ.

TABLE 1.7. The assessment of the effective coefficient of friction at vehicle-barrier interaction[19].

μ	Assessment
0 - 0.25	Good
0.26 - 0.35	Fair
>0.35	Marginal

This coefficient is equal to,

$$\mu = \frac{\cos\theta - \frac{V_p}{V}}{\sin\theta} \qquad (1.1)$$

where θ = impact angle, [deg.]

V_p = speed of vehicle when it becomes parallel to railing, [km/h or mph]

V = impact speed, [km/h or mph].

Guideline values for maximum vehicle decelerations (at center of mass) are presented in TABLE 1.8 according to vehicle reference axes and three performance ratings[18]. The values given are maximum limits beyond which fatality and injury may be expected. As a rule it can be suggested to use a maximum 50 msec average deceleration occurring near the vehicle's center of mass during impact for design purposes.

TABLE 1.8. Maximum vehicle decelerations[18].

Barrier Performance Rating†	Maximum Vehicle Decelerations (g's)*			
	Lateral	Longitudinal	Total	Remarks
A	3	5	6	Preferred Range
B	5	10	12	
C	15	25	25	

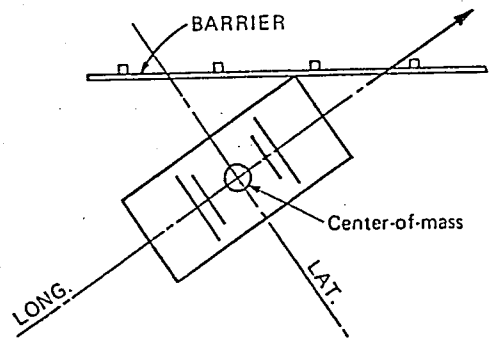

*Vehicle rigid body decelerations; maximum 500 g/sec onset rate; highest 50 msec average.

†A - limits for unrestrained passenger.
B - limits for passenger restrained by lap belt.
C - limits for passenger restrained by lap and shoulder belts.

1.3.3.2. Crash Cushions Crash cushions are designed for locations such as off-ramp gores, retaining walls and bridge piers in the medians, for which the primary problem is a head-on collision[18]. By spreading the impact energy over time and space, they reduce the severity of crash. A number of impact attenuation devices that can be used for this purpose such as rows of barrels, entrapment nets and arrays of containers filled with sand or water are available. TABLE 1.9 gives the classification of crash cushions. In FIGURE 1.8 the successive crushing of a crash cushion system is represented.

TABLE 1.9. Classification of crash cushions[18].

Status	Designation	Description
1. Operational	C-1	Steel Drums
	C-2	Water Cells
	C-3	Sand Containers
	C-4	Tor-Shok *
2. Experimental	XC-(a)	Entrapment Net
3. R & D	YC-(b)	Lightweight Cellular Concrete
	YC-(c)	Timber Post Field
	YC-(d)	Rigid Foams
	YC-(e)	Frangible Post Field
	YC-(f)	Yielding Beam
* Restricted for highways with posted speed of 50 mph(80 km/h) or less.		

For direct-on tests of crash cushions (i.e., where vehicle lateral deceleration is minimum), a maximum average permissible vehicle deceleration is 12 g's, as calculated

from vehicle impact speed and stopping distance[18]. For side impacts, the criterion given in TABLE 1.8 for longitudinal barriers is applicable.

Crash cushion behavior can be analyzed by two methods, namely the work-energy approach or the linear impulse momentum approach. The work-energy approach is used in cases where the vehicle kinetic energy is dissipated in plastic deformation. Barrel nests and entrapment nets are good examples of this situation. The second (linear impulse-momentum) approach is used for devices such as sand container systems, where the kinetic energy is dispersed into individual sand particles.

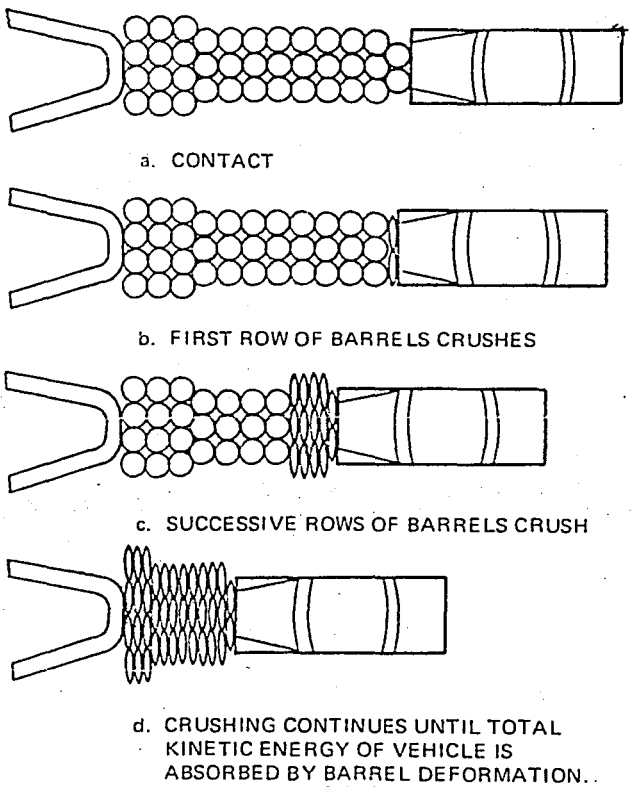

FIGURE 1.8. Successive crushing of crash cushion system[18].

The kinetic energy of a moving body is given by:

$$KE = \frac{Wv^2}{2g} \qquad (1.2)$$

where W = body weight, [kg or lb]
v = body speed, [m/sec or ft/sec]
g = acceleration due to gravity, [m/sec^2 or ft/sec^2].

In normal stopping conditions the kinetic energy is eventually dissipated by air drag, rolling friction and braking forces, but this is a matter of several hundred feet. Since at critical highway locations, the normal stopping distance and time are not available, crash cushions are used.

In FIGURE 1.9 the average deceleration in g units as a function of distance are given. The applied formulas are:

$$G_A = \frac{V_o - V_f}{t} \tag{1.3}$$

$$V_{avg} = \frac{V_o + V_f}{2} \tag{1.4}$$

$$D = V_{avg} \times t \tag{1.5}$$

where G_A = average deceleration, [m/sec^2 or ft/sec^2]
v_o = initial vehicle speed (speed of impact), [m/sec or ft/sec]
v_f = final speed = 0, [m/sec or ft/sec]
t = time of deceleration, [sec]
D = stopping distance after impact, [m or ft]
v_{avg} = average velocity, [m/sec or ft/sec].

For a reasonably flat deceleration-time history G_A can be expressed in gravitational units (g's) by extracting t from Equation (1.5) and inserting it to Equation (1.3) as seen in Equation (1.6).

$$G_A = \frac{V_o^2}{2gD} \tag{1.6}$$

(A) Work-energy analysis : In this analysis, vehicle's kinetic energy, KE, dissipated by the crash cushion is equated to the work, U, performed on the car by the crash cushion.

$$KE = U = \int_0^d F_x dx \tag{1.7}$$

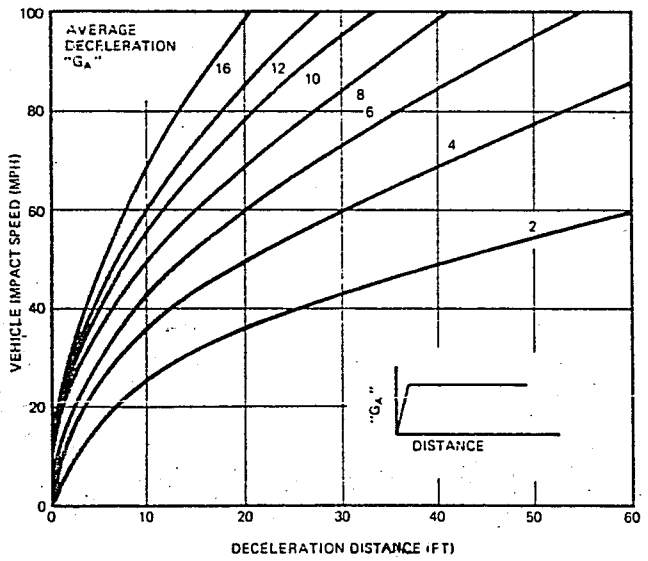

(1 ft = 0.305 m) (1 mph = 1.6 km/h)

FIGURE 1.9. Theoretical vehicle speed-deceleration distance relationship[18].

where U = work, [kg-m or ft-lb]

F_X = crash cushion force acting on the car through a small deformation, [kg or lb]

d_X = a small part of the crash-cushion deformation at the point of impact, [m or ft]

d = total crash-cushion deformation, [m or ft].

If F, the crash cushion force, is a constant then work can be calculated from Equation (1.8).

$$U = F \times d \tag{1.8}$$

There are an infinite number of force and displacement combinations that will produce a specified work. For instance, a 100 N force displaced through one meter is the same work as one newton force acting through 100 m. There are two constraints imposed on a crash cushion that restrict these combinations, namely space availability and the maximum permissible deceleration level.

For a crash cushion the deformation, d, might be restricted due to the geometrical conditions. The crash cushion force, F, must be less than that which will produce dangerous decelerations for the vehicle occupants.

Deceleration is a function of crash cushion force and vehicle weight. It is inversely proportional to vehicle weight - the heavier the car, the smaller the deceleration. Using Newton's second law, deceleration can be expressed by;

$$a'' = \frac{Fg}{w} \qquad [ft / sec^2] \tag{1.9}$$

$$a' = \frac{F}{w} \qquad [g's] \tag{1.10}$$

where a" = deceleration in [m/sec^2 or ft/sec^2] units
a' = deceleration in [g] units
F = crash cushion force, [kg or lb]
w = vehicle weight, [kg or lb].

A crash cushion design example solved by using the work-energy analysis and obtained from references [18] and [15] has been provided in APPENDIX A.

(B) Linear impulse-momentum analysis: The collision between two bodies, such as a car and a barrier, where relatively large contact forces exist during a very short interval of time, is called "impact"[18]. If there are no external forces of magnitude and the mass of the barrier put into motion is small, the law of conservation of momentum is applied.

$$M \cdot dV = V \cdot dm \tag{1.11}$$

where M = vehicle mass
V = vehicle speed
dm = mass of small stationary barrier
dV = small loss of vehicle speed.

The barrier mass per unit length is expressed as;

$$\frac{dm}{ds} = \frac{M \cdot \frac{dV}{dt}}{V \cdot \frac{ds}{dt}} \tag{1.12}$$

by solving Equation (1.11) for dm and dividing by ds; an increment along barrier side referenced to vehicle terminal point of penetration; and also by dt (time) on the numerator and the denominator on the right. Here dV/dt is acceleration and ds/dt is velocity. Equation (1.12) is restated for acceleration as Equation (1.14).

$$\frac{dm}{ds} = \frac{M \cdot a}{V^2} \tag{1.13}$$

$$a = \frac{dm}{ds}\frac{V^2}{M} \tag{1.14}$$

Maximum vehicle decelerations will occur during the initial phase of impact and then decrease rapidly as the vehicle slows, if the barrier mass is constant through out its length. To maintain a deceleration level within human tolerance, the system mass should be low. Hence, length of the constant-mass barrier will be unnecessarily long because the average deceleration force will be well below human tolerance[18]. A more appropriate design approach is to proportion the barrier mass in such a manner that vehicle deceleration, a, is constant through out impact[18]. By equating the work done by the vehicle during impact to its kinetic energy before impact, the stopping distance, s, is expressed as Equation (1.17).

$$F \cdot s = \frac{1}{2} MV^2 \tag{1.15}$$

$$M \cdot a \cdot s = \frac{1}{2} MV^2 \tag{1.16}$$

$$s = \frac{V^2}{2a} \tag{1.17}$$

After making the substitutions Equation (1.14) becomes Equation (1.18).

$$\frac{dm}{ds} = \frac{M}{2s} \tag{1.18}$$

Equation (1.18) suggests that, for constant deceleration, the mass per unit length required at any point in the barrier is one half the mass of the vehicle divided by the distance to a fixed stopping point. The barrier mass approaches infinity as the distance approaches zero. In practice, for a corresponding final value of s, namely s_f, dm/ds has a feasible maximum value.

$$s_f = \frac{M}{2\left(\frac{dm}{ds}\right)_{max}} \tag{1.19}$$

where $(dm/ds)_{max}$ = the maximum feasible module mass per unit length.

Incremental module masses are determined from,

$$\frac{dm}{ds} = \left(\frac{dm}{ds}\right)_{max} \frac{s_f}{s_f + s_i} \tag{1.20}$$

where s_i = consecutive integers (module diameters).

Constant vehicle deceleration depends on barrier length and vehicle impact speed. A design speed and an acceptable vehicle deceleration is selected first and the length of inertia, D, is calculated from Equation (1.6), in which G_A is the acceptable average vehicle deceleration in gravitational units.

Equation (1.22) can not be practically satisfied as the value of s becomes small. Fortunately, the vehicle is

decelerated to a relatively low speed (i.e., 10 to 15 mph) as it nears the end of the barrier's inertia phase[18]. At this point, vehicle kinetic energy is dissipated by friction in the sand as the car bulldozes into this final barrier part[18]. It has been determined that the bulldozing phase should consist of approximately five tons of sand. A typical crash cushion system designed according to the linear impulse momentum principles is presented in FIGURE 1.10. A solved design problem taken from reference [18] has been submitted as an example in APPENDIX A.

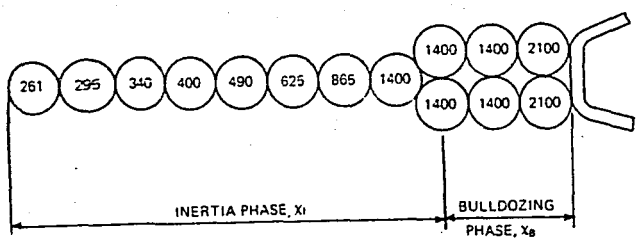

FIGURE 1.10. Layout of crash cushion system C3[18].

2. SAMPLE PREPARATION AND TESTING METHODOLOGY

2.1. Materials

The materials used are fly ash, rubber, lime and spherical and crushed ice. Specific gravities and grain size distributions of fly ash, lime and rubber are determined using the test methods specified by ASTM under the following names and codes as; Standard Method of Test for Specific Gravity of Soils - ASTM D854-58 (reapproved 1965)[22] and Standard Method for Grain-Size Analysis of Soils - ASTM D422-63[24].

The basic material utilized during laboratory research is high-calcium fly ash, obtained from the Soma TEK-B Thermal Power Plant, third unit, third (last) section. This section, when compared with the other two, is known to produce the finest particles. The grain size distribution of fly ash obtained by hydrometer analysis performed in the laboratories of the General Directorate of Turkish Highways is given in FIGURE 2.1. It is a poorly graded material with a specific gravity of 2.6.

The chemical composition of coarse, medium and fine sized fly ash (from the Soma TEK-B Thermal Power Plant) determined by the General Directorate of Turkish Highways is given in TABLE 2.1.

Fly ash is stored in cloth bags which are placed in plastic bags after being thoroughly mixed to ensure uniformity. Its exposure to air, moisture and light is prevented.

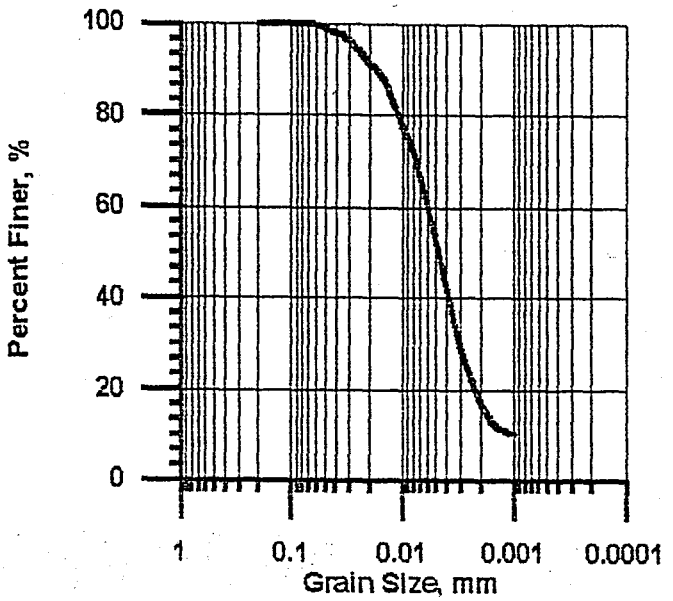

FIGURE 2.1. Grain size distribution of fly ash.

TABLE 2.1. The chemical composition of fly ash obtained from the Soma TEK-B Thermal Power Plant.

Components (%)	Size		
	Coarse	Medium	Fine
SiO_2	46.60	26.50	21.00
$R2O_3$ (Fe_2O_3+Al_2O_3)	33.80	53.29	60.12
Fe_2O_3	2.29	1.89	1.54
Al_2O_3	31.51	51.40	58.58
CaO	14.16	14.01	12.65
MgO	1.29	1.95	2.04
SO_3	1.49	2.87	3.02
Loss on ignition	0.49	0.63	0.66

The hydrated lime used in this study is produced by Işıklar Holding A.Ş. under the commercial name Barkisan. It is sold in 25 kg. paper bags and has the qualifications listed in T.S. 4022/April 1993[20]. The chemical properties of hydrated limes as specified by T.S. 4022/April 1993[20] are presented in TABLE 2.2. Its specific gravity is equal to 2.43. FIGURE 2.2 shows the grain size distribution (obtained

TABLE 2.2. The chemical properties of hydrated limes[20].

Properties (in per cent by weight)	Commercial Lime Types				
	S-KK 90	S-KK 80	S-KK 70	S-DK 85	S-DK 80
CaO+MgO (min.)	90	80	70	85	80
MgO	≤5	≤5	≤5	≥30	>5
CO_2 (max.)	4	7	12	7	7
Materials non-soluble in acid(including SiO_2) (max.)	1.5	1.5	1.5	1.5	1.5
Metal oxides (Al_2O_3+Fe_2O_3) (R_2O_3) (max.)	1	1	1	1	1
SO_3 (max.)	2	2	2	2	2
Note: These values are found by excluding the moisture and bonded water contents.					

by hydrometer analysis performed in the Boğaziçi University Soil Mechanics and Foundation Engineering Laboratory) of this uniform, poorly graded material.

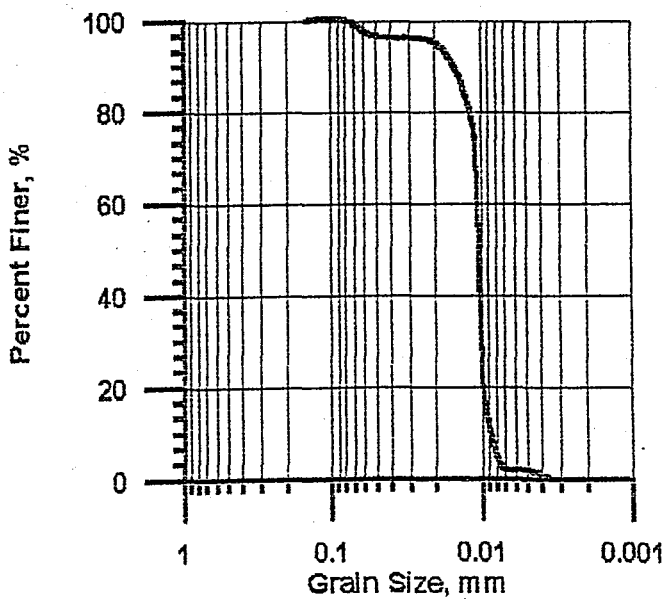

FIGURE 2.2. Grain size distribution of lime.

Rubber is obtained in pulverized form from Turlas A.Ş., Kayışdağı, Istanbul. It is produced as a waste during the retreating of worn-out truck tires. The specific gravity of rubber is 1.1. It is a well graded material with a coefficient of uniformity (C_u) of 4 and a coefficient of concavity (C_c) of 1. The grain size distribution (obtained by sieve analysis performed in the Boğaziçi University Soil Mechanics and Foundation Engineering Laboratory) of rubber is given in FIGURE 2.3. It has almost no economical value and very few areas of utilization. It is stored in plastic bags to prevent exposure to sunlight.

Ice is produced in the laboratory using distilled water. Crushed ice is obtained by breaking ice blocks to arbitrarily shaped and sized particles. Spherical ice, 2 cm. in diameter, is produced using special molds.

2.2. Samples

The scope of the laboratory research was to find out the effects of adding lime, rubber and ice in different compositions to fly ash samples to obtain energy absorbing behavior. A total number of 126 samples were prepared in three main, 21 sub-groups, each sub-group consisting of six elements with similar properties. In TABLE 2.3 the grouping of samples is explained in detail.

The effects of changing the per cent lime and rubber added to the samples on strength properties were determined by adding zero, 10, 20 and 30 per cent lime or rubber by weight during sample preparation. It was proposed that adding lime to a certain level would increase ultimate strength and adding rubber would decrease it but would increase the energy absorbing capacity.

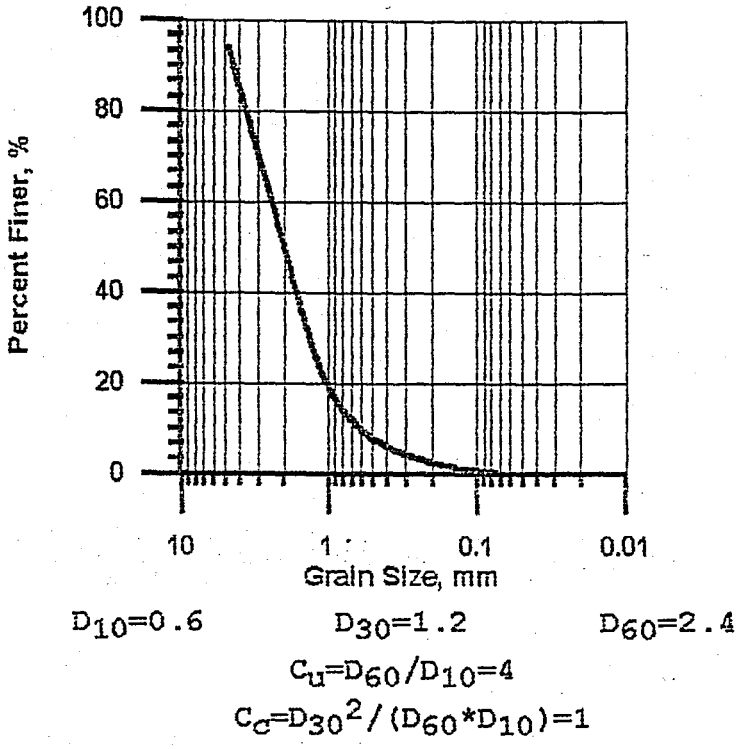

FIGURE 2.3. Grain size distribution of rubber.

The scope of adding ice was to provide extra water for hydration after the sample was molded into shape. This water was introduced by the thawing of ice. Also it was proposed that the voids, especially the spherical ones left in the sample after the thawing and the depletion of water would increase the energy absorbing capacity by introducing small air cushions.

2.2.1. Sample Preparation

The moisture content-dry density relationship of fly ash, fly ash-lime (10, 20, 30 per cent lime by weight) and fly ash-rubber (10, 20, 30 per cent rubber by weight) mixtures were determined as described in Tentative Methods of Test for Moisture-Density Relations of Soils Using 5.5 lb (2.5 kg) Rammer and 12-in (30.5 cm) Drop - ASTM D698-66T[25] specifications. Two complete sets of compaction tests were performed on every different mixture. The moisture content-

TABLE 2.3. Sample groups

TYPE OF ADDITIVE		ICE CONTENT		
		No Ice	10 Per Cent by Weight Crushed Ice	10 Per Cent by Weight Spherical Ice
	CONTROL	1)100 per cent fly ash	1)100 per cent fly ash	1)100 per cent fly ash
	LIME	2)90 per cent fly ash and 10 per cent lime*	2)90 per cent fly ash and 10 per cent lime*	2)90 per cent fly ash and 10 per cent lime*
		3)80 per cent fly ash and 20 per cent lime*	3)80 per cent fly ash and 20 per cent lime*	3)80 per cent fly ash and 20 per cent lime*
		4)70 per cent fly ash and 30 per cent lime*	4)70 per cent fly ash and 30 per cent lime*	4)70 per cent fly ash and 30 per cent lime*
	RUBBER	5)90 per cent fly ash and 10 per cent rubber*	5)90 per cent fly ash and 10 per cent rubber*	5)90 per cent fly ash and 10 per cent rubber*
		6)80 per cent fly ash and 20 per cent rubber*	6)80 per cent fly ash and 20 per cent rubber*	6)80 per cent fly ash and 20 per cent rubber*
		7)70 per cent fly ash and 30 per cent rubber*	7)70 per cent fly ash and 30 per cent rubber*	7)70 per cent fly ash and 30 per cent rubber*

* All per centages in the table are per cent by weight

dry density curves are given in FIGURE B.1 through FIGURE B.7 in APPENDIX B. The averaged results from the data obtained from the two sets for each mixture are given in TABLE 2.4 and in FIGURE 2.4 and FIGURE 2.5.

TABLE 2.4. Average optimum water content-maximum dry unit weight values for fly ash, lime and rubber mixtures.

DESCRIPTION	Optimum Water Content, w_{opt} (%)	Maximum Dry Unit Weight, γ_{max} (kN/m^3)
100 per cent fly ash	22.40	12.10
90 per cent fly ash and 10 per cent lime	22.65	12.23
80 per cent fly ash and 20 per cent lime	23.14	12.48
70 per cent fly ash and 30 per cent lime	24.30	12.43
90 per cent fly ash and 10 per cent rubber	22.18	12.20
80 per cent fly ash and 20 per cent rubber	20.85	11.86
70 per cent fly ash and 30 per cent rubber	20.43	11.50

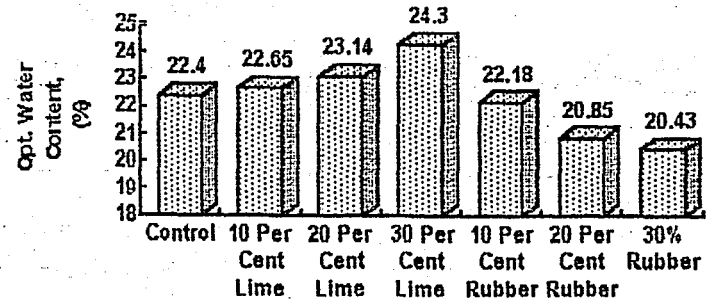

FIGURE 2.4. Variation of optimum water content with per cent added lime and rubber

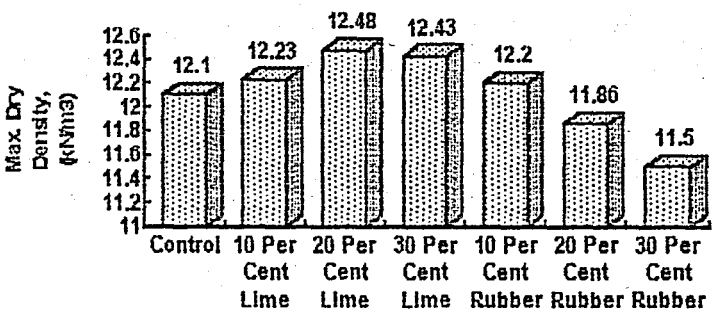

FIGURE 2.5. Variation of maximum dry density with per cent added lime and rubber.

The 944 cm^3 Standard Proctor molds with average diameters of 10.16 cm and average heights of 11.65 cm were used for the preparation of specimens. First it was proposed to compact the samples in three layers with 25 blows per layer using a 24.5 N compaction hammer dropping from 0.305 m on to the fly ash mixture. The nominal compaction energy, CE, delivered by the hammer in this case is equal to;

$$CE = \frac{3 * 25 * 24.5 * 0.305}{9.44 * 10^{-4} * 1000} = 593.7 \ kJ / m^3$$

It was seen that the ice particles were being crushed at every drop of the hammer in samples which were prepared by adding 10 per cent by weight spherical ice. Since it was especially required to have spherical voids in that group of specimens, another method of compaction, namely static compaction, had to be used in the preparation of all of the samples. The compression machine available in the laboratory for CBR tests was used to apply the required static load. A cap with a cross-sectional area equal to the cross-sectional area of the Standard Proctor mold was placed between the loading piston and the fly ash mixture during compaction to ensure uniform distribution of load. Compaction was performed in a single layer. The load required to compact fly ash to the maximum dry density at optimum moisture content was calculated by equating the nominal compaction energy, CE, delivered by the compaction hammer to the work per volume done by the CBR compression machine piston in compressing the mixture through a distance of t. Energy loss due to friction was not taken into account.

$$CE = \frac{L * C_m * g}{V_c} * t_p \qquad (2.1)$$

where CE = nominal compaction energy delivered by the rammer, [kJ/m^3].

L = load applied by the piston, [divisions]

C_m = calibration constant of the compression machine = 0.579 kg/division

g = gravitational acceleration = 9.81 kg/sec^2

t_p = distance traveled by the piston during compression (assumed to be approximately equal to 5 cm)

V_C = volume of the Standard Proctor compaction mold = 944 cm^3.

The load (L) necessary for delivering the Standard Compaction energy was calculated from equation (2.1) to be approximately equal to 14 MPa (2000 psi) without considering the frictional loss.

Static compaction was applied to 100 per cent fly ash to determine its water content-dry density relationship under 7(1000), 14(2000), 21(3000), 28(4000) and 35(5000) MPa(psi) static loading and to compare the results with the ones obtained from Standard Proctor. It was seen that no matter how much the load was increased, static compaction was not yielding optimum water content and maximum dry density values as high as those obtained from Standard Proctor. An applicable, standard shaped curve for static compaction could not be drawn. The static compaction test results for 100 per cent fly ash are presented in FIGURE 2.6. In the end it was decided to use a compressive load of 21(3000) MPa(psi), taking into consideration the value obtained by equating the nominal compaction energy to the work done by the compression machine piston (Equation (2.1)) and assuming an energy loss due to friction of 50 per cent.

The samples were molded in single layers. Compressive load was applied at a rate of approximately 1.8 kg/cm^2-sec (25 psi/sec). After reaching the ultimate value [21 MPa (3000 psi)] the load was kept constant for a period of five minutes, until the load gage pointer resumed static state. After the removal of the load, the samples were wrapped up to prevent moisture loss and let to stand in the molds for three hours. Within this period of time, they gained enough strength by hydration to be able to support their own weight without deforming. The molds were removed, the samples were wrapped in plastic sheets and were stored in the moisture room.

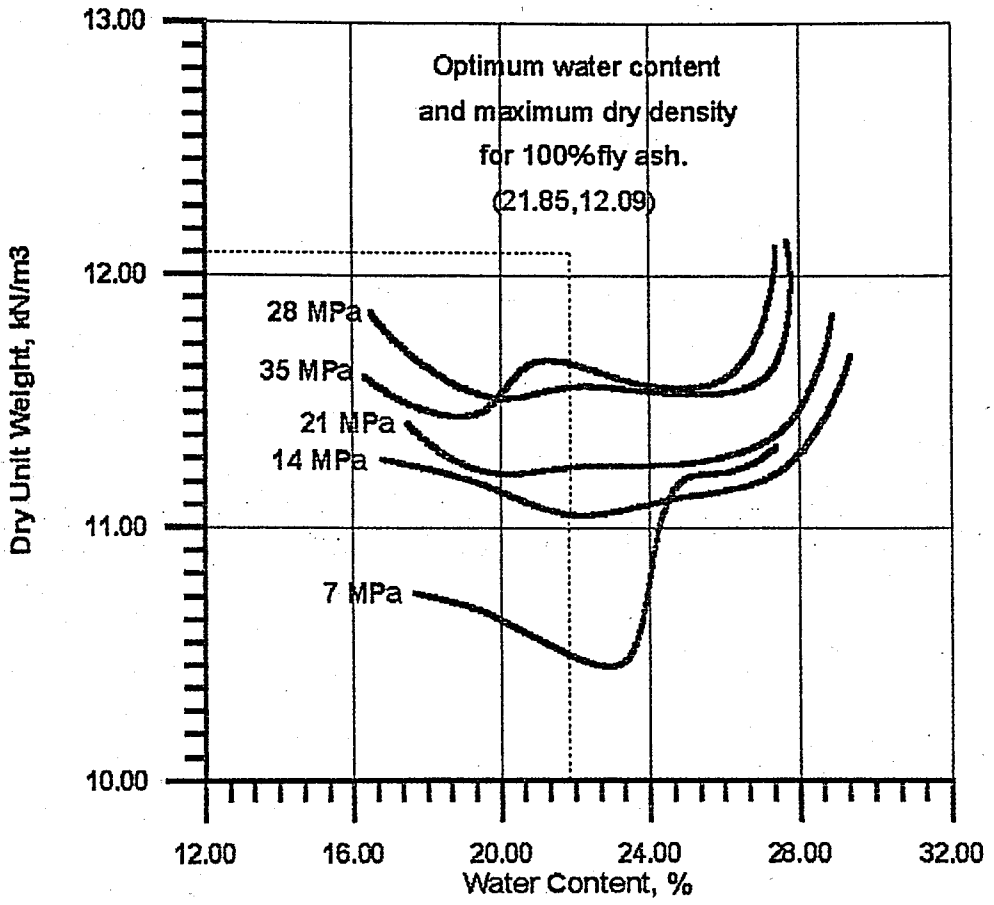

FIGURE 2.6. Water content - dry density relations for 100 per cent fly ash determined by static compaction.

2.2.2. Sample Curing

The samples were cured for a period of 56 days. The more traditional curing period of 28 days could not be used due to the problems encountered in adjusting the test set-up. In the beginning it was decided to cure the samples at ideally recommended conditions; namely at 21+/-2°C and 100 per cent relative humidity. But due to the limitations of the moisture room, it was not possible to maintain this medium in the beginning. The air conditioner was not working in the first 25 days of curing. But according to the readings taken every day, it is possible to say that the temperature never fell below 15°C and the humidity below 50 per cent through

out this period. As can be seen, the temperatures obtained were high enough to sustain the hydration reaction which is known to cease at 4°C. The humidity in this case did not have too much significance any way since the samples were packed up in plastic sheets to prevent exposure to atmosphere and moisture loss. At the end of the curing period, it was seen that the samples had lost only a small amount of moisture varying from two to five gr. The curing conditions recorded every day are submitted in APPENDIX C, TABLE C.1.

2.3. Sample Testing

Compression, double punch tension and ultrasound tests were performed on the samples. Ultrasonic testing, which is a non-destructive method of determining compressive strength, modulus of elasticity and some other physical properties of a material was carried on all of the samples, namely on 126 of them. Then the samples were grouped into two parts according to the test performed on them. Three samples representing each group (there were 21 sub-groups) were tested under compression and three under splitting tension. The stress-strain relationship and the ultimate failure loads were determined.

2.3.1. Ultrasonic Testing

This test is performed using the Ultrasonic Tester Type BP III. The Ultrasonic Tester is utilized in the measurement of the sound velocity in solids, fluids and gasses. Using the obtained values and certain correlations, it is possible to calculate the dynamic elasticity modulus, to determine the compressive strength, to detect fissures and to localize the damaged zones without destroying the samples.

The Ultrasonic Tester can be used outside the laboratory to investigate any form or shape such as piers, rock, marble or concrete slabs, road surfaces and bricks etc. The Ultrasonic Tester is seen in FIGURE 2.7.

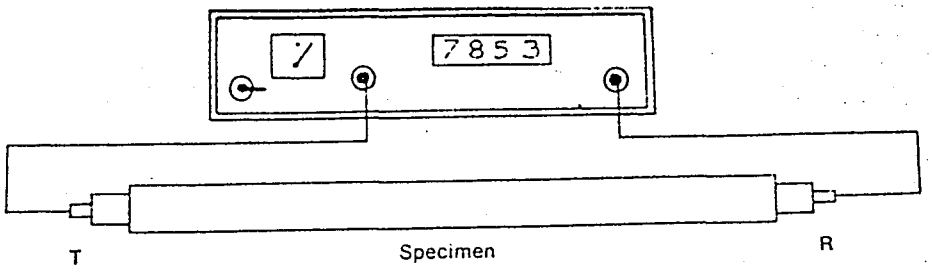

FIGURE 2.7. The Ultrasonic Tester.

When the apparatus is operated, the transmitting probe, T, receives electrical pulses at interval of one second and transforms them into ultrasonic pulses. These pulses are picked up by the receiving probe, R, after having traveled through the specimen and reconverted into electrical pulses which are then conducted to a timing device. The time it takes the ultrasonic pulses to travel through the specimen are indicated in microseconds (μs). The transit time of sound may be read from 0.1 to 999.9 μs with an accuracy of ±0.1 μs. For good sound conductivity between the specimen and the probes, a coupling medium such as grease, putty or rubber sheets must be used to ensure optimum contact.

The velocity of sound can be determined from,

$$v_s = \frac{s_u}{t_u} \qquad (2.2)$$

where v_s = sound velocity, [km/sec]

s_u = nearest distance between two probe surfaces, [mm]

t_u = time of transmission, [μs].

From the determined sound velocities, the quality of the tested material can be decided upon. TABLE 2.5 gives the quality ranges of old concrete determined from sound velocities. The compressive strength of concrete is directly proportional to its quality. High quality of concretes have very minor discontinuities in the form of cracks or voids and high compressive strengths.

The dynamic modulus of elasticity (Young's Modulus) can be determined for long, rod shaped bodies using the formula,

$$E = \rho \cdot v_s^2 \qquad (2.3)$$

TABLE 2.5. Concrete quality determined from sound velocities.

Velocity (m/sec)	Quality
> 4500	excellent
4500 > v >3500	good
3500 > v >3000	doubtful
3000 > v >2000	poor to bad
v < 2000	very bad

where E = Young's Modulus, $[N/m^2]$
ρ = net density of the material, $[kg/m^3]$
v_S = sound velocity, [m/sec].

It must be noted that the modulus increases with increasing sound velocity. When the transverse dimension of the tested object is not small as compared with the wavelength of the specimen (three dimensional sample), equation (2.3) changes into,

$$E = \rho \cdot v_s^2 \frac{(1 + \nu) \cdot (1 - 2\nu)}{1 - \nu} \qquad (2.4)$$

where ν = the Poisson's ratio.

The Poisson's ratio is a constant relationship between lateral strains and longitudinal or axial strains caused by an uni-axial force, provided a material remains elastic and is homogeneous and isotropic.

$$\nu = \frac{\text{lateral strain}}{\text{axial strain}} \qquad (2.5)$$

The value of ν fluctuates for different materials over a relatively narrow range ($-1 < \nu < 0.5$). Generally it is in the neighborhood of 0.25 to 0.35. In extreme cases values as low as 0.1 (some concretes) and as high as 0.5 (rubber) occur. The latter value is the largest possible. If the Poisson's ratio of concrete is assumed to equal to 0.2, equation (2.4) can be expressed as equation (2.6).

$$E = 0.9 \cdot \rho \cdot v_s^2 \qquad (2.6)$$

In this study, the transverse dimensions of the samples can not be assumed to be negligibly small. In other words, the samples are three dimensional. For this reason, equation (2.6) has been used in the calculations and the value of the Poisson's ratio has been assumed to equal to 0.2 for all fly ash mixtures.

Three readings were taken for each sample and the sound velocities were calculated by averaging them. The densities of the samples were calculated by dividing the

weight of each sample by the corresponding volume, which is approximately equal to 944 cm^3 (the volume of the Standard Proctor mold). The dynamic elasticity moduli for each of the 21 sub-groups were calculated by taking the average of the values obtained from the six samples belonging to that sub-group. It has been observed that the moduli calculated for the six samples making up a sub-group showed consistency. Individual sound velocity and elasticity modulus values calculated for each sample are given in APPENDIX D, TABLE D.1 through TABLE D.3. In TABLE 2.6 dynamic elasticity moduli for each subgroup are given.

Variations among sub-groups occurred due to the compositional differences depending on the per cent lime or rubber in the samples or due to the presence of the 10 per cent added by weight crushed or spherical ice.

2.3.2. Compressive Loading and Stress-Strain Curves

The reactions of a material to external loading conditions are called the mechanical properties of that material. The first property that comes into mind is strength. Other mechanical properties are elasticity, ductility, creep, hardness and toughness[21]. Each of these properties are associated with the ability of the material to resist mechanical forces[21].

Stress rather than force is the more significant parameter in the study of materials, since the effect of an applied force P depends primarily on the cross-sectional area of the member[22]. The cross-sectional area of the tested specimen changes through out compressive loading so area correction should be applied for better results. This way the so-called true stress can be obtained.

TABLE 2.6. Dynamic elasticity moduli obtained by ultrasonic testing.

	DYNAMIC ELASTICITY MODULUS (*10^3) (MPa)		
Sample compositions	No ice	10% spherical ice by weight	10% crushed ice by weight
100% fly ash	6.0	7.6	7.1
90% fly ash & 10% lime	7.2	8.8	8.7
80% fly ash & 20% lime	6.7	9.1	6.9
70% fly ash & 30% lime	6.0	6.6	7.5
90% fly ash & 10% rubber	6.4	5.8	5.6
80% fly ash & 20% rubber	4.2	4.4	3.9
70% fly ash & 30% rubber	3.8	2.0	2.8

In the compression test, not only the ultimate strength, but other properties are observed, especially those connected with the study of deformation as a function of the applied force. Thus, while a specimen is being subjected to an increasing force P, a change in length between two arbitrary points is observed. The initial distance between these two points is called the gage distance, L. The gage distance can be taken equal to the initial length of the sample, L_o, but some errors can be encountered due to the in homogeneity of the top and bottom surfaces. It is better to determine two points some where in the middle and more fundamental to calculate strain as the observed reduction per unit length of the gage.

Strain may be elastic or plastic. Elastic strain is the strain which is present only during stressing and

disappears after the load is removed[21]. It is proportional to the amount of applied stress. This linear relationship is described by Hooke's law. The modulus of elasticity or Young's Modulus (E) is the ratio between the stress that is applied and the elastic strain that results and is in the units of stress.

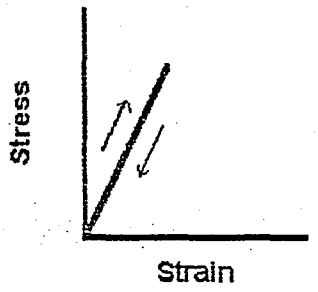

FIGURE 2.8. Elastic stress-strain relationship. Elastic strain is proportional to the amount of stress[21].

Plastic strain is the result of a permanent displacement of the atoms inside the material and is encountered when the elastic limit, which corresponds closely to the proportional limit, is exceeded.

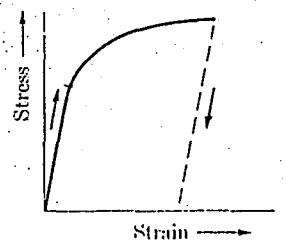

FIGURE 2.9. Plastic stress-strain relationships. Plastic strain, which follows initial elastic strain, is not reversible. The elastic strain is reversible[21].

The strength of a material to resist plastic deformation is called the yield strength, and is computed by dividing the force initiating the yield by the cross-sectional area[21]. During loading, in materials such as some

of the softer steels, the yield strength is marked by a definite yield point. In other materials, where the proportional limit is less obvious, it is common to define the yield load as that force required to give 0.2 per cent (or some other specified value) plastic offset[21].

Ductility is the amount of plastic deformation at the breaking point and can be expressed as reduction in length with the same units as strain. Non-ductile materials show no plastic deformation. Ductile materials, such as metals, have elasticity modulus, proportional limit and yielding limit values in compression which are very close to those they have under tension. Highly ductile materials will be greatly enlarged in cross-section under compression but sudden breaking is never achieved. Ductility can be measured from the difference in area at the point of failure, and can be expressed as a percentage, too.

$$\text{enlargement of area} = \frac{\text{original area - final area}}{\text{original area}} \qquad (2.7)$$

Brittle materials like concrete undergo very small deformations under compression. Their failure is usually due to shear or tension caused by lateral enlargement of the cross-sectional area. Their stress-strain diagrams are usually linear, indicating that no plastic deformations occur. Their compressive strength is greater than their tensile strength by an average factor of eight.

Toughness is a measure of the energy required to break a material[21]. Energy, a product of force and distance, is closely related to the area under the stress-strain curve. A ductile material with the same strength as a non-ductile material will require more energy for breaking and be tougher[21].

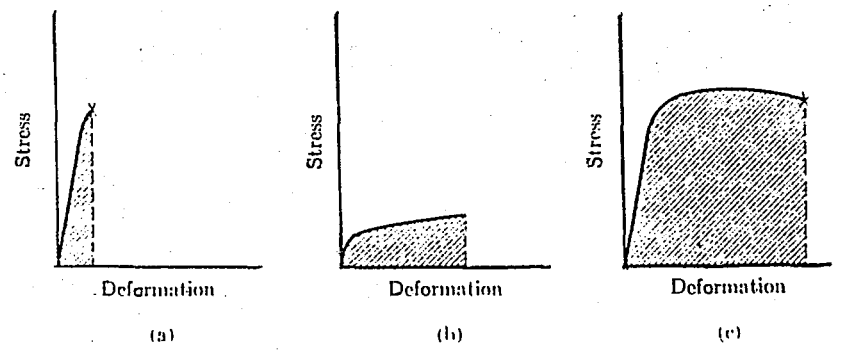

FIGURE 2.10. Toughness. This is a measure of the energy required to break a material. As such, it is closely related to the area under the stress-strain curve. a) is a brittle, b) is a ductile and c) is a tough material[21].

Compressive testing of the samples was carried on at the Boğaziçi University Structures Laboratory. The purpose was to determine the increase or decrease in load bearing capacity caused by adding different per centages of lime, rubber and ice to the samples. The samples were loaded manually using a hydraulic jack, so the loading rate could not be kept constant. Two electronic dial gages were used to record the reduction in length of the samples at two points 180° apart. The load cell had a measuring capacity of 50 tons. The dial gages and the load cell were connected to a data logger. All of the readings were recorded as data files by a computer connected to the data logger.

The deformation dial gages were attached to a frame made up of two plexi-glass plates with circular holes, big enough to insert the sample in between, at a gage length of 8.5 cm. Since they were very sensitive to every small vibration, even the noises or small air currents within the laboratory affected the readings taken. All the data were recorded in the order of 10^{-2} mm. The strain was calculated

by averaging the data obtained from the two deformation dial gages and dividing by the gage length which is equal to 8.5 cm as stated before.

The load readings were taken with an accuracy of ±50 kg. True stresses were calculated by dividing the load by the corrected area for every load-deformation reading.

The samples without rubber failed in the brittle mode. Multiple cracks were observed. All of the cracks were oriented at 90° angles. The stress-strain curves were plotted and the dynamic elasticity moduli were calculated from slopes of the elastic range for each sample.

Samples with rubber had cracks oriented at 90° angles on their surfaces, but the failure angle was 45° on the inside. They did not fail completely; that is they continued to carry a large portion of the maximum load even after they were completely cracked. Despite being cracked the samples almost completely returned to their original shape after the removal of the load, since the rubber fibres kept them in one piece.

It was also essential to determine the differences in energy absorbing capacities due to the composition of the samples, from the compression test results. The energy absorbing capacity (toughness), as stated before, was equal to the area under the stress-strain curve. The area under a curve with a known equation could be found by taking the integral within the boundaries. In this case, the equations were found by fitting curves using the stress and strain values (x and y coordinates) determined from the recorded data. An approach based on the definition of integration was followed.

If it is necessary to determine the area under the curve seen in FIGURE 2.11 with the equation $y = f(x)$, this area can be divided into n pieces separated by a distance of

δx_i within the boundaries [a,b]. If a value of $x = x_i'$ is chosen within these partial intervals and if lines parallel to the x-axis are drawn from points on the curve with x_i' abscissa then the rectangles seen in the figure are obtained. Each of these rectangles have an area equal to δA_i.

$$\delta A_i = f(x_i') \cdot \delta x_i \qquad (2.8)$$

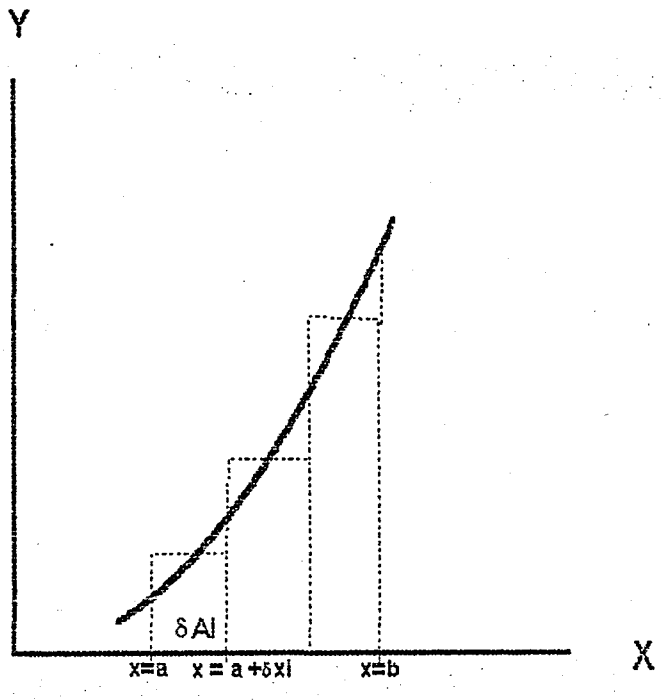

FIGURE 2.11. Determination of the area under a curve.

As the abscissa moves from x to $x+\delta x_i$ the total area changes by an amount δA_i. The total area of n of these rectangles is calculated using equation (2.9).

$$\sum_{i=1}^{n} \delta A_i = \sum_{i=1}^{n} f(x_i')\delta x_i \qquad (2.9)$$

Taking the limit of equation (2.9) $\delta x_i \to 0$ and $n \to \infty$, the total area of the curve is obtained as A.

$$A = \lim_{n\to\infty} \sum_{i=1}^{n} f(x_i') \cdot \delta x_i = \int_a^b f(x)dx = \int_a^b y \cdot dx \qquad (2.10)$$

Stress-strain diagrams of the 63 samples tested under compressive loading are drawn by curve fitting and their energy absorbing capacities are determined from equation (2.10). The areas under the stress-strain curves have been calculated up to the strain value where the stress reached zero. The stress-strain curves and the determined mechanical properties as well as the water content and dry unit weight values of the samples are submitted in APPENDIX E as FIGURES E.1 through E.21 and in APPENDIX F as TABLE F.1 through TABLE F.3 Young's Modulus, energy absorbing capacity and maximum compressive strength values obtained for the 21 subgroups by averaging the results from three samples tested under compression for each subgroup are presented in TABLE 2.7. Comparison of these results are made in FIGURE 2.12 through FIGURE 2.14.

TABLE 2.7. Some mechanical properties of fly ash mixtures obtained from compressive loading test.

	Per cent lime or rubber	Water content (%)	Dry unit weight (kN/m^3)	Young's Modulus ($*10^3$) (MPa)	Maximum compressive strength (kPa)	Energy absorbing capacity (kJ/m^3)
CONTROL	1) -	17.87	11.72	4.65	5061	32.4
	2) 10% lime	20.56	11.29	5.61	8976	152.8
	3) 20% lime	19.22	11.38	10.4	8361	194.2
	4) 30% lime	20.33	10.95	4.73	6019	31.4
	5) 10% rubber	20.62	12.60	3.26	4746	85.3
	6) 20% rubber	19.78	12.17	1.87	2578	53.1
	7) 30% rubber	20.07	11.66	1.25	1273	65.5
SPHERICAL ICE	1) -	28.99	11.15	2.65	5304	51.1
	2) 10% lime	29.86	11.08	4.84	8699	27.5
	3) 20% lime	27.87	11.19	6.47	10281	322
	4) 30% lime	30.23	10.30	5.48	8726	23.2
	5) 10% rubber	27.32	11.02	2.98	3080	60.4
	6) 20% rubber	25.50	10.80	3.8	2472	65.4
	7) 30% rubber	20.87	11.24	0.9	1080	121.4

TABLE 2.7 continued.

	Per cent lime or rubber	Water content (%)	Dry unit weight (kN/m^3)	Young's Modulus ($*10^3$) (MPa)	Maximum compressive strength (kPa)	Energy absorbing capacity (kJ/m^3)
CRUSHED ICE	1) -	25.83	12.05	4.97	5661	76
	2) 10% lime	27.46	11.61	4.9	13359	56.2
	3) 20% lime	27.06	11.75	5.4	7766	100.3
	4) 30% lime	28.12	11.32	4.9	8715	193.1
	5) 10% rubber	26.55	11.22	5.17	4714	53.6
	6) 20% rubber	27.01	10.69	3.63	3242	44.9
	7) 30% rubber	24.54	10.62	1.2	1837	59.2

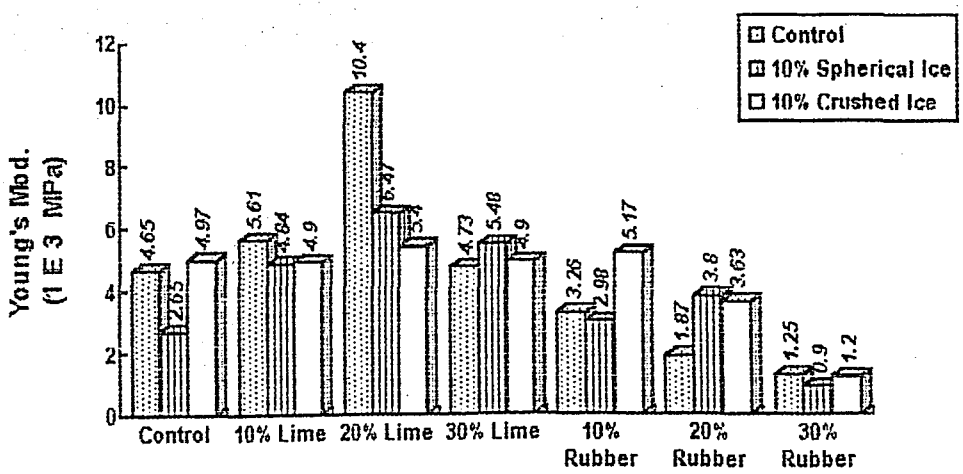

FIGURE 2.12. Variation of the Young's Modulus values with ice content.

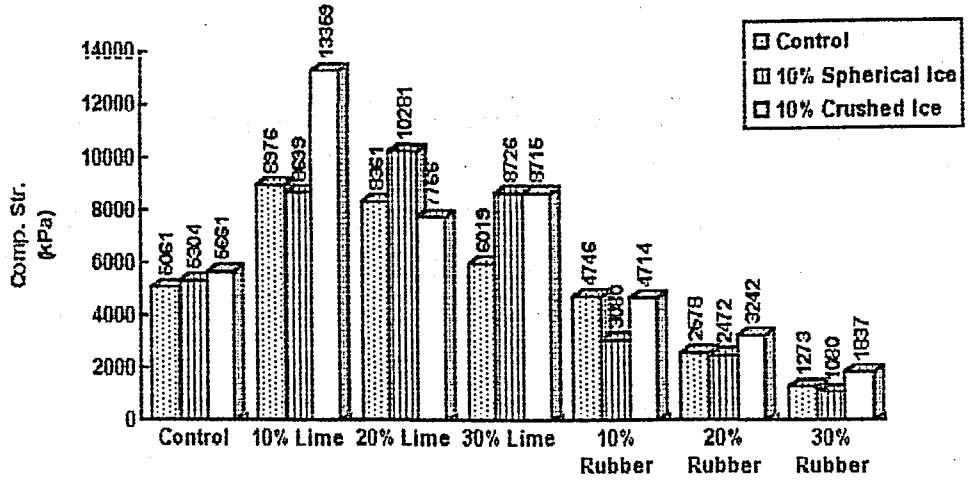

FIGURE 2.13. Variation of the maximum compressive strength with ice content.

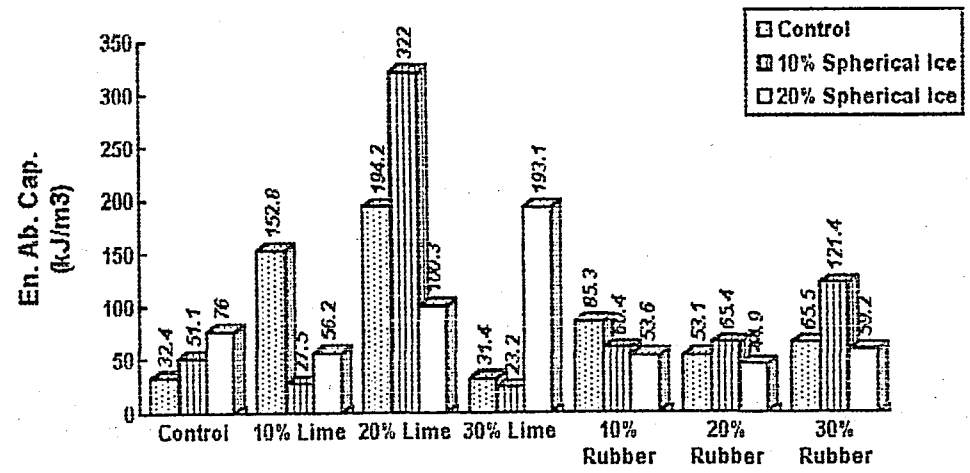

FIGURE 2.14. Variation of the energy absorbing capacity with ice content.

2.3.3. Double Punch Testing for Tensile Strength Measurement

Concrete and soil are the two materials used under compressive loading, but their tensile strength is also of importance under various situations. The condition under which cracks form on the tension side of reinforced concrete

flexural members and cracking failure related to the tensile strength of materials in many highway pavements and earth-fill dams has been attracting attention in the recent years.

There are experimental difficulties in determining the tensile strength of concrete and soil. In direct tension minor misalignments and stress concentrations in the gripping devices are apt to mar the results[27]. In recent years it became more customary to use split tensile test for the measurement of the tensile strength. In this test the specimen cylinder is inserted to the compression machine in a horizontal position and loaded slowly until failure. Pads are inserted between the machine and the cylinder to ensure equal distribution of load.

The double punch test has been developed as an alternative to the split tensile test for the determination of the tensile strength of concrete and soil. Most of the time the tensile strength of these materials is assumed to be zero because it is a relatively small value when compared to the compressive strength and because of the lack of a satisfactory measuring technique.

In the double punch test, a vertical load is applied slowly through two steel disks centered on both top and bottom surfaces of a cylindrical sample until failure. Schematic diagrams of the double punch test can be seen in FIGURE 2.15.

It has been found that a height to diameter ratio of the specimen varying from 0.8 to 1.2 and a ratio of diameter of the specimen to the diameter of the steel disks varying from 0.2 to 0.3 are more suitable for this test. For convenience, the Proctor mold (4 by 4.6 in. (10.15 by 11.7 cm)) and CBR mold (6 by 6 in. (15.2 by 15.2 cm)) with 1 in. (2.54 cm) and 1.33 in. (3.4 cm) (CBR piston) disc respectively are recommended[26].

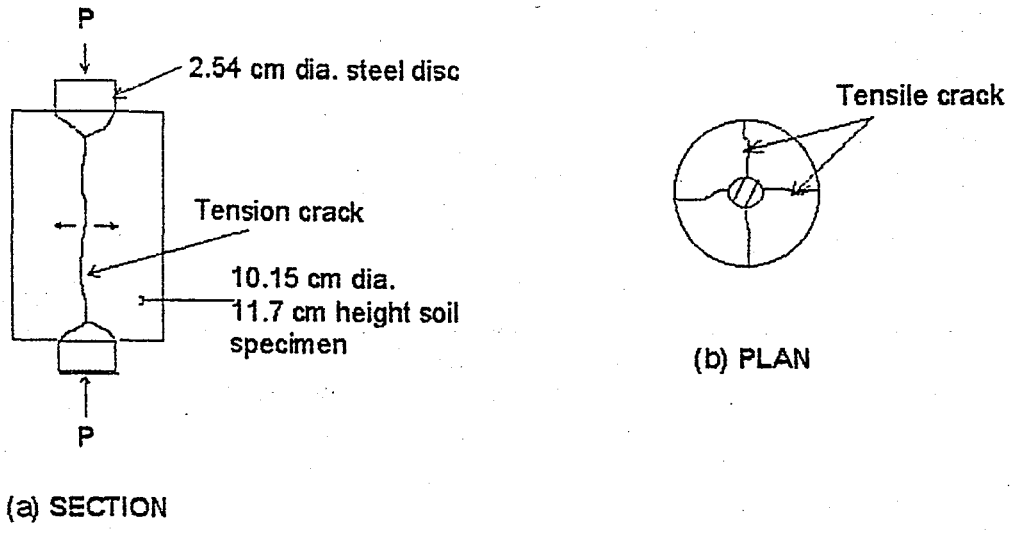

FIGURE 2.15. Schematic diagram of a double punch test[26].

The tensile strength of the specimen can be calculated by the theory of perfect plasticity. As a result of the analysis the formula stated below has been obtained for computing the tensile strength in a double punch test for all soils.

$$\sigma_t = \frac{P \cdot g}{\pi(1.0bH - a^2)} \qquad (2.11)$$

where σ_t = simple tensile strength, [kPa] or [psi],
P = applied load, [kg] or [lb],
g = acceleration due to gravity, 9.81 [m/sec^2],
b = radius of specimen, [m],
H = height of sample, [m],
a = radius of the steel disc, [m].

The double punch test is a simple, easy to perform method of measuring the tensile strength of concrete, soil and like materials. Samples compacted on the dry side of the optimum moisture content have displayed higher tensile strength (FIGURE 2.16) when tested with this method. Samples

of the same composition tested by double punch and splitting tension tests have yielded similar load-deflection curves and very close tensile strength values as can be seen in FIGURE 2.17 and FIGURE 2.18. In cases where cracking failure is significant, double punch test can easily be used for both laboratory and field construction control.

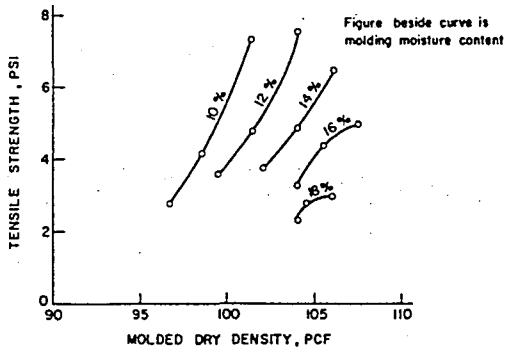

(1 psi = 7 kPa) (1 pcf = 16.04 kg/m^3)

FIGURE 2.16. Tensile strength versus molded dry density for various materials[26].

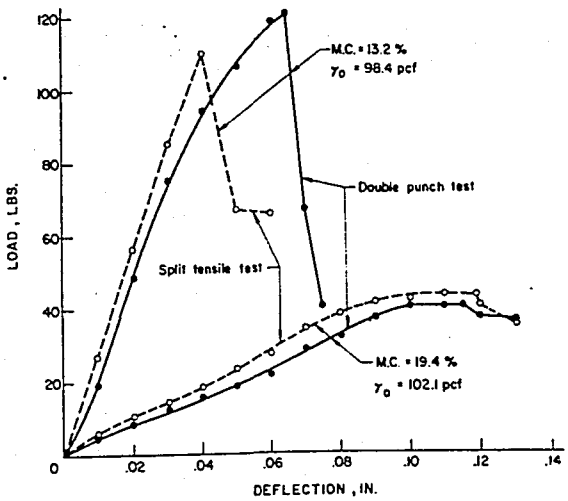

(1 lb = 0.455 kg) (1 in = 0.0254 m)

FIGURE 2.17. Load-deflection curves [26].

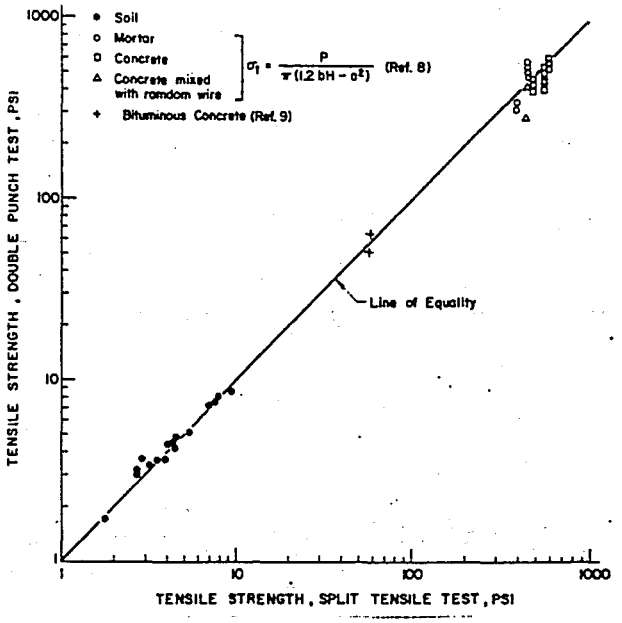

(1 psi = 7 kPa)

FIGURE 2.18. Comparison of tensile strength of various materials determined by double punch and split tensile test[26].

Double punch testing of the samples was carried on in the Boğaziçi University Structures Laboratory. The test set-up used for compressive loading was slightly modified and used for this test as well. The rate of loading could not be measured since a manually operated hydraulic jack was used for that purpose. The samples were molded in Standard Proctor molds with an average diameter of 10.16 cm and an average height of 11.65 cm as mentioned in Section 2.2.1 of this work. The diameters of the steel disks placed between the sample and the compression machine were 2.4 cm, which is within the specified ranges of 0.2 to 0.3 times the diameter of the sample. The load cell had a measuring capacity of 50 tons. Data were transmitted to the data logger connected to the load cell. Then they were transmitted to and recorded by the computer as data files. Data gathered were in the units of kilograms and had an accuracy range of +/- 200 kg.

The samples failed in two or three pieces with 120° to 180° angles in between. The tensile strength of the samples has been calculated using equation (2.11) from the maximum tensile loads. The averaged values of tensile strength for each sub-group are presented in TABLE 2.8 together with the average optimum water content and maximum dry density values. Comparison of the tensile strength variation between the sub-groups is presented in FIGURE 2.19. Tensile strength values for each of the samples are presented in TABLE G.1 through TABLE G.3 in APPENDIX G.

TABLE 2.8. Maximum tensile strength of fly ash, lime, rubber and ice mixtures determined by double punch testing.

	Per cent lime or rubber	Optimum water content, (%)	Maximum dry density, (KN/m^3)	Maximum tensile strength, (kPa)
CONTROL	1) -	17.85	11.89	928.9
	2) 10% lime	19.79	11.77	1242.5
	3) 20% lime	19.42	11.22	1043.5
	4) 30% lime	19.32	11.05	995.2
	5) 10% rubber	20.09	12.69	940.9
	6) 20% rubber	18.89	12.21	681.6
	7) 30% rubber	17.17	11.96	500.6
SPHERICAL ICE	1) -	27.77	11.39	946.9
	2) 10% lime	27.78	11.38	1435.5
	3) 20% lime	28.18	11.12	1308.9
	4) 30% lime	28.65	10.54	983.2
	5) 10% rubber	27.03	11.12	627.3
	6) 20% rubber	26.09	10.83	536.8
	7) 30% rubber	19.71	11.30	422.2

TABLE 2.8 continued.

	Per cent lime or rubber	Optimum water content, (%)	Maximum dry density, (KN/m^3)	Maximum tensile strength, (kPa)
CRUSHED ICE	1) -	23.62	12.47	1236.5
	2) 10% lime	27.48	11.47	1351.1
	3) 20% lime	28.04	11.57	1284.7
	4) 30% lime	29.06	11.21	1121.9
	5) 10% rubber	27.33	11.09	898.7
	6) 20% rubber	25.47	10.95	560.9
	7) 30% rubber	23.99	10.63	536.8

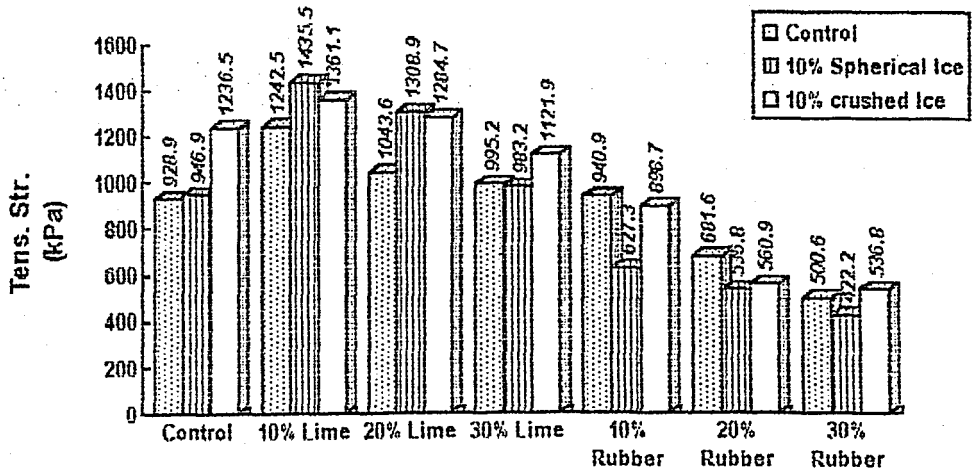

FIGURE 2.19. Variation of tensile strength with fly ash, lime, rubber and ice content.

3. DISCUSSION OF THE TEST RESULTS

- 3.1. Evaluation of the Ultrasonic Testing Results

The first evaluation of the samples have been made according to the sound velocity calculated from the wave transmission time. In TABLE 2.5 quality ratings for old concrete determined according to sound velocity criteria were given. According to this table samples made up of 20 per cent rubber and 80 per cent fly ash and 30 per cent rubber and 70 per cent fly ash by weight (with or without ice) are rated as bad quality. The rest of the samples belong to the poor to bad quality group. These samples may not be good in terms of load carrying capacity but they are certainly good noise isolators. Being a bad sound conductor can be an advantage if these mixtures can be used for noise isolation.

3.1.1. Comparison of Young's Modulus Values

The elasticity moduli (Young's Moduli) have been calculated from the data obtained by both destructive and non-destructive testing of the fly ash samples for the purpose of comparison. The moduli obtained from the ultrasonic testing are dynamic. The values from both of these methods are in the order of 10^3 MPa, but they still show some variations in magnitude. The comparison of these results are presented in FIGURE 3.1 through FIGURE 3.3.

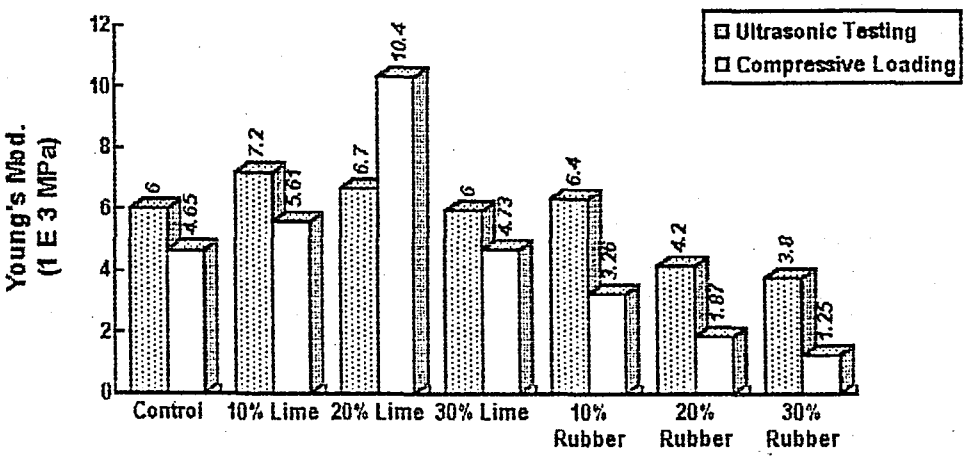

FIGURE 3.1. Variation of the Young's Modulus values determined by ultrasonic testing and compressive loading for samples without ice.

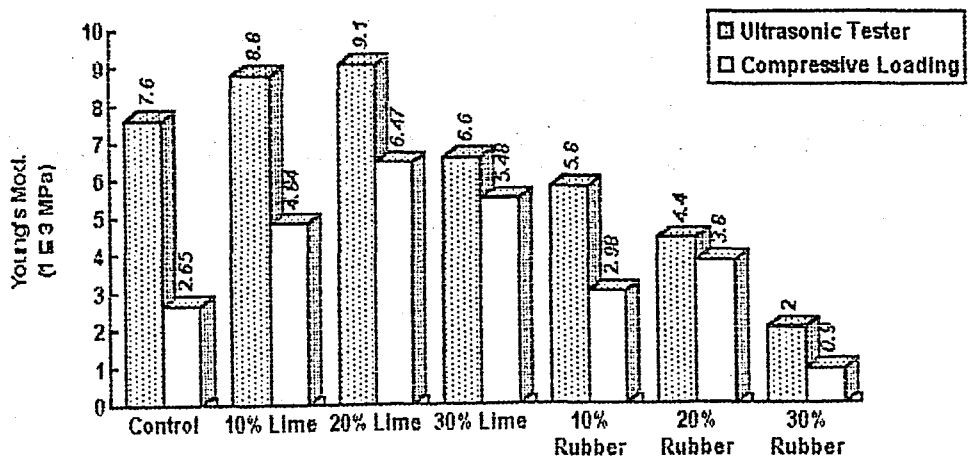

FIGURE 3.2. Variation of the Young's Modulus values determined by ultrasonic testing and compressive loading for samples with 10 per cent spherical ice.

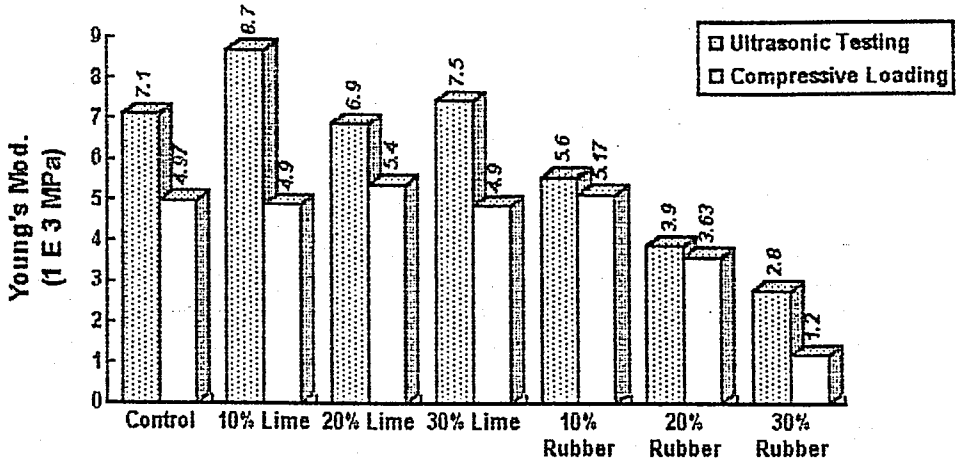

FIGURE 3.3. Variation of the Young's Modulus values determined by ultrasonic testing and compressive loading for samples with 10 per cent crushed ice.

As can be seen, ultrasonic testing has yielded larger Young's Modulus values for most of the mixtures. This is expectable, since it is known that the dynamic elasticity moduli are greater than the ones obtained by static loading by a factor of 1.5 to two. So it can be said that the results from ultrasonic testing are useful for providing a general idea about the magnitude of the Young's Modulus without destroying the sample.

3.2. Evaluation of the Compressive Loading Test

The variations of the Young's Modulus, maximum compressive strength and energy absorbing capacity due to per cent added ice are given in FIGURE 2.12 through FIGURE 2.14 of this work.

In general, high Young's Modulus values are indications of high stress and low strain and a steep slope of the stress-strain curve in the elastic range. If FIGURE 2.12 is examined it can be seen that, adding up to 20 per

cent by weight lime has increased the Young's Modulus values. Samples with 30 per cent lime by weight and all of the samples with rubber have lower modulus values than those with no lime or rubber. Adding 10 per cent by weight spherical ice has increased Young's Modulus in all samples with lime and decreased it in the rest. Young's Moduli of samples with crushed ice have decreased in samples with 20 and 30 per cent rubber and remained approximately the same or slightly increased in the rest of the samples. The highest modulus value of the 21 subgroups has been obtained from samples with 20 per cent by weight lime and no ice.

From FIGURE 2.13 it can be seen that samples with lime have increased and samples with rubber have decreased maximum compressive strengths when compared with samples of 100 per cent fly ash. The greatest increase without adding ice has been obtained in samples with 10 and 20 per cent lime. Adding crushed ice has generally improved the compressive strength more than adding spherical ice. The additional 10 per cent spherical ice has increased the compressive strength in samples of 100 per cent fly ash and samples with 20 and 30 per cent lime but decreased it in the rest. 10 per cent crushed ice has increased the compressive strength in all samples except those with 20 per cent lime. Maximum compressive strength has been obtained in samples made up of 10 per cent lime, 90 per cent fly ash by weight with 10 per cent additional crushed ice. Usually, it is not expected to have higher compressive strengths in samples with holes or cracks, when they are compared with samples of the same composition without cracks. This increase in the compressive strength must be due to the additional water for the hydratation reaction introduced in the samples by adding ice. As a conclusion, it can be said that adding lime has been beneficial and that maximum compressive strength can be increased in all samples if crushed ice is added.

If FIGURE 2.14 is examined, it can be seen that the energy absorbing capacity of samples without ice has greatly

increased in 10 and 20 per cent lime samples, has increased in 10 to 30 per cent rubber samples but has decreased in 30 per cent lime samples. Adding spherical ice has increased the energy absorbing capacity of 100 per cent fly ash, 20 per cent lime and 20 to 30 per cent rubber samples. Adding crushed ice has increased this capacity in 100 per cent fly ash and 30 per cent lime samples. In general it can be stated that the samples with lime have greater energy absorbing capacities than samples with rubber even though the former fails in more brittle and the latter in more ductile mode. The reason to this phenomenon is that the maximum compressive strengths of samples with lime are approximately 10 times those with rubber. Adding spherical ice has been more beneficial than adding crushed ice in terms of energy absorbing capacity. The reason might be the effect of the voids, acting as air cushions, introduced in the samples after the thawing of the spherical ice particles.

3.3. Evaluation of the Double Punch Test Results

The variation of the tensile strength determined by double punch test had been presented in FIGURE 2.19. The tensile strength of samples without ice has increased in samples with 10 to 30 per cent lime and with 10 per cent rubber. The maximum increase is seen in samples with 10 per cent lime. Adding 10 per cent spherical ice has increased the tensile strength of samples with 10 and 20 per cent lime and samples made up of 100 per cent fly ash. In the rest of the samples, the tensile strength has decreased with added spherical ice. Adding 10 per cent crushed ice has increased the tensile strength in 100 per cent fly ash, 10 to 30 per cent lime and 30 per cent rubber samples. In general spherical ice has improved the tensile strength in greater magnitude than crushed ice in samples with lime. The tensile strength of samples with lime are approximately twice that of samples with rubber. Adding up to 20 per cent lime and

spherical or crushed ice is beneficial in terms of increasing tensile strength. The best results have been obtained from samples with 10 per cent lime.

3.4. Utilization as Traffic Barriers

The variation of the compressive and tensile strengths and energy absorbing capacities of fly ash, lime, rubber and ice mixtures has been investigated to determine whether they can be used as traffic barriers has been investigated.

3.4.1. Utilization as Longitudinal Barriers

As stated before, longitudinal barriers can be constructed from steel wires or profiles and from precast concrete elements. It was proposed to construct the precast elements from fly ash mixtures instead of concrete. There are certain specifications that have to be followed in terms of shape and strength of such elements. According to the Technical Specifications of Highways[28] published by the General Directorate of Turkish Highways, BS 25 quality (as designated by TS 500[29]) concrete should be used in the production of precast concrete elements. The BS 25 concrete is characterized by a cylindrical compressive strength of 25 N/mm^2 (25 MPa) and a tensile strength of 1.8 N/mm^2 (1.8 MPa). The maximum compressive strength obtained from the material under consideration is 13.4 MPa (from samples made up of 10 per cent lime and 90 per cent fly ash, with 10 per cent crushed ice added) and the maximum tensile strength is 1.44 MPa (from samples made up of 10 per cent lime and 90 per cent fly ash, with 10 per cent spherical ice added). So it can be stated that this material can not be used in longitudinal barrier construction.

The state of stress on a longitudinal barrier during an impact is not purely compressive. Bending moments are also involved. If a stronger material can be produced using fly ash mixtures, it might be a good idea to perform bending tests as well as compressive and tensile loading tests on it before recommending it as eligible for longitudinal barrier construction.

3.4.2. Utilization as Crash Cushions

Crash cushions can be made up of different materials (TABLE 1.8) such as steel drums, water cells, sand containers, lightweight cellular concrete cylinders etc. It is also possible to make cylinders from fly ash mixtures and build crash cushion systems out of them.

Work-energy approach described in Section 1.3.3.2 may be used to design such a system in case of head-on impact. A detailed example solved using this approach has been presented in APPENDIX A. If it is proposed to construct cellular cylinders 60 cm in diameter and one meter in height out of this material, the volume of such cylinders is calculated to be equal to 0.28 m^3. If an energy absorbing capacity (energy consumption to completely crush the cylinder) of 100 kJ/m^3 is obtained for a specimen, the energy absorbing capacity of 0.28 m^3 of the same material can be calculated as,

$$100\ kJ/m^3 * 0.28\ m^3 = 28\ kJ\ (kN\text{-}m).$$

A dynamic force is required to crush this cylinder from its original 0.6 m diameter to a diameter of 0.05 meters. This force can be calculated from equation (1.8). The

total crash-cushion deformation d is equal to (0.6m - 0m = 0.6m). The dynamic force F is equal to,

$$U = 28 \text{ kN-m} = F*d = F*(0.6 \text{ m})$$
$$F = 47 \text{ kN}.$$

The kinetic energy of a 1000 kg car traveling at 100 km/h (28m/sec) can be determined from equation (1.2) as,

$$KE = Wv^2/2g = 392000 \text{ J} = 392 \text{ kJ}.$$

The minimum number of barrels necessary to stop this car is,

$$N_b = 392/28 = 14 \text{ barrels}.$$

These cylinders should be arranged in such a way that the maximum permissible deceleration level of 12 g's is not exceeded. The 16 cylinder nest configuration shown in FIGURE 3.4 can be used for this purpose. The barrier stopping force is dependent on the number of cylinders in a row. By equating the kinetic energy, KE, to the area under the vehicle penetration- barrier stopping force curve, the stopping distance after impact (D) can be calculated.

$$KE= 392 = (47)(0.6) + (2)(47)(1.8) + (3)(47)(0.6)(x)$$
$$x = 2.3 \text{ m (number of rows to stop this car)}$$
$$D = 0.6 + 1.8 + (0.6)(2.3) = 3.78.$$

Placing this D value in equation (1.6), the average deceleration level in [g] units can be calculated as,

$$G_A = v^2/(2gD) = 28^2/2(9.81)(3.78) = 10.57 \text{ g} < 12 \text{ g}.$$

As can be seen, the design is acceptable. This procedure has been used in the calculation of the number of fly ash cylinders, vehicle stopping distance and average deceleration levels for crash-cushion nests constructed from

the 21 different mixtures taken into consideration in this work. The design has been carried on for a vehicle speed of 100 km/hr and a vehicle weight of 1000 kg. The results obtained are submitted in TABLE 3.1 through TABLE 3.3.

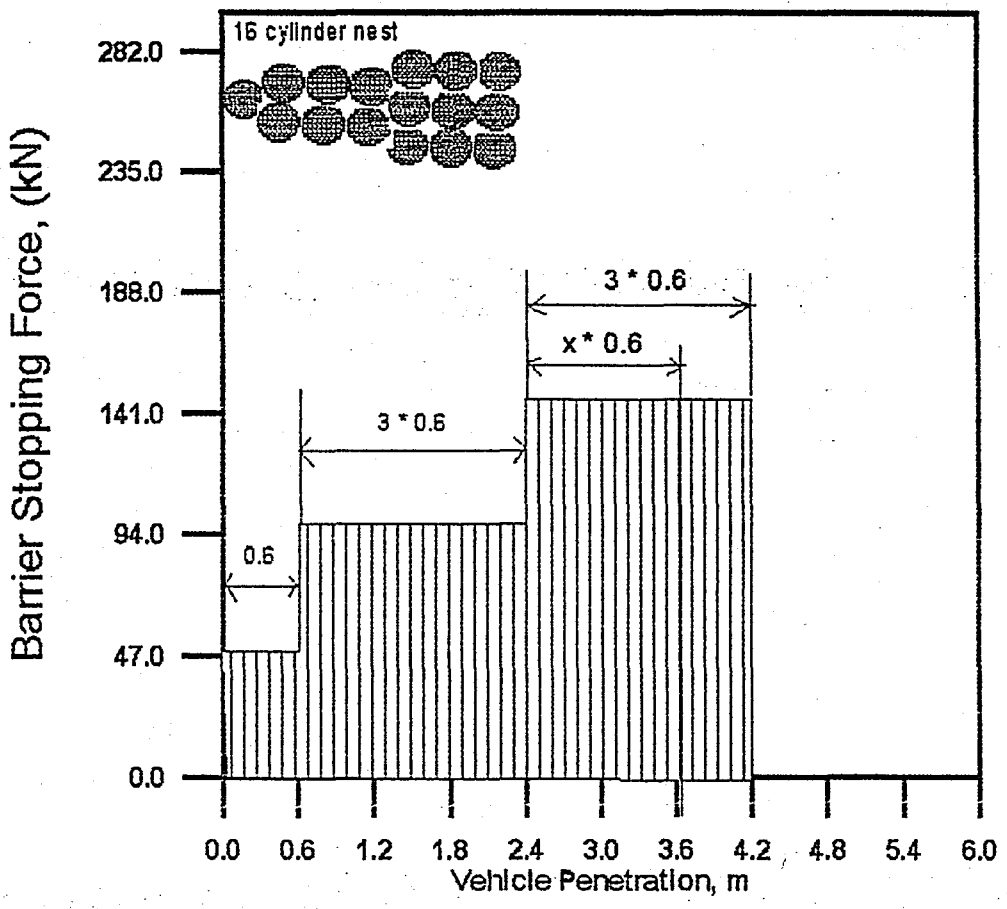

FIGURE 3.4. Analysis of crash-cushion system with 16 cylinders.

Cylinder nests made up of material with very high energy absorbing capacities (such as the ones made up of 20 per cent lime by weight with 10 per cent spherical ice added) may have deceleration levels above the maximum permissible deceleration level (12 g's). Using these barriers could cause fatalities among the passengers of an impacting vehicle. It is better to use a different design or a less energy absorbent material in such cases. It is better to use a material with medium energy absorbing capacity for safety and

economy. If judged in this way, elements made up of fly ash mixtures containing rubber are more advantageous.

TABLE 3.1. Design of crash-cushions constructed using cylindrical nests made up of fly ash mixtures with no ice.

						Crash Cushion Definition		
Per Cent Lime or Rubber	Energy Ab. Cap. (kJ)*	Min. No. of Cylinders needed	Dynamic Force (kN)	Stopping Dist.-D (m)	G_A (g)	No. of Cylinders used	No. Cylinders in a row	No. of Rows
1) -	9.6	41	16.02	7.17	5.57	41	1 2 3 4	1 3 6 4
2) 10% Lime	45.3	9	75.54	3.79	10.5	10	1 2	4 3
3) 20% Lime	57.6	7	96.0	3.54	11.3	7	1 2	5 1
4) 30% Lime	9.3	43	15.5	8.56	4.67	45	1 2 3 4	1 3 6 5
5) 10% Rubber	25.3	16	42.16	4.1	9.74	16	1 2 3	1 3 3
6) 20% Rubber	15.75	25	26.25	5.97	6.69	25	1 2 3	1 3 6
7) 30% Rubber	19.4	21	32.38	5.04	7.93	22	1 2 3	1 3 5

* Energy absorbing capacity of cylinders with 0.28 m^3 volume.

TABLE 3.2. Design of crash-cushions constructed using cylindrical nests made up of fly ash mixtures with spherical ice.

						Crash Cushion Definition		
Per Cent Lime or Rubber	Energy Ab. Cap. (kJ)*	Min. No. of Cylinders needed	Dynamic Force (kN)	Stopping Dist.-D (m)	G_A (g)	No. of Cylinders used	No. Cylinders in a row	No. of Rows
1) -	15.16	26	25.26	6.13	6.52	29	1 2 3 4	1 3 6 1
2) 10% Lime	8.16	49	13.6	9.43	4.24	49	1 2 3 4	1 3 6 6
3) 20% Lime	95.5	5	159.1	2.46	16.2 not OK.	5	1	5
4) 30% Lime	6.9	57	11.46	10.8	3.7	57	1 2 3 4	1 3 6 8
5) 10% Rubber	17.92	22	29.86	5.38	7.43	22	1 2 3	1 3 5
6) 20% Rubber	19.4	21	32.33	5.04	7.93	22	1 2 3	1 3 5
7) 30% Rubber	36.0	11	60.0	4.17	9.58	11	1 2	3 4

* Energy absorbing capacity of cylinders with 0.28 m^3 volume.

TABLE 3.3. Design of crash-cushions constructed using cylindrical nests made up of fly ash mixtures with crushed ice.

						Crash Cushion Definition		
Per Cent Lime or Rubber	Energy Ab. Cap. (kJ)*	Min. No. of Cylinders needed	Dynamic Force (kN)	Stopping Dist.-D (m)	G_A (g)	No. of Cylinders used	No. Cylinders in a row	No. of Rows
1) -	22.54	18	37.57	4.48	8.93	19	1 2 3	1 3 4
2) 10% Lime	16.67	24	27.8	5.7	7.01	25	1 2 3	1 3 6
3) 20% Lime	29.75	14	49.6	3.63	11.0	16	1 2 3	1 3 3
4) 30% Lime	57.3	7	95.46	3.55	11.3	7	1 2	5 1
5) 10% Rubber	15.9	25	29.5	5.43	7.36	25	1 2 3	1 3 6
6) 20% Rubber	13.32	30	22.2	7.31	5.47	33	1 2 3 4	1 3 6 2
7) 30% Rubber	17.6	23	29.3	5.46	7.32	25	1 2 3	1 3 6

* Energy absorbing capacity of cylinders with 0.28 m^3 volume.

4. CONCLUSIONS AND RECOMMENDATIONS

Compressive and tensile strength and energy absorbing capacities of fly ash, lime, rubber and ice mixtures have been investigated in this work. Rubber and lime has been used to improve the mechanical properties mentioned above. Ice has been used to provide additional water for the pozzolanic reaction after the compaction of the samples and to introduce air voids to increase energy absorbing capacity.

The variations in elasticity moduli have been determined using ultrasonic testing and statical loading. The dynamic elasticity moduli obtained from ultrasonic testing is greater than the elasticity moduli calculated from the slopes of the stress-strain curves by a factor varying between 1.27 and 3.04 in samples without ice. In samples with spherical ice this factor varies between 1.2 and 2.87. A factor varying between 1.07 and 2.33 is obtained in samples with crushed ice. These factors are not very different from the expected variation factors of 1.5 to two. Errors due to bad contact between specimen and probe surfaces or a noisy environment might have occurred in ultrasonic readings. Ultrasonic testing is still a recommendable method of determining the dynamic elasticity moduli.

Young's Modulus is maximum in samples with 20 per cent lime and no ice. The modulus has increased by a factor of 2.24 in such samples. This is expectable since samples with lime have high compressive strength and low strain values in the elastic range. In other samples the variation is not that obvious. Adding spherical ice has increased the moduli values by a factor varying between 1.04 and 1.4. It is recommended to add lime up to 20 per cent by weight and spherical ice to increase the Young's Modulus.

The compressive strength of samples with 10 per cent lime and crushed ice have increased by a factor of 2.64. This is the maximum increase in compressive strength. The compressive strength has increased by a maximum factor of 1.77 in samples with lime but no ice. Adding lime and spherical ice has increased the compressive strength by a maximum factor of 2.03. It is recommended to add lime and ice, preferably crushed ice to increase the compressive strength. This unexpected increase in the compressive strength after the addition of crushed ice, which is introducing some voids and imperfections in the samples, must be due to the additional water provided for the hydratation reaction. Adding rubber does not improve the compressive strength, as expected.

The energy absorbing capacities of samples have increased by a factor of six at maximum by adding lime. This factor has increased up to 9.94 in samples with 20 per cent lime and spherical ice. It seems that the variation in energy absorbing capacity tends to follow a more random distribution. Samples with spherical ice have higher energy absorbing capacities since the voids left after the thawing of ice act as air cushions during loading. Samples with lime tend to have greater energy absorbing capacities, since they have higher compressive strength values.

Energy absorbing capacity calculations have been carried on by assuming that the samples are free of any pores or cracks. But in reality, pores have been introduced to the samples intentionally. For this reason, the values obtained are not the real values. But they provide a basis of comparison between samples of different compositions. Using these values, it is possible to find the additive that has been more beneficial than the others.

Energy absorbing capacities have been determined by statical loading and crash cushion design has been carried on using these values even though the formulas used were

developed for dynamic loading conditions. In reality the behavior of a material under dynamic loads (i.e. impact) is very different. Due to the limitations of the laboratories, the samples could not be tested under dynamic loads. A mixture that proves inefficient under static loads can prove to be very successful under dynamic loads. In the future, dynamic loading tests should be performed on these mixtures for more accurate results.

The tensile strength of samples with 10 per cent lime and spherical ice has increased by a maximum factor of 1.55. In samples with lime the tensile strength has increased more with added spherical ice. The tensile strength has not improved with added ice in samples with rubber. When compared with other mechanical properties, the tensile strength of samples with rubber is closer in magnitude to the tensile strength of samples with lime. There was a larger gap in the magnitude of the other properties in samples with lime and rubber. In general, it can be recommended to add lime and ice, especially spherical ice to increase the tensile strength.

For more dependable compressive and tensile strengths and energy absorbing capacities, the exact shape, distribution and volume fraction of the pores introduced by adding ice should be determined. In this way, similar samples can be produced and the analysis of the test results can be carried out with higher accuracy.

This work has involved the utilization of two waste products, namely fly ash and rubber, which are otherwise pollutants. Being able to use these materials in production offers a solution to some environmental problems and earns economical value to these wastes.

The materials obtained can be used in crash cushion construction. If it is decided to use the material in crash cushion construction, full scale vehicular crash testing

should be performed to determine behavior under dynamic loading conditions. Freeze-thaw tests should be performed as well, to determine the effects of environmental changes on the samples. The compressive strength of the materials is not high enough for use as a structural member, but since they have air voids and don't transmit sound waves very easily, they can be used for sound insulation in precast form as well.

APPENDIX A. DESIGN EXAMPLES FOR CRASH CUSHIONS

A.1. Design Using Work-Energy Principle

A crash cushion device is to be placed at an elevated gore to safely decelerate 2000(910) to 4500(2050) lb(kg) vehicles traveling at 60 mph (=88 ft/sec = 97 km/h). A 20-gauge, 55-gal (208 lt.) steel barrel with a seven inch (18 cm) hole in the center of each end is the basic element. Laboratory studies have indicated that a dynamic force of 9000 lb (4090 kg) is required to crush one barrel from its original two feet (61 cm) diameter to approximately 0.5 feet (15 cm). Determine the number and the arrangement of barrels that will fulfill these criteria.

F = dynamic force = 9000 lb (4090 kg)
d = reduction in barrel diameter = 2 - 0.5 = 1.5 ft (46 cm)
e_d = the dynamic energy consumption of one barrel = U (work done by the barrel)
e_d = F*d (eq.(1.8)) = 9000 * 1.5 = 13500 ft-lb (1873.46 kg-m)
KE = the kinetic energy of the vehicles = $Wv^2/2g$ (eq.(1.2))
for W = 2000 lb,

$$KE = (2000*88^2)/(2*32.2) = 240496 \text{ ft-lb}(33000 \text{ kg-m})$$

for W = 4500 lb,

$$KE = (4500*88^2)/(2*32.2) = 541118 \text{ ft-lb}(74250 \text{ kg-m}).$$

Minimum number of barrels (N_b) required:
for W = 2000 lb $N_b = KE/e_d = 40.08 = 40$ barrels,
for W = 4500 lb $N_b = 17.8 = 18$ barrels.

These barrels should be arranged to achieve an acceptable deceleration level. As mentioned in Section 1.3.3.2 of this work, the maximum permissible deceleration level is 12 g's, averaged over the entire stopping distance. There are certain barrel nest configurations that can be used in design, such as the one shown in FIGURE A.1 referred to as

system C1. The barrier stopping force is a stepped function corresponding to the number of barrels in a row. Vehicle penetration into the crash cushion is determined by equating vehicle impact kinetic energy to the area under the curve in FIGURE A.1 and bound by the unknown vehicle penetration abscissa.

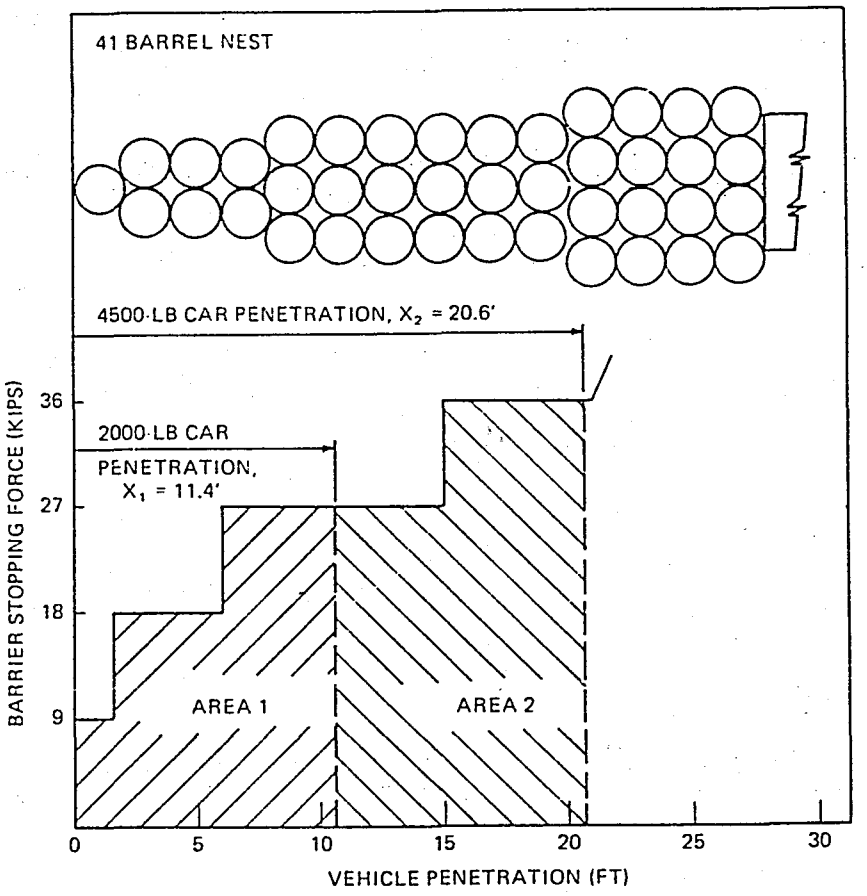

FIGURE A.1. Analysis of crash cushion system C1.

The general formula is,

$$U = \int_0^d F_x \cdot dx = \sum_{\substack{\text{cushion} \\ \text{segments}}}^{n} a_i \cdot f_d \cdot b_i \qquad (A.1)$$

where,

a_i = number of barrels in the width of the crush cushion segment

f_d = average dynamic crushing force of a single barrel

b_i = cushion segment deformation.

for W = 2000 lb (910 kg) (Using equation (A.1) and FIGURE A.1)

$$240496 \text{ ft-lb} = (1)(9000)(1.5) + (2)(9000)(6-1.5) + (3)(9000)(X_1-6)$$

X_1 = 11.41 ft (3.5 m) from impact with barrier

for W = 4500 lb (2050 kg)

$$541118 \text{ ft-lb} = 240496 + (3)(9000)(15-11.4) + (4)(9)(X_2-15)$$

X_2 = 20.6 ft (6.3 m) from impact with barrier

The average deceleration level for each vehicle impact on the proposed barrier configuration is calculated to ensure compliance using equation (1.6).

for the 2000 lb vehicle,

$$G_a = V^2/(2gX_i) = (88)^2/2(32.2)(11.4) = 10.5g < 12g$$

for the 4500 lb vehicle,

$$G_a = (88)^2/2(32.2)(20.6) = 5.8g < 12g$$

A.2. Linear Impulse-Momentum Analysis

A C3-type (FIGURE 1.10) crash cushion is to be placed at an elevated gore to safely decelerate a 2000 lb (910 kg) and a 4500 lb (2050 kg) car impacting at 60 mph (97 km/h).

A vehicle deceleration of 5g's is selected. Also, inertial barrier modules of 3-ft (0.91 m) diameter will be used, maximum module weight is 1400 lb (636 kg).

(a) Length of inertia part : Solving equation (1.6) for x_i (FIGURE 1.10),

$x_i = V^2/2gG_a = 88^2/2(32.2)(5) = 24$ ft (7.3 m), or about eight modules long.

(b) Determine s_f from equation (1.19)

$s_f = (4500/32.2)/[2(1400)/32.2] = 1.61$ module diameters.

(c) Determine modules weights from equation (1.20)

weights = [1400] * (1.61/(1.61+0,1,2,3,4,5,6,7))
= 1400, 865, 625, 490, 400, 340, 295, 261 lb.
= 636, 393, 284, 222, 182, 154, 134, 118 kg.

(d) Bulldozing phase, x_B: Five tons of sand can be provided by four 1400 lb (636 kg) modules and two 2100 lb (953 kg) modules.

APPENDIX B. DRY UNIT WEIGHT-MOISTURE CONTENT CURVES

Moisture content-dry unit weight curves for 100 per cent fly ash, 90 per cent fly ash and 10 per cent lime, 80 per cent fly ash and 20 per cent lime, 70 per cent fly ash and 30 per cent lime, 90 per cent fly ash and 10 per cent rubber, 80 per cent fly ash and 20 per cent rubber and 70 per cent fly ash and 30 per cent rubber by weight are presented in the following pages. For optimum moisture content and maximum dry unit weight values refer to TABLE 2.4.

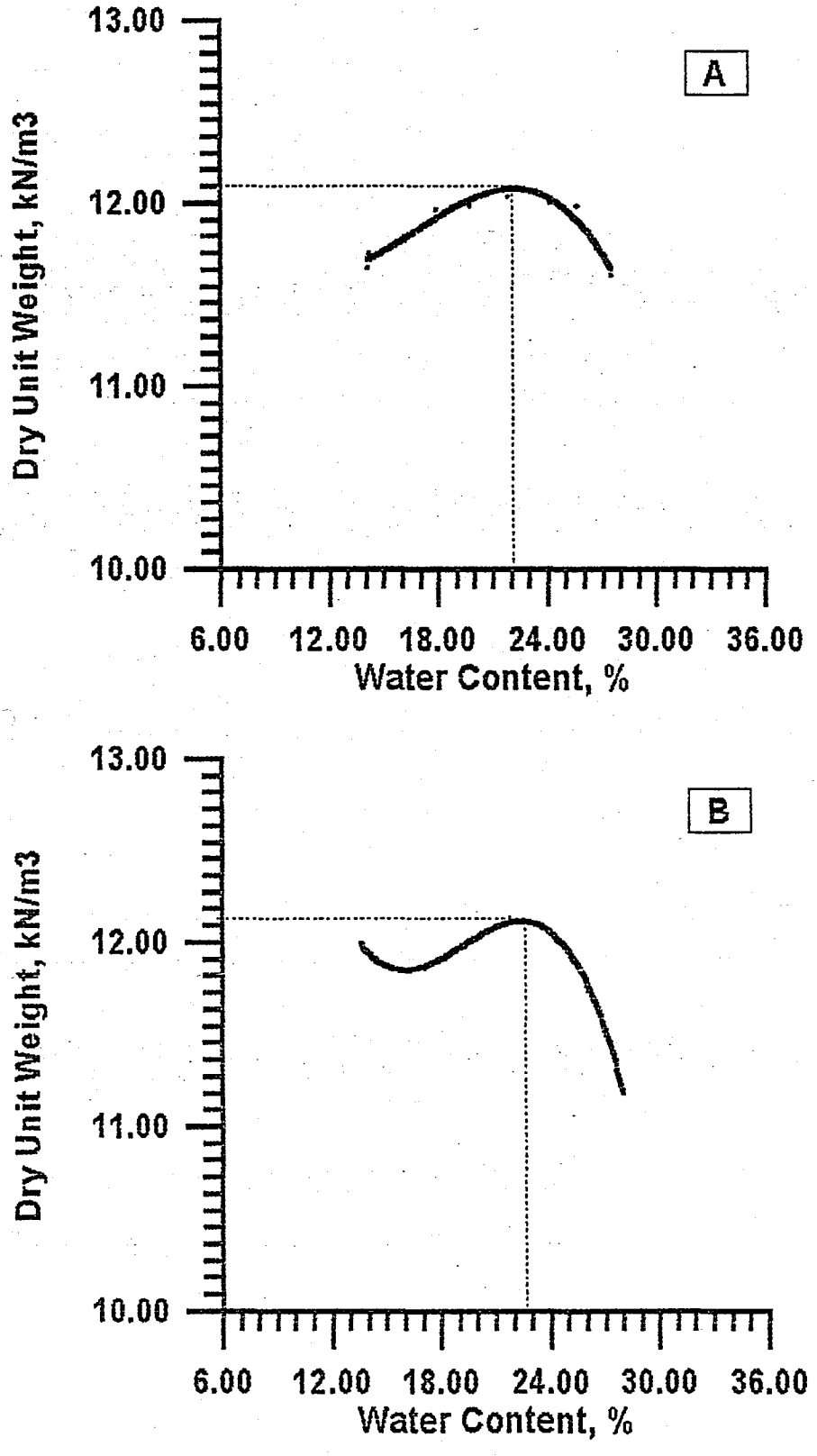

FIGURE B.1. Water content-dry unit weight curves for 100 per cent fly ash.

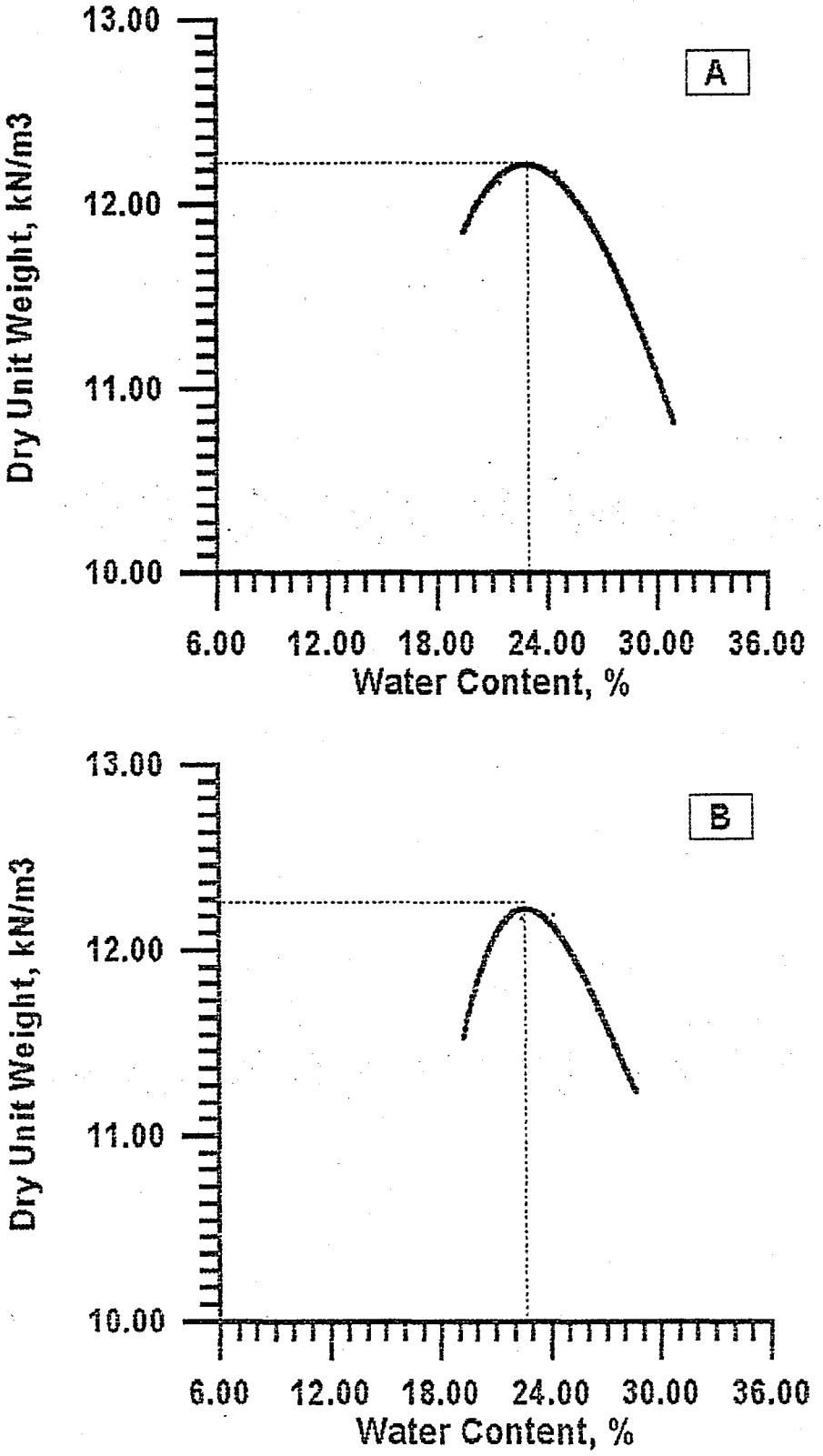

FIGURE B.2. Water content-dry unit weight curves for 90 per cent fly ash and 10 per cent lime by weight.

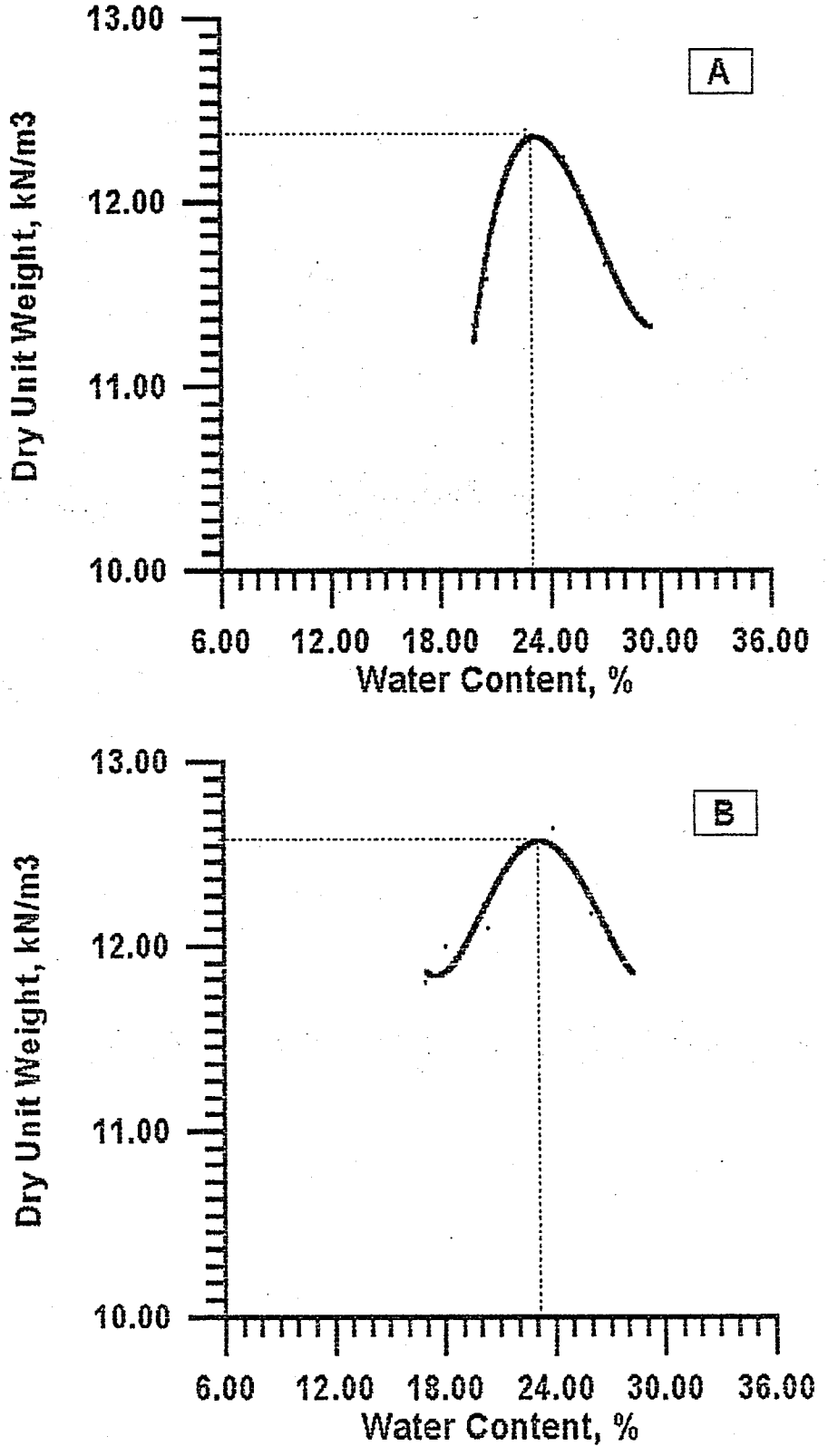

FIGURE B.3. Water content-dry unit weight curves for 80 per cent fly ash and 20 per cent lime by weight.

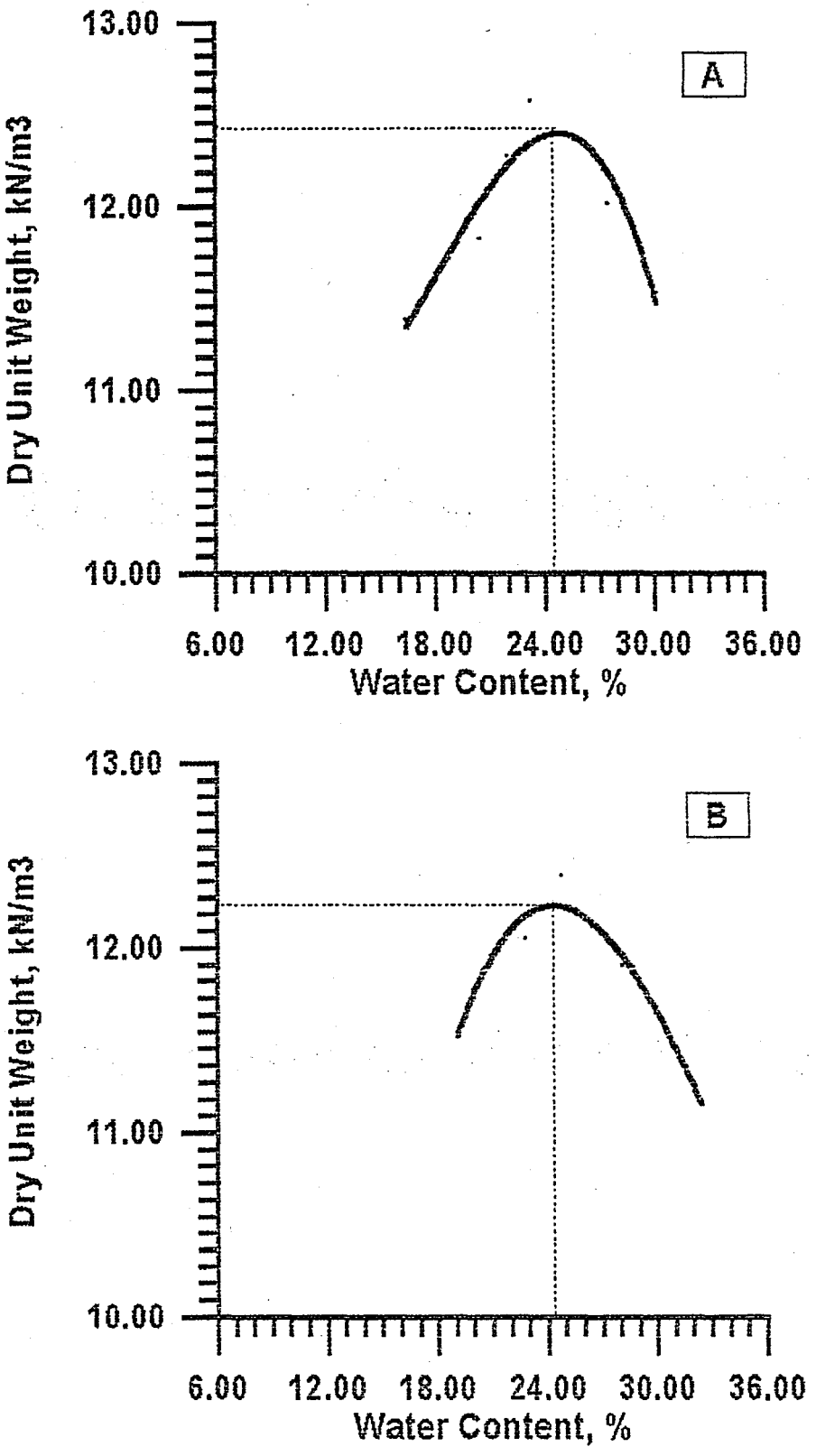

FIGURE B.4. Water content-dry unit weight curves for 70 per cent fly ash and 30 per cent lime by weight.

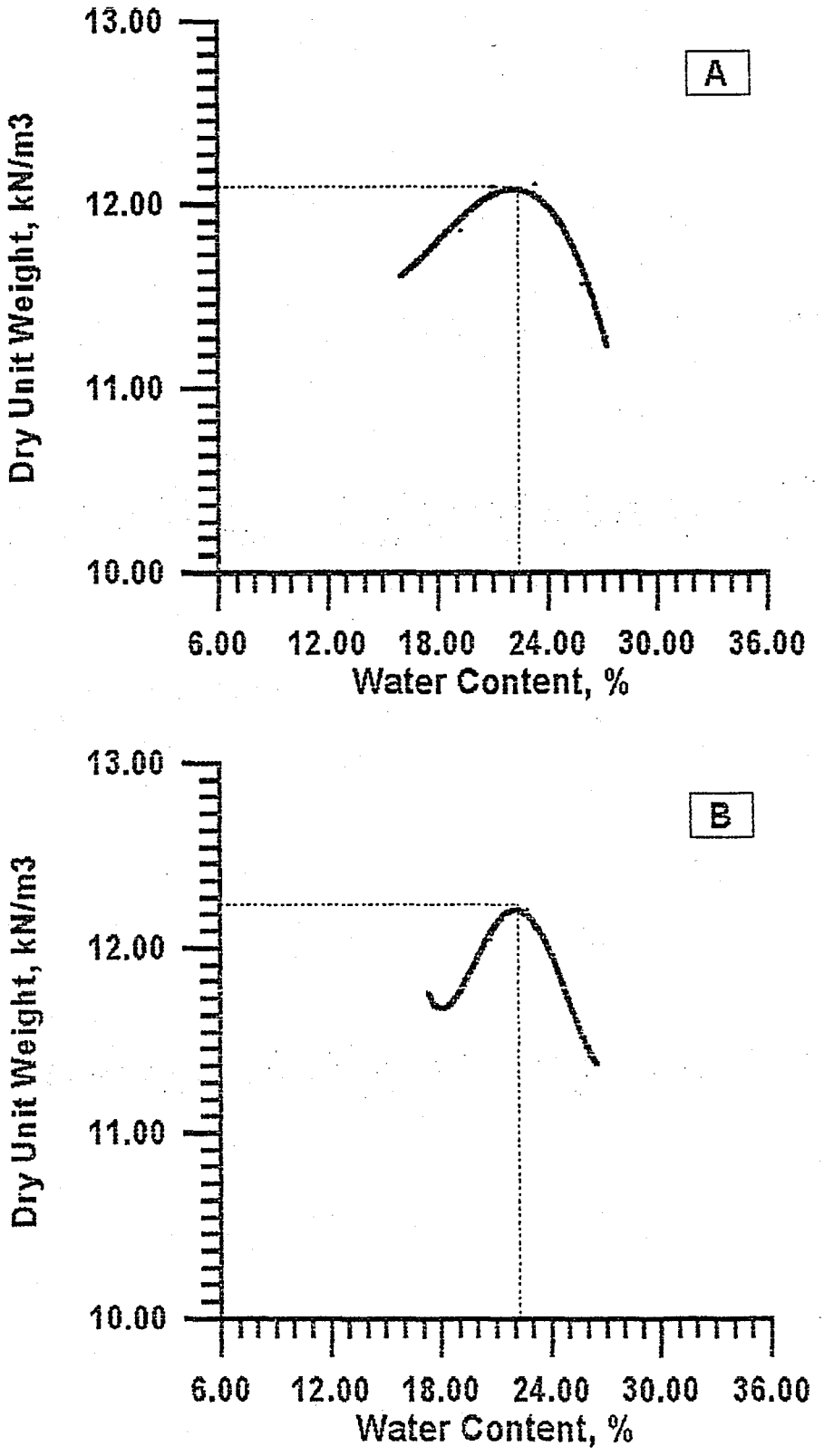

FIGURE B.5. Water content-dry unit weight curves for 90 per cent fly ash and 10 per cent rubber by weight.

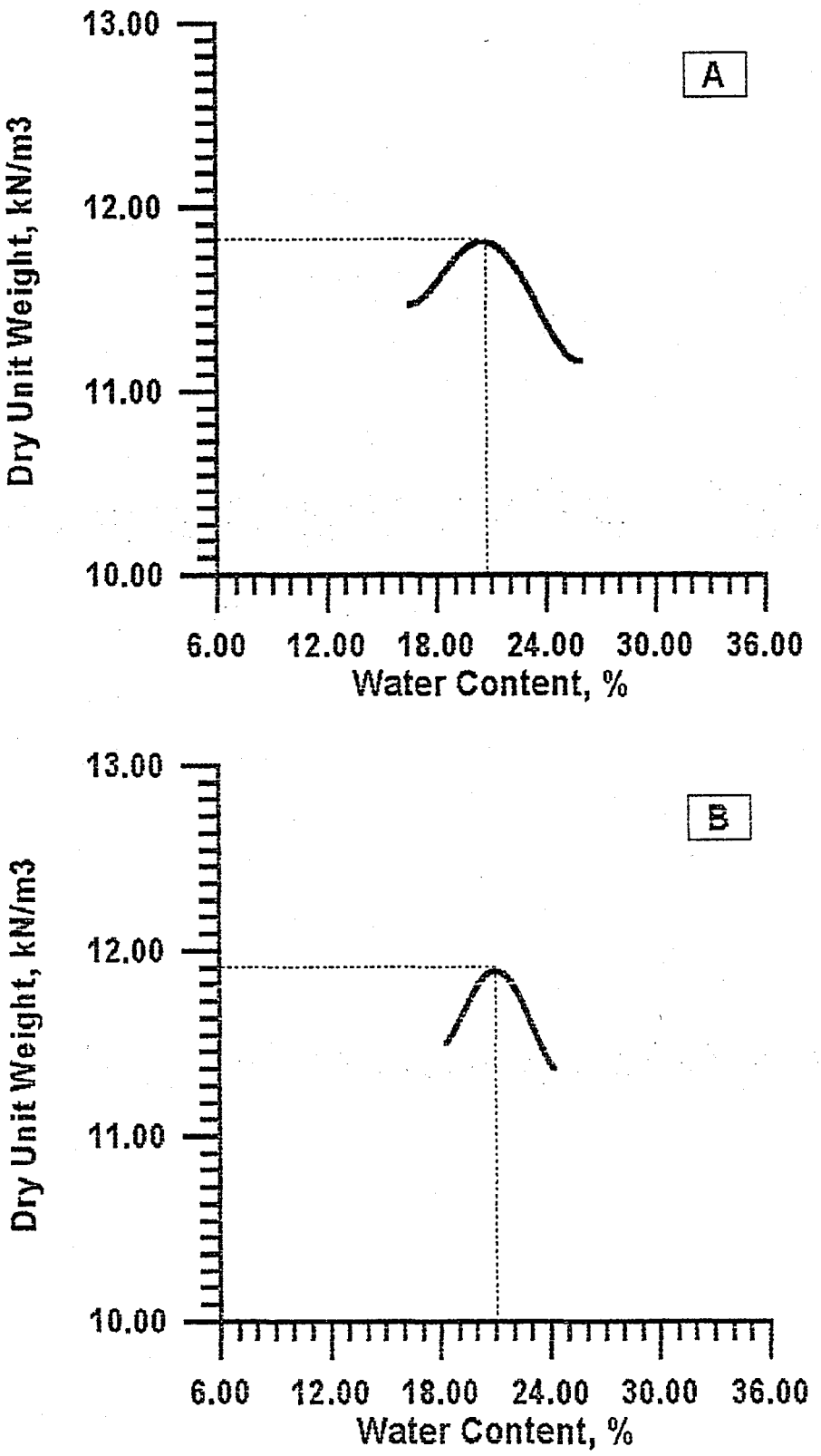

FIGURE B.6. Water content-dry unit weight curves for 80 per cent fly ash and 20 per cent rubber by weight.

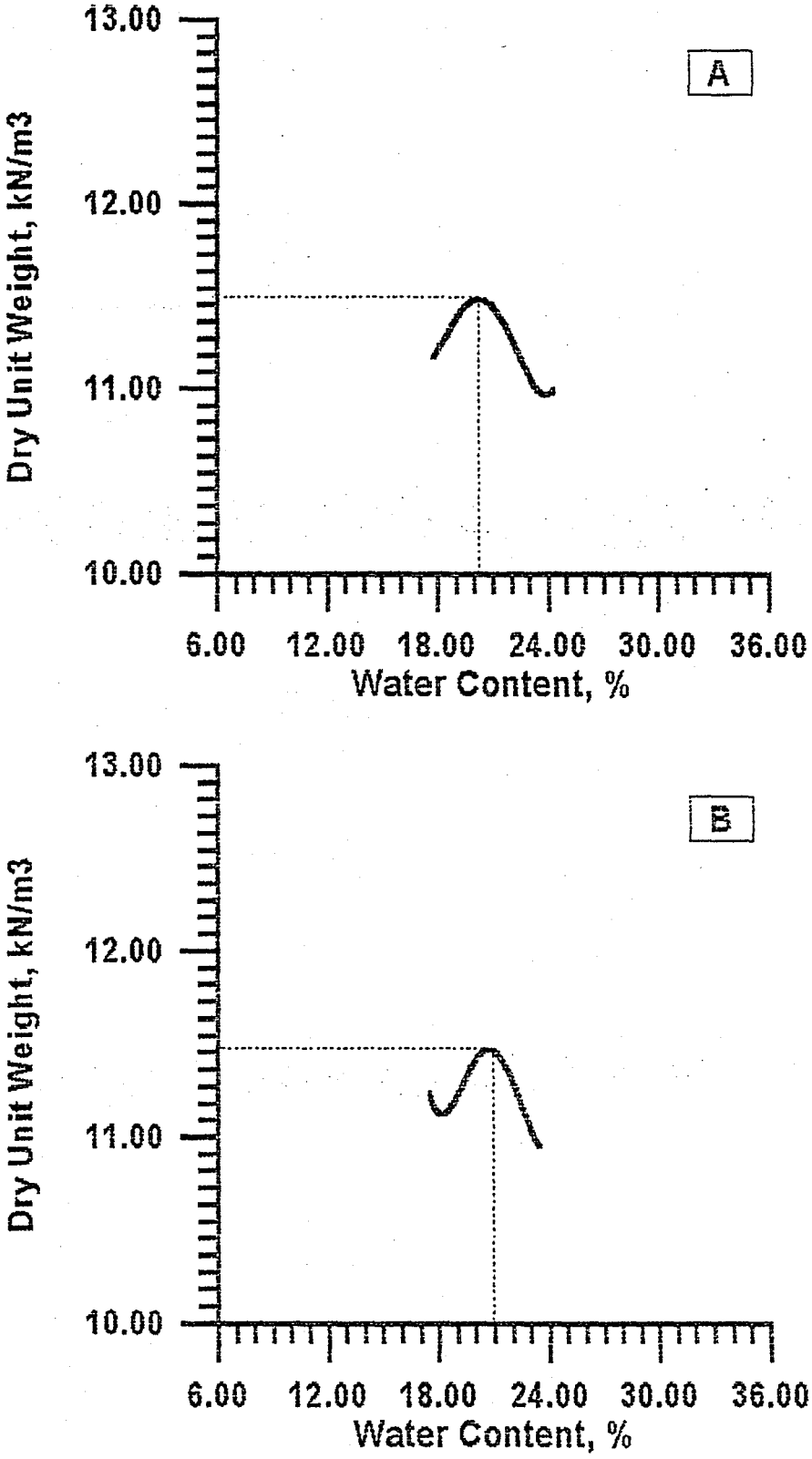

FIGURE B.7. Water content-dry unit weight curves for 70 per cent fly ash and 30 per cent rubber by weight.

APPENDIX C. SAMPLE CURING CONDITIONS

TABLE C.1. Curing conditions data.

DATE	TEMPERATURE (°C)	RELATIVE HUMIDITY OF THE CURING ROOM (%)
5.4.1994 [a]	15	70
6.4.1994	16	71
7.4.1994	16.3	74
8.4.1994	16.5	76.5
9.4.1994	16.3	73
10.4.1994	16.8	72
11.4.1994	16.8	73
12.4.1994	16.5	74
13.4.1994	16.6	73
14.4.1994	16.6	73
15.4.1994	16.7	73
16.4.1994 [b]	16.6	73
17.4.1994	16.8	72
18.4.1994	16.9	72
19.4.1994	16.8	73
20.4.1994	17	72
21.4.1994	17	72
22.4.1994	16.9	72
23.4.1994	16.8	72
24.4.1994	16.8	73
25.4.1994	16.5	73
26.4.1994	16.5	74
27.4.1994	16.5	73
28.4.1994	16.5	74
29.4.1994	16.5	74
30.4.1994	25	60
1.5.1994	26	55
2.5.1994	26.3	55

TABLE C.1 continued.

DATE	TEMPERATURE (°C)	MOISTURE (%)
3.5.1994	26.3	50
4.5.1994	26	52
5.5.1994	22	60
6.5.1994	23	62
7.5.1994	19	64
8.5.1994	21	60
9.5.1994	20.5	62
10.5.1994	20.5	62
11.5.1994	22	61
12.5.1994	22	63
13.5.1994	22	64
14.5.1994	22	64
15.5.1994	22	64
16.5.1994	22	65
17.5.1994	21	67
18.5.1994	21	68
19.5.1994	21	66
20.5.1994	20	69
21.5.1994	22	68
22.5.1994	20	70
23.5.1994	21	68
24.5.1994	21	66
25.5.1994	21	66
26.5.1994	21	70
27.5.1994	21	70
28.5.1994	21	70
29.5.1994	21	69
30.5.1994	21	68
31.5.1994 [c]	22	68
1.6.1994	22	67
2.6.1994	22	67
3.6.1994	22	68

TABLE C.1 continued.

DATE	TEMPERATURE (°C)	MOISTURE (%)
4.6.1994	21	68
5.6.1994	22	67
6.6.1994	20	70
7.6.1994	20.5	71
8.6.1994	20.5	71
9.6.1994	21	71
10.6.1994	22	72
11.6.1994 [d]	22	70

[a] : first day of sample preparation
[b] : last day of sample preparation
[c] : first day of sample testing
[d] : last day of sample testing

APPENDIX D. ULTRASONIC TEST RESULTS

TABLE D.1. Sound velocity and elasticity modulus values for samples without ice.

Per Cent Lime or Rubber	Sample Number	Average Transit Time (μs)	Sound Velocity (km/sec)	Modulus of Elasticity (*10^3 MPa)
-	1	54.1	2.15	6.05
	2	54.9	2.12	5.88
	3	55.7	2.09	5.76
	4	56.9	2.05	5.68
	5	53.1	2.9	6.27
	6	52.2	2.23	6.58
10 PER CENT LIME	7	50.0	2.33	7.09
	8	50.3	2.31	6.99
	9	49.6	2.35	7.22
	10	48.4	2.41	7.63
	11	52.9	2.20	6.82
	12	48.9	2.38	7.46
20 PER CENT LIME	13	52.8	2.21	6.26
	14	49.4	2.36	7.24
	15	48.7	2.39	7.41
	16	50.6	2.30	6.81
	17	51.2	2.28	6.62
	18	53.8	2.17	5.96
30 PER CENT LIME	19	53.3	2.19	6.0
	20	53.1	2.19	6.12
	21	55.3	2.11	5.6
	22	56.1	2.08	5.34
	23	51.7	2.25	6.38
	24	52.5	2.22	628

TABLE D.1 continued.

Per Cent Lime or Rubber	Sample Number	Average Transit Time (μs)	Sound Velocity (km/sec)	Modulus of Elasticity (*10^3 MPa)
	25	54.6	2.13	6.63
10 PER	26	55.2	2.11	6.5
CENT	27	61.6	1.89	5.22
RUBBER	28	52.6	2.22	7.15
	29	55.9	2.08	6.36
	30	54.6	2.13	6.61
	31	62.5	1.86	4.82
20 PER	32	64.5	1.81	4.53
CENT	33	68.9	1.69	4.03
RUBBER	34	68.4	1.70	3.95
	35	65.7	1.77	4.39
	36	71.1	1.64	3.72
	37	73.1	1.59	3.39
30 PER	38	64.2	1.81	4.43
CENT	39	65.7	1.77	4.22
RUBBER	40	71.1	1.64	3.56
	41	71.2	1.64	3.57
	42	72.0	1.62	3.46

TABLE D.2. Sound velocity and elasticity modulus values for samples with 10 per cent spherical ice.

Per Cent Lime or Rubber	Sample Number	Average Transit Time (μs)	Sound Velocity (km/sec)	Modulus of Elasticity (*10^3 MPa)
	43	49.0	2.38	8.12
	44	53.5	2.18	6.84
	45	50.2	2.32	7.78
-	46	50.9	2.29	7.52
	47	50.5	2.31	7.7
	48	51.5	2.26	7.46
	49	48.6	2.40	8.4
10 PER	50	46.7	2.49	8.89
CENT	51	47.1	2.47	8.89
LIME	52	49.1	2.37	8.15
	53	43.1	2.70	10.5
	54	49.1	2.37	8.17
	55	45.7	2.55	9.25
20 PER	56	46.8	2.49	8.8
CENT	57	47.1	2.47	8.8
LIME	58	45.0	2.59	9.69
	59	45.4	2.57	9.27
	60	46.6	2.50	8.8
	61	52.5	2.22	6.62
30 PER	62	51.4	2.27	7.07
CENT	63	54.6	2.14	6.12
LIME	64	5.5	2.26	6.84
	65	55.5	2.10	6.1
	66	51.7	2.25	6.85

TABLE D.2 continued.

Per Cent Lime or Rubber	Sample Number	Average Transit Time (μs)	Sound Velocity (km/sec)	Modulus of Elasticity (*10^3 MPa)
	67	68.6	1.7	4.03
10 PER	68	58.2	2.0	5.6
CENT	69	56.6	2.06	5.82
RUBBER	70	56.9	2.05	5.83
	71	54.4	2.14	6.38
	72	52.5	2.22	6.93
	73	62.2	1.87	4.68
20 PER	74	62.8	1.86	4.62
CENT	75	65.3	1.78	4.18
RUBBER	76	60.0	1.94	5.01
	77	66.6	1.75	4.06
	78	71.0	1.64	3.71
	79	96.5	1.21	1.9
30 PER	80	97.1	1.2	1.88
CENT	81	90.9	1.28	2.14
RUBBER	82	97.3	1.2	1.84
	83	91.1	1.28	2.12
	84	97.1	1.2	1.86

TABLE D.3. Sound velocity and elasticity modulus values for samples with 10 per cent crushed ice.

Per Cent Lime or Rubber	Sample Number	Average Transit Time (μs)	Sound Velocity (km/sec)	Modulus of Elasticity (*10^3 MPa)
-	85	51.8	2.25	7.54
	86	59.4	1.96	5.73
	87	56.1	2.08	6.47
	88	52.2	2.23	7.48
	89	54.2	2.15	6.89
	90	49.2	2.37	8.4
10 PER CENT LIME	91	51.8	2.25	7.58
	92	46.1	2.53	9.31
	93	46.5	2.51	9.12
	94	46.6	2.50	9.07
	95	51.1	2.28	7.53
	96	45.1	2.58	9.67
20 PER CENT LIME	97	55.4	2.10	6.6
	98	54.5	2.14	6.73
	99	51.5	2.26	7.53
	100	50.4	2.31	7.82
	101	56.6	2.06	6.29
	102	55.2	2.11	6.57
30 PER CENT LIME	103	50.8	2.29	7.65
	104	50.0	2.33	7.82
	105	52.6	2.21	7.04
	106	53.0	2.20	7.0
	107	52.5	2.22	7.17
	108	48.6	2.40	8.28

TABLE D.3 continued.

Per Cent Lime or Rubber	Sample Number	Average Transit Time (μs)	Sound Velocity (km/sec)	Modulus of Elasticity (*10^3 MPa)
	109	58.3	2.0	5.65
10 PER	110	60.2	1.94	5.19
CENT	111	56.9	2.05	5.89
RUBBER	112	60.4	1.93	5.18
	113	56.3	2.07	6.01
	114	59.4	1.96	5.41
	115	68.8	1.69	3.9
20 PER	116	67.5	1.73	3.97
CENT	117	70.9	1.64	3.61
RUBBER	118	67.0	1.74	4.07
	119	69.2	1.68	3.83
	120	67.1	1.74	4.06
	121	81.3	1.43	2.66
30 PER	122	76.5	1.52	2.99
CENT	123	77.4	1.50	2.93
RUBBER	124	81.2	1.43	2.65
	125	81.7	1.43	2.62
	126	77.1	1.51	2.9

APPENDIX E. STRESS-STRAIN CURVES

The stress-strain curves for compressive loading of the samples belonging to the 21 sub-groups are presented in the following pages. Polynomial and linear curves passing through the data points have been fitted. Curve fitting has been carried on until the last data point for each sample.

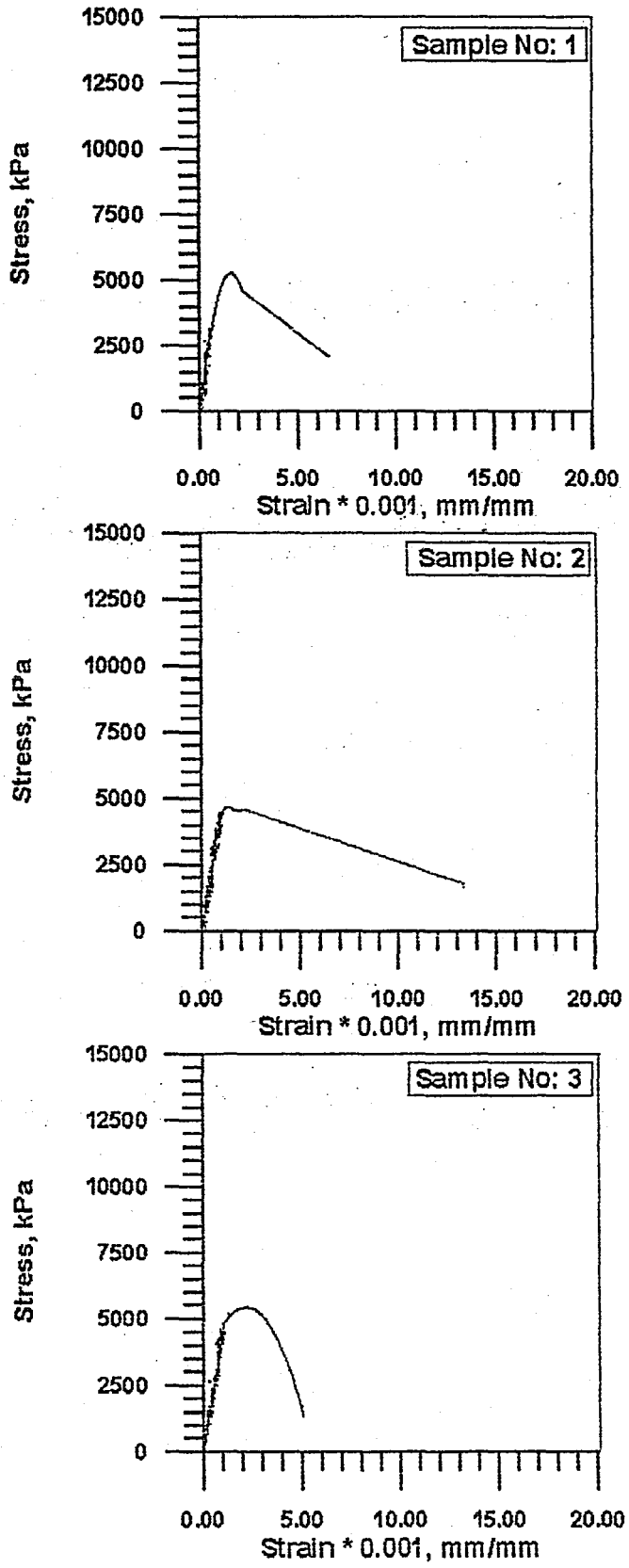

FIGURE E.1. Stress-strain curves for 100 per cent fly ash.

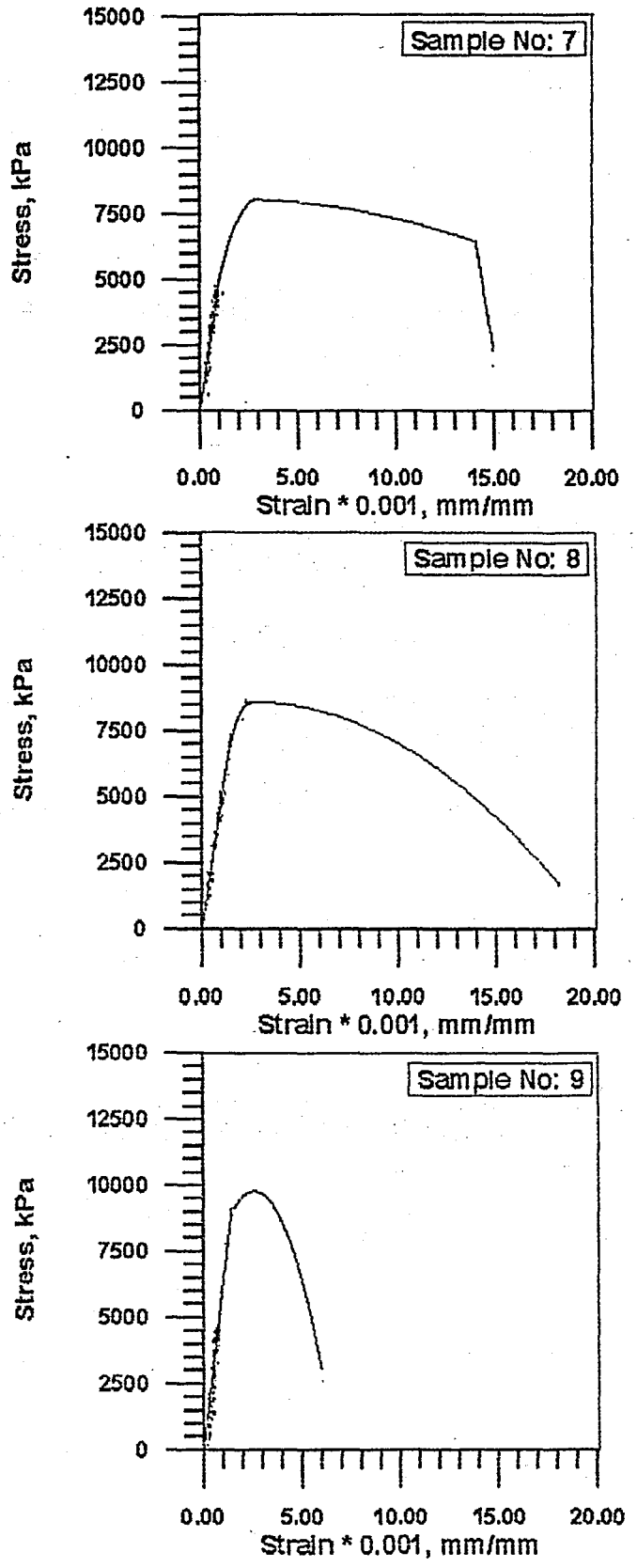

FIGURE E.2. Stress-strain curves for 90 per cent fly ash and 10 per cent lime.

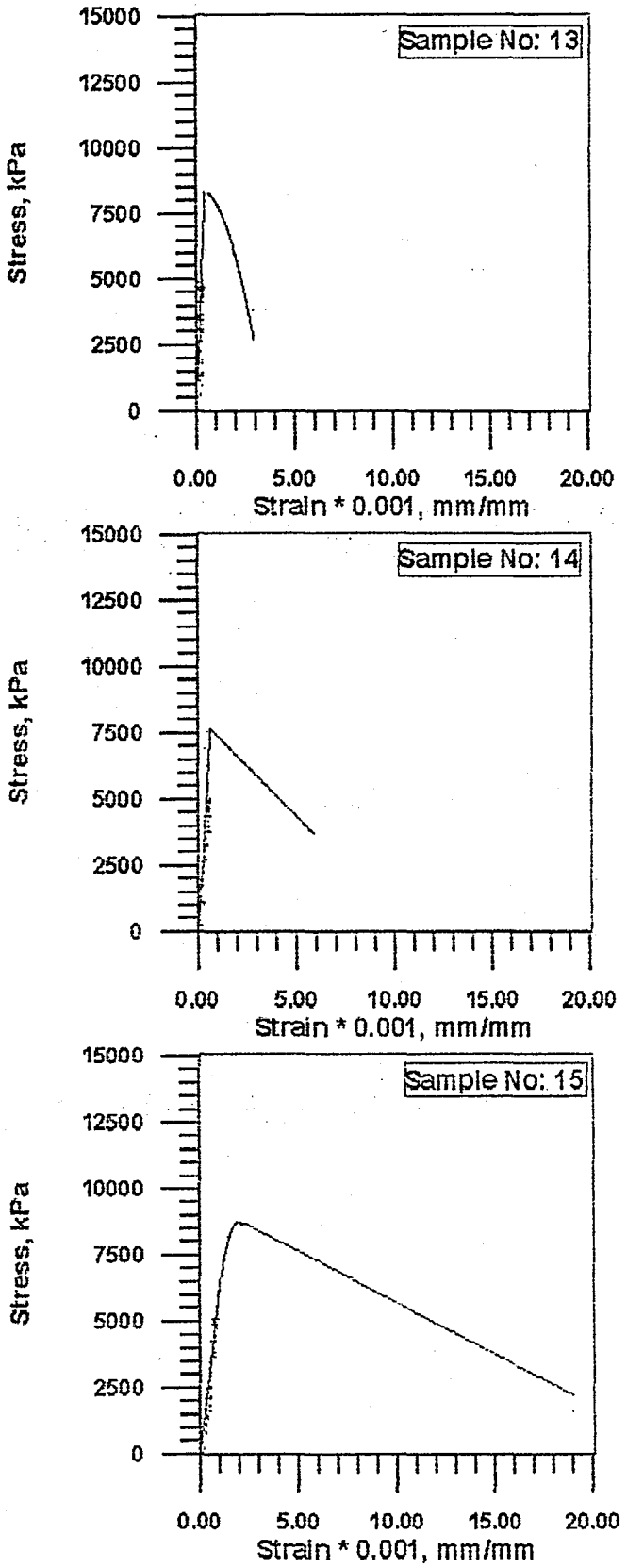

FIGURE E.3. Stress-strain curves for 80 per cent fly ash and 20 per cent lime.

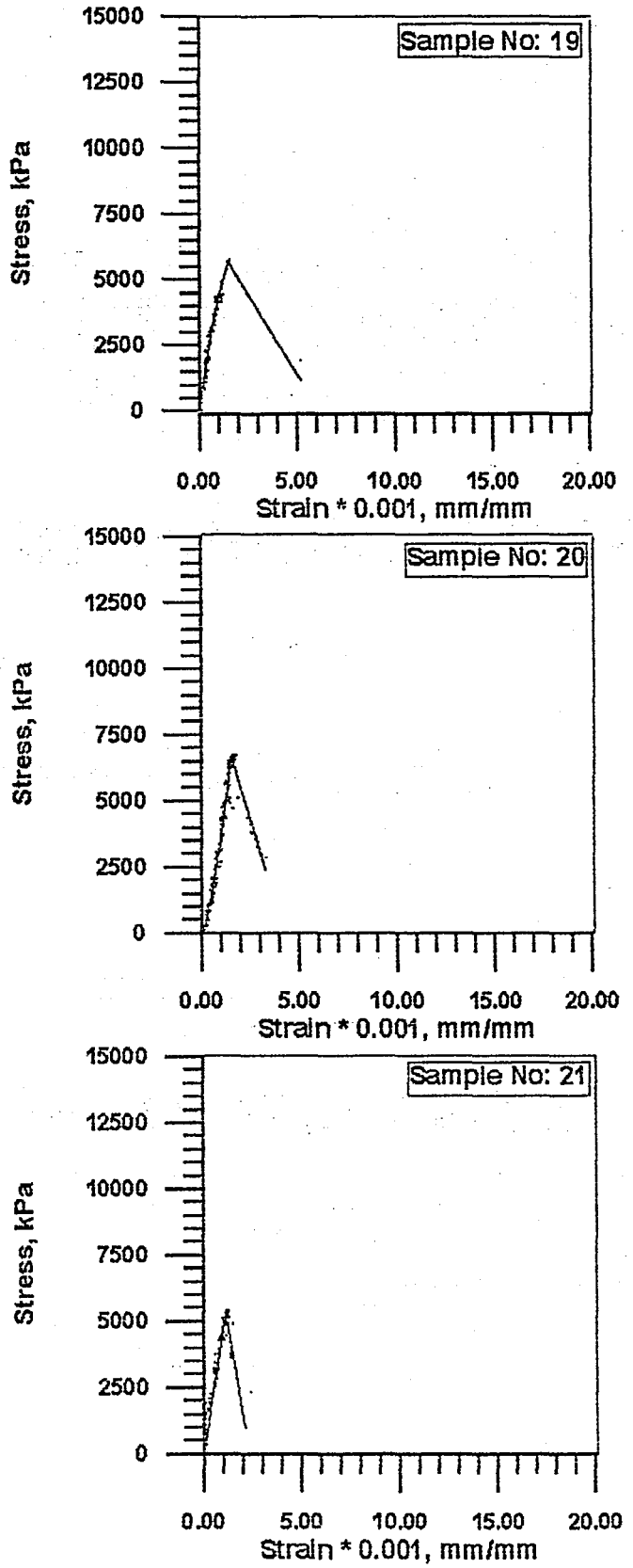

FIGURE E.4. Stress-strain curves for 70 per cent fly ash and 30 per cent lime.

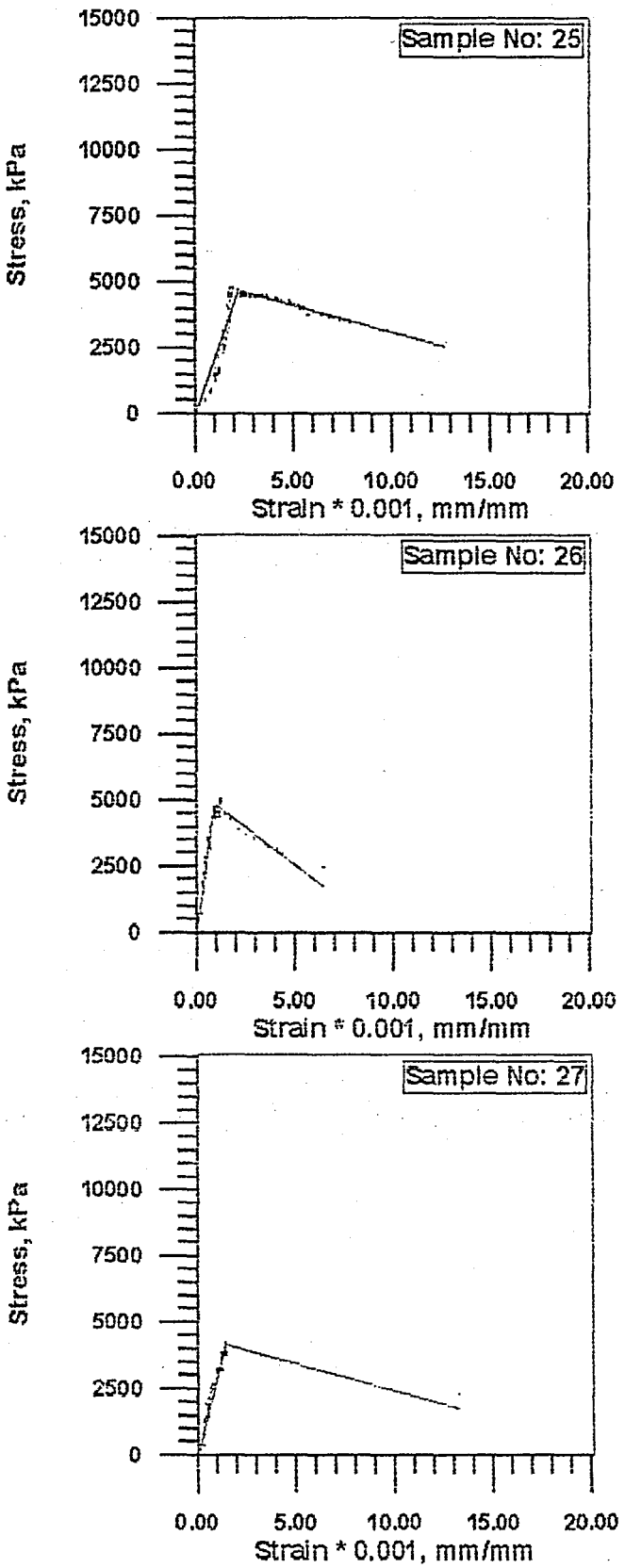

FIGURE E.5. Stress-strain curves for 90 per cent fly ash and 10 per cent rubber.

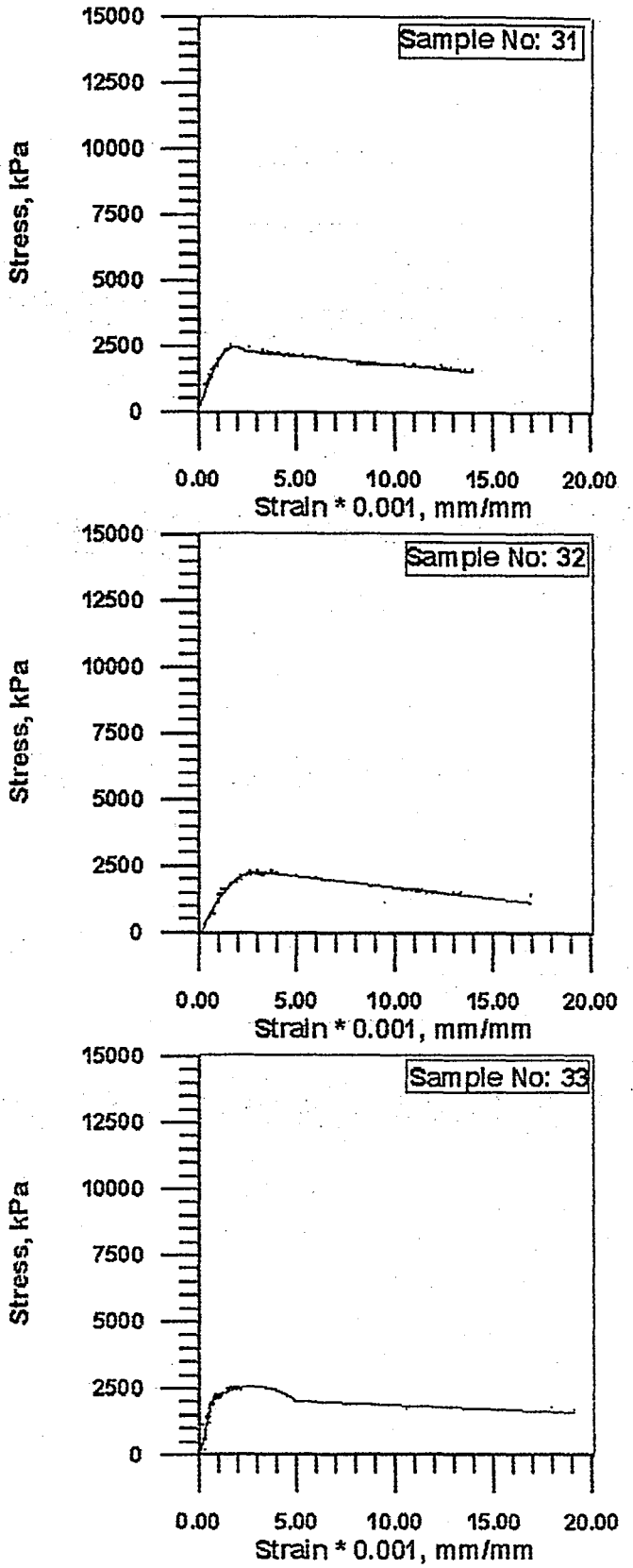

FIGURE E.6. Stress-strain curves for 80 per cent fly ash and 20 per cent rubber.

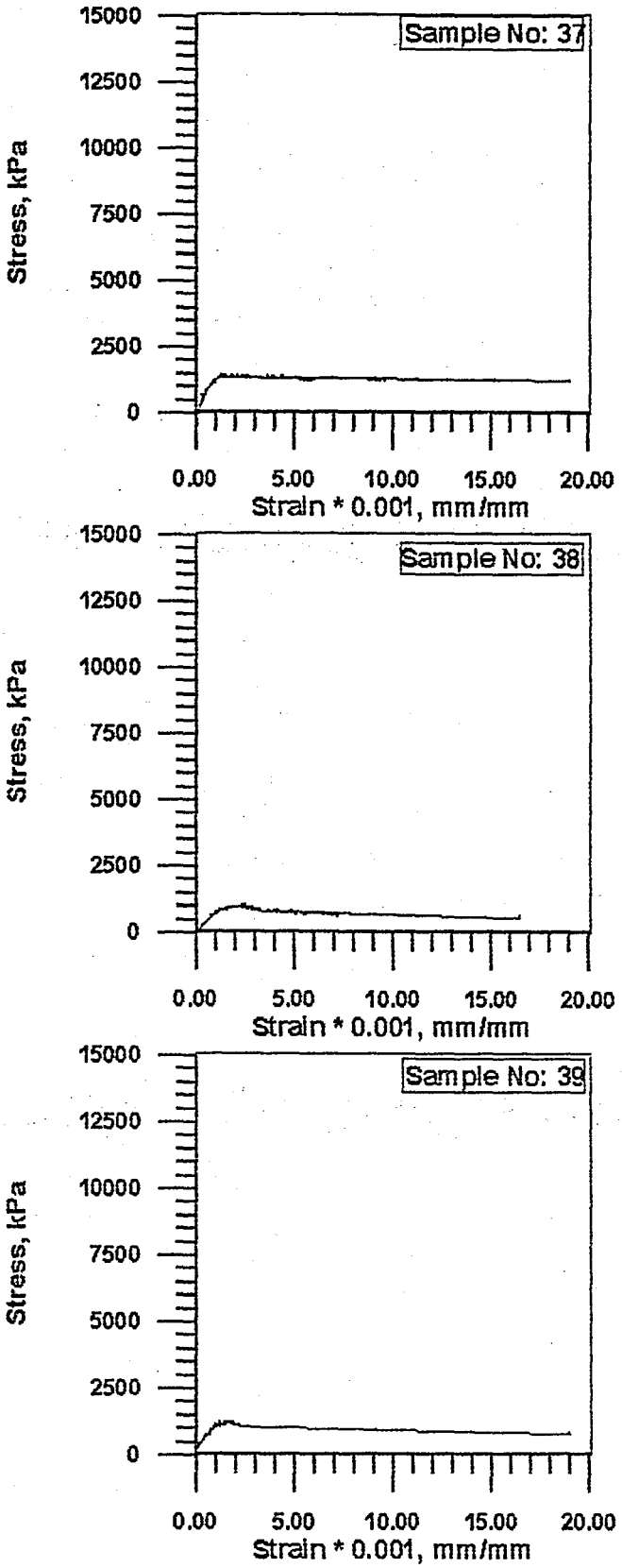

FIGURE E.7. Stress-strain curves for 70 per cent fly ash and 30 per cent rubber.

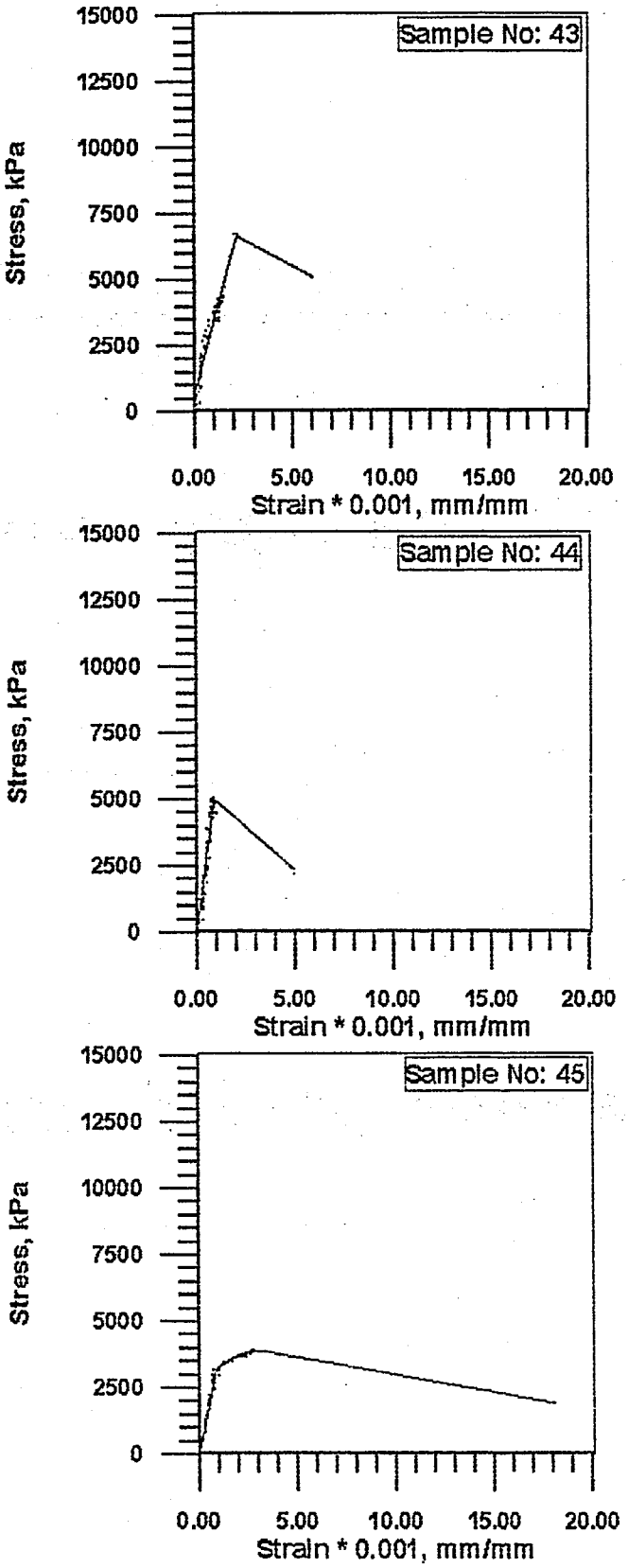

FIGURE E.8. Stress-strain curves for 100 per cent fly ash with 10 per cent spherical ice.

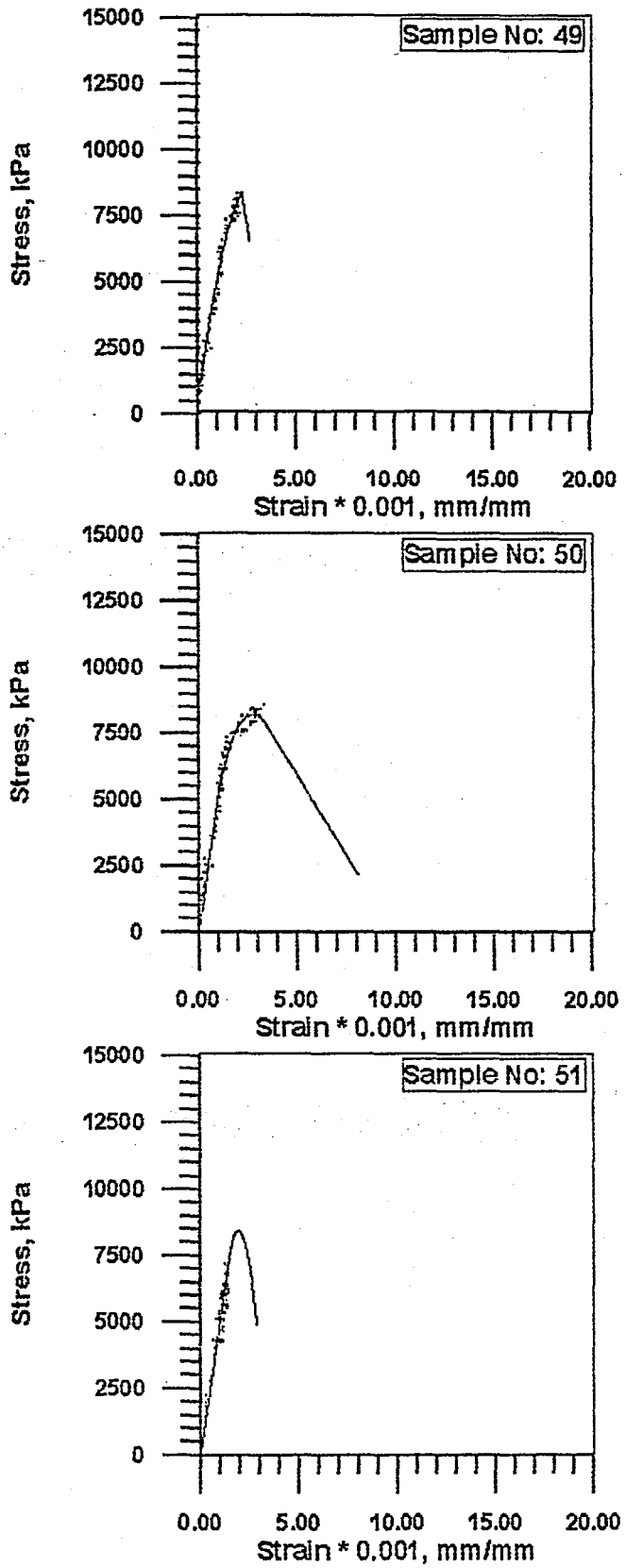

FIGURE E.9. Stress-strain curves for 90 per cent fly ash and 10 per cent lime with 10 per cent spherical ice.

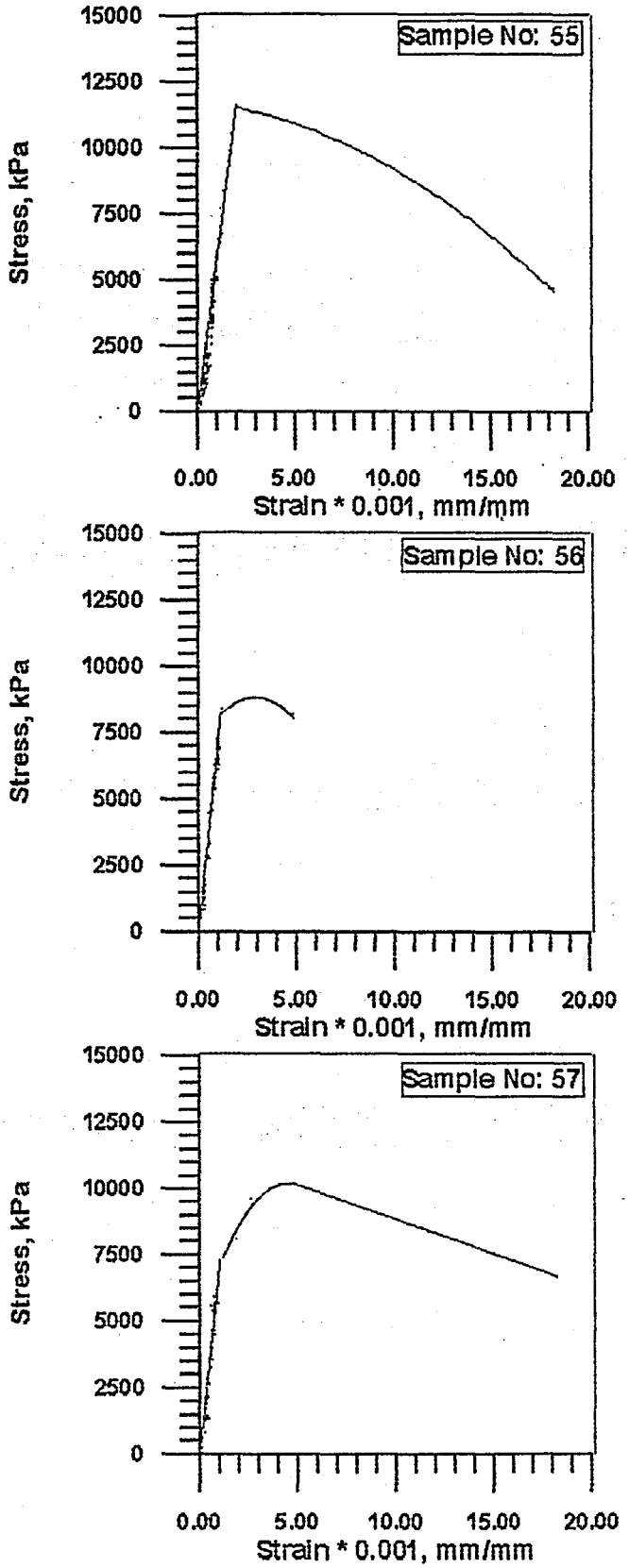

FIGURE E.10. Stress-strain curves for 80 per cent fly ash and 20 per cent lime with 10 per cent spherical ice.

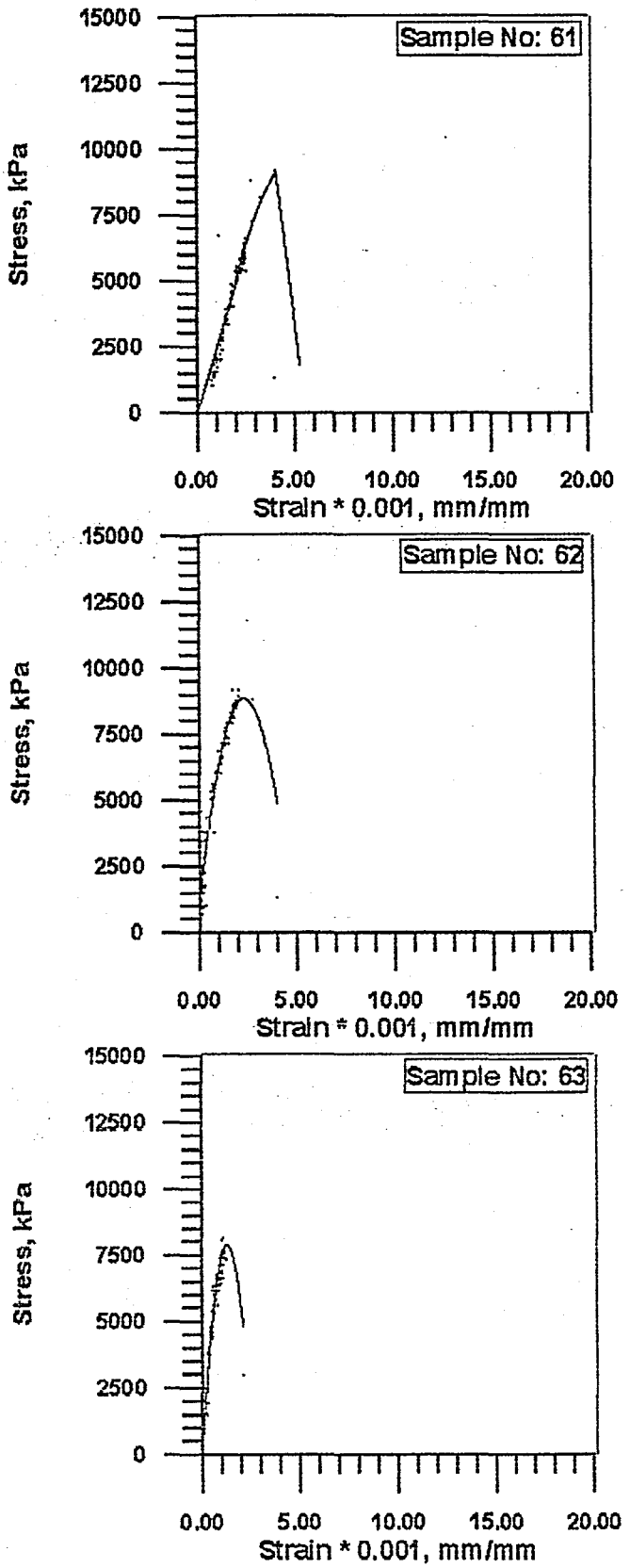

FIGURE E.11. Stress-strain curves for 70 per cent fly ash and 30 per cent lime with 10 per cent spherical ice.

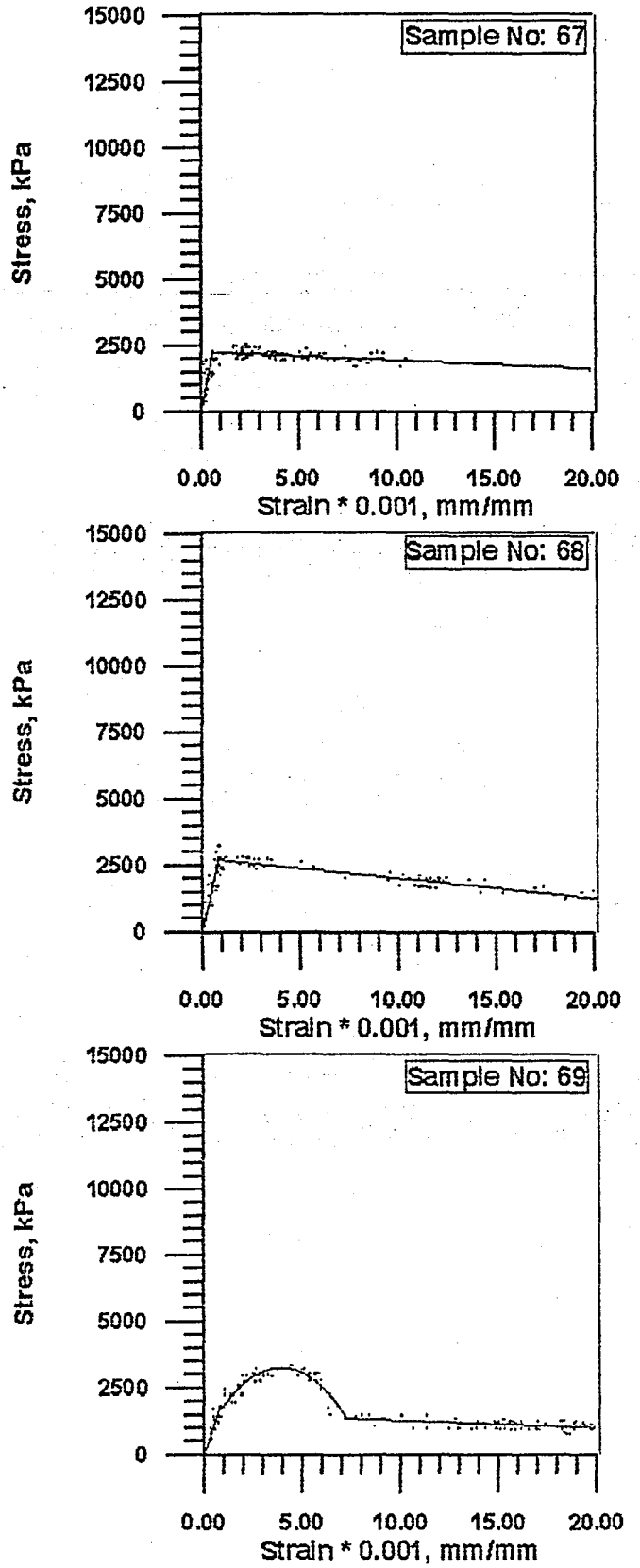

FIGURE E.12. Stress-strain curves for 90 per cent fly ash and 10 per cent rubber with 10 per cent spherical ice.

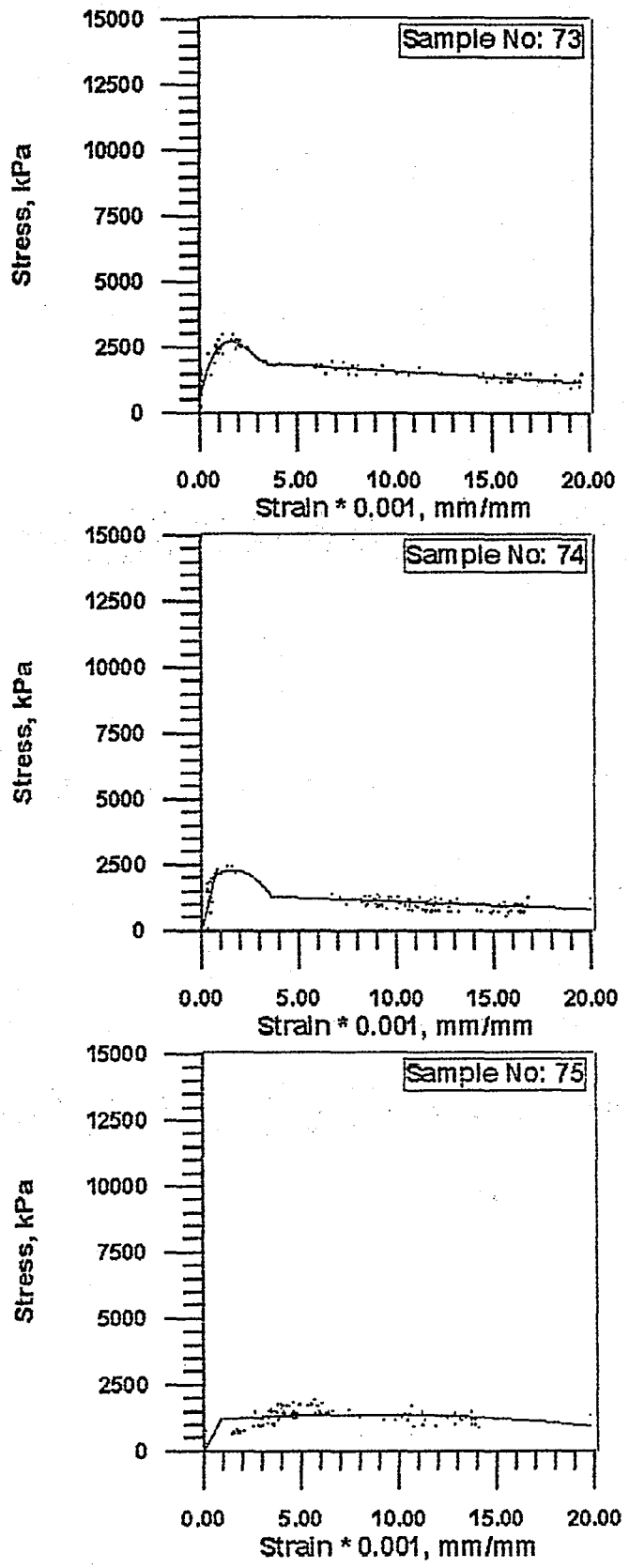

FIGURE E.13. Stress-strain curves for 80 per cent fly ash and 20 per cent rubber with 10 per cent spherical ice.

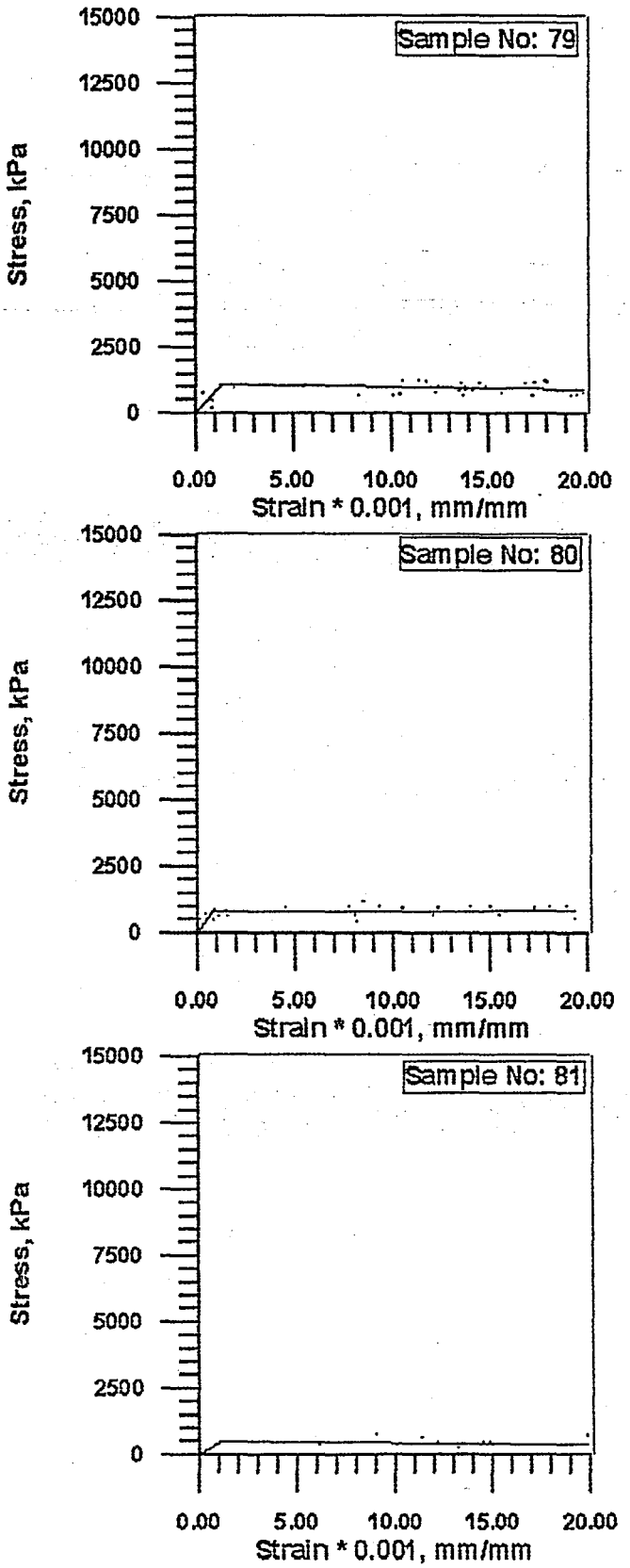

FIGURE E.14. Stress-strain curves for 70 per cent fly ash and 30 per cent rubber with 10 per cent spherical ice.

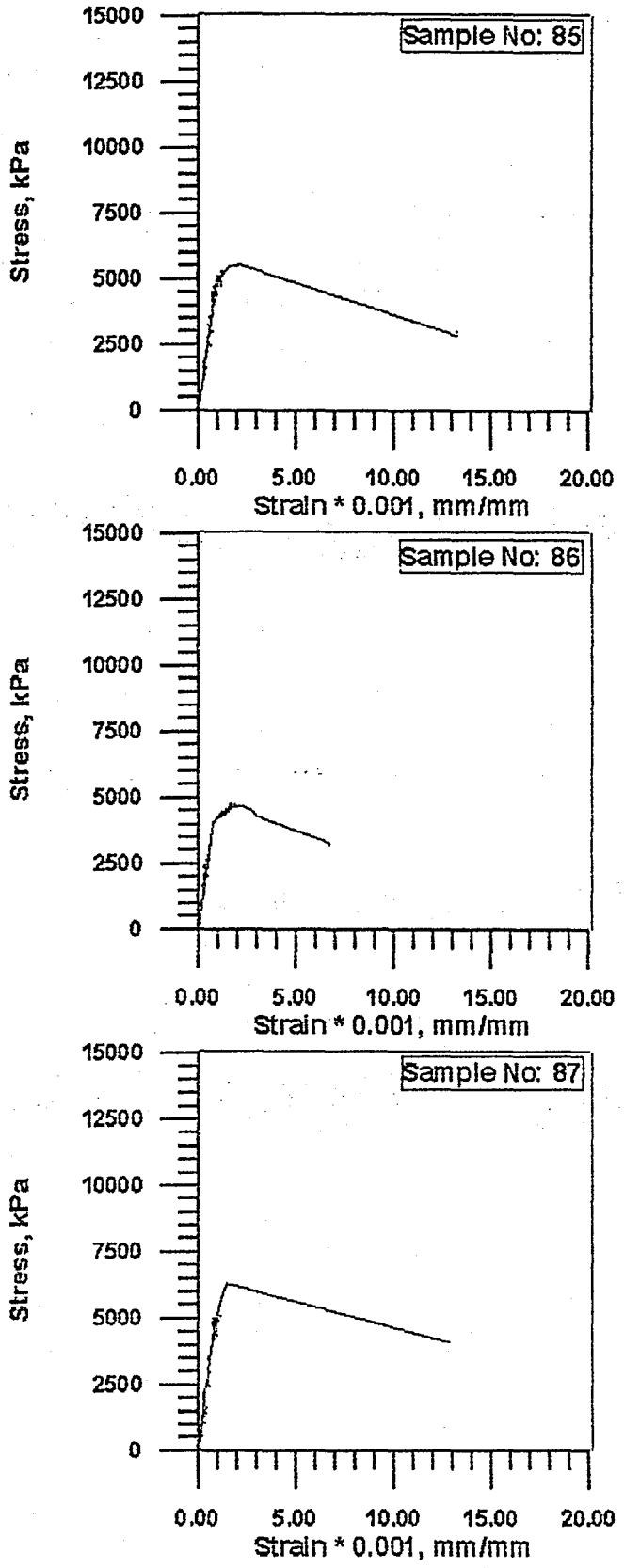

FIGURE E.15. Stress-strain curves for 100 per cent fly ash with 10 per cent crushed ice.

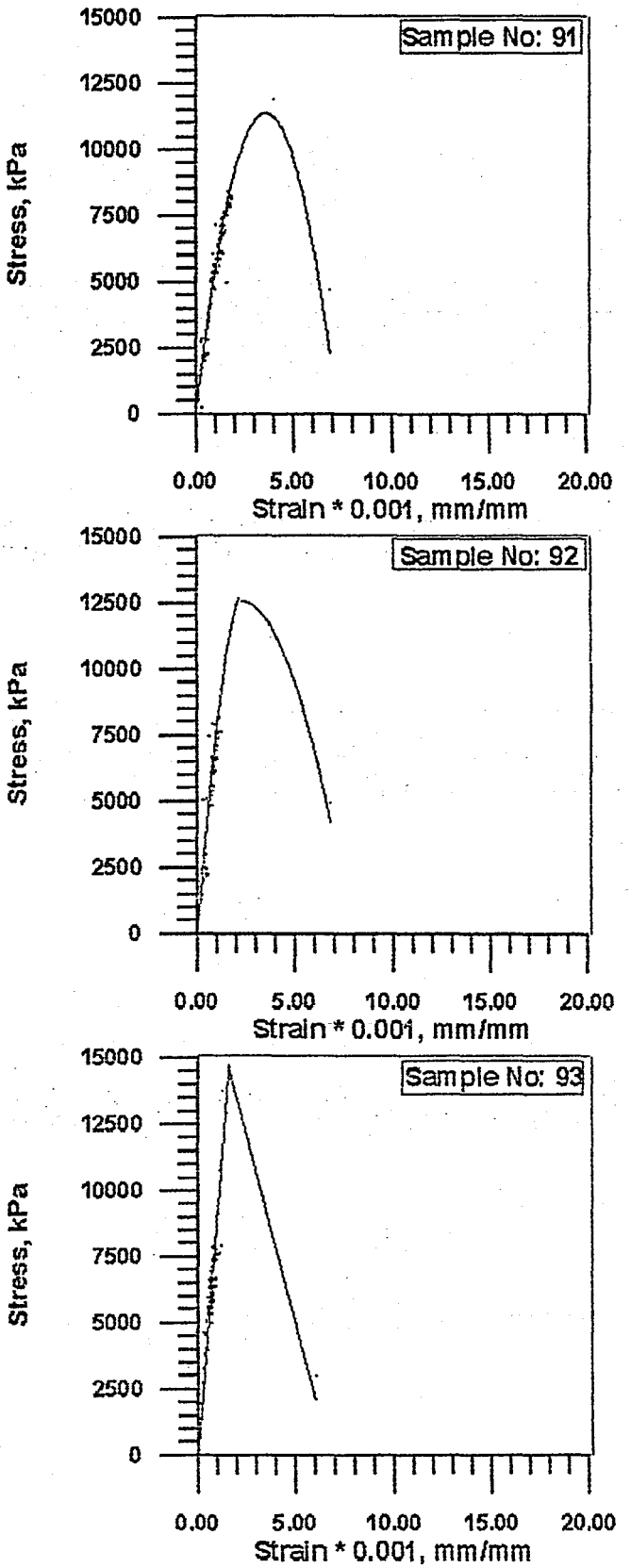

FIGURE E.16. Stress-strain curves for 90 per cent fly ash and 10 per cent lime with 10 per cent crushed ice.

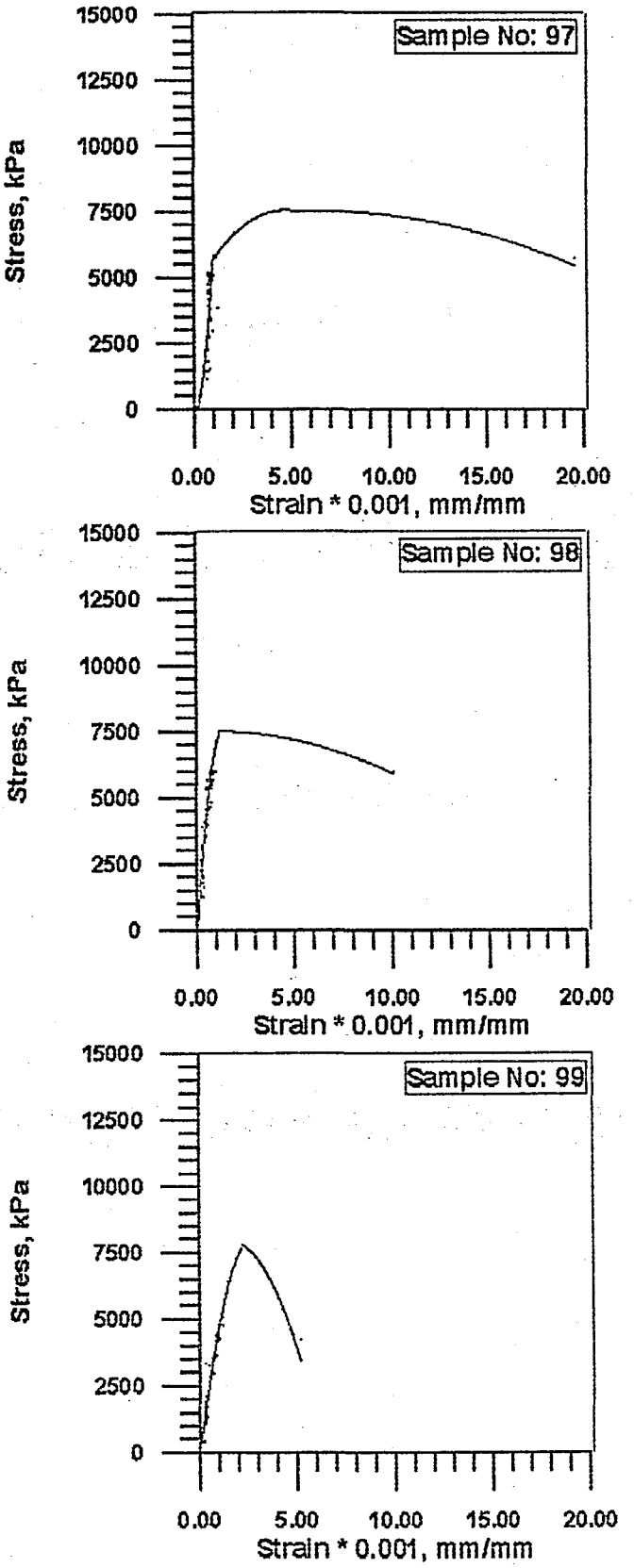

FIGURE E.17. Stress-strain curves for 80 per cent fly ash and 20 per cent lime with 10 per cent crushed ice.

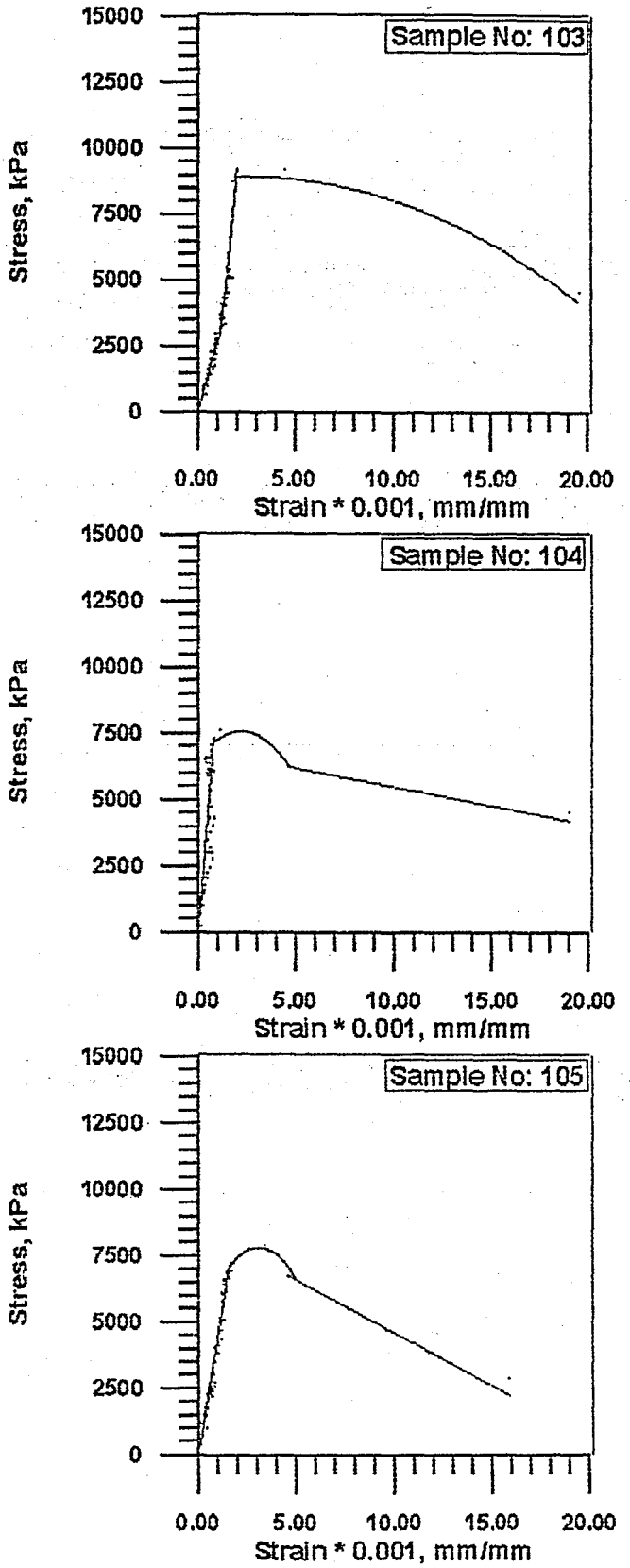

FIGURE E.18. Stress-strain curves for 70 per cent fly ash and 30 per cent lime with 10 per cent crushed ice.

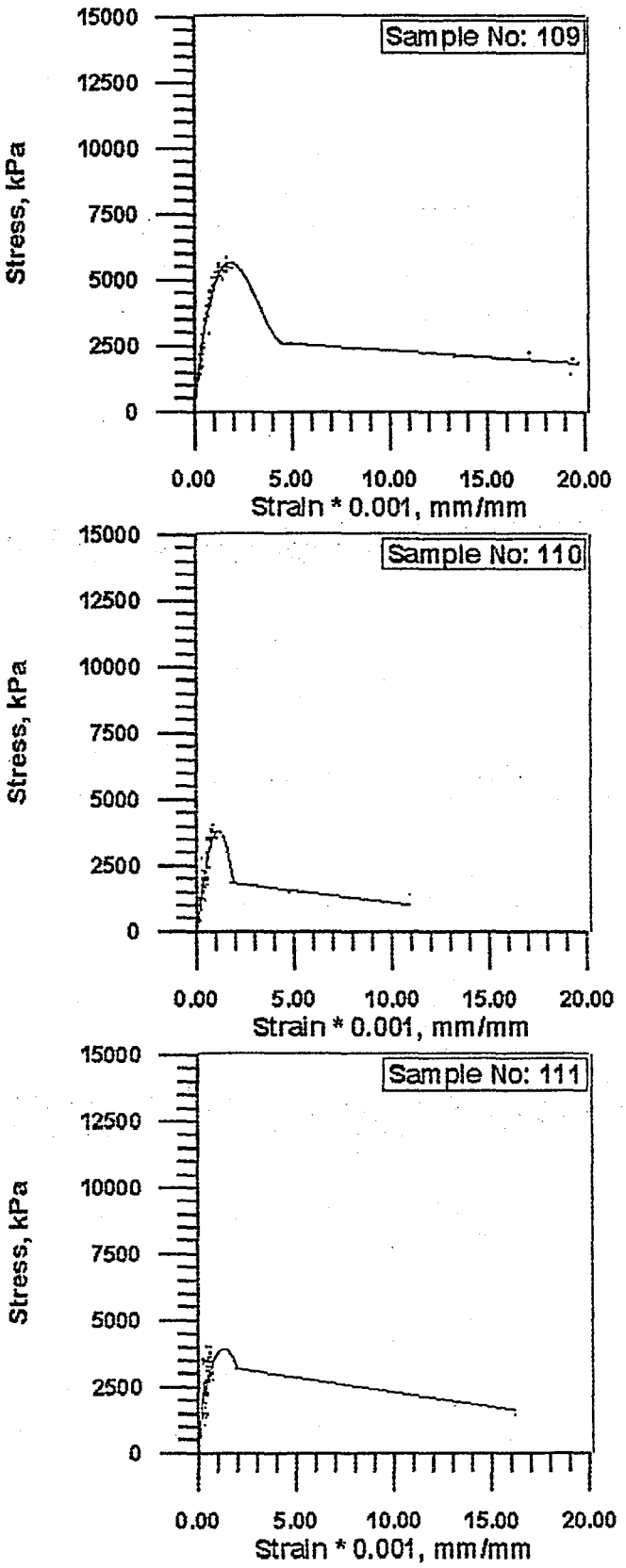

FIGURE E.19. Stress-strain curves for 90 per cent fly ash and 10 per cent rubber with 10 per cent crushed ice.

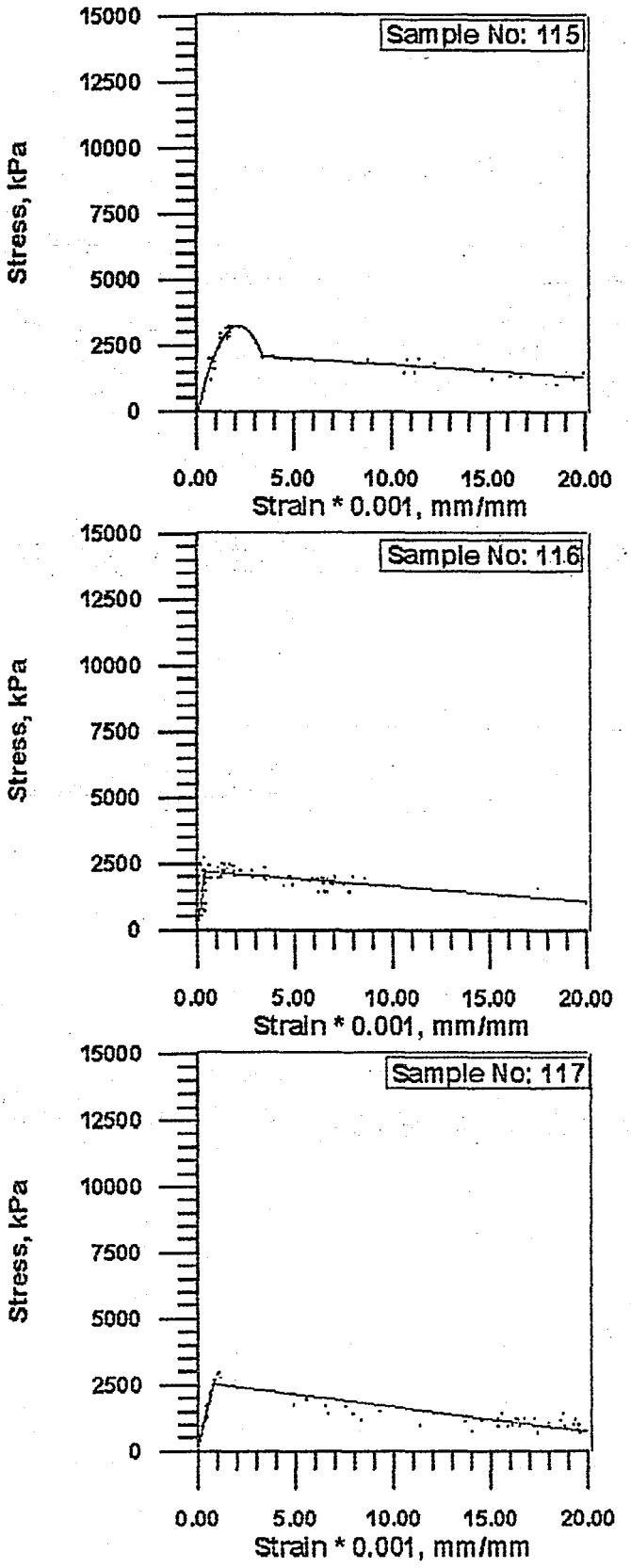

FIGURE E.20. Stress-strain curves for 80 per cent fly ash and 20 per cent rubber with 10 per cent crushed ice.

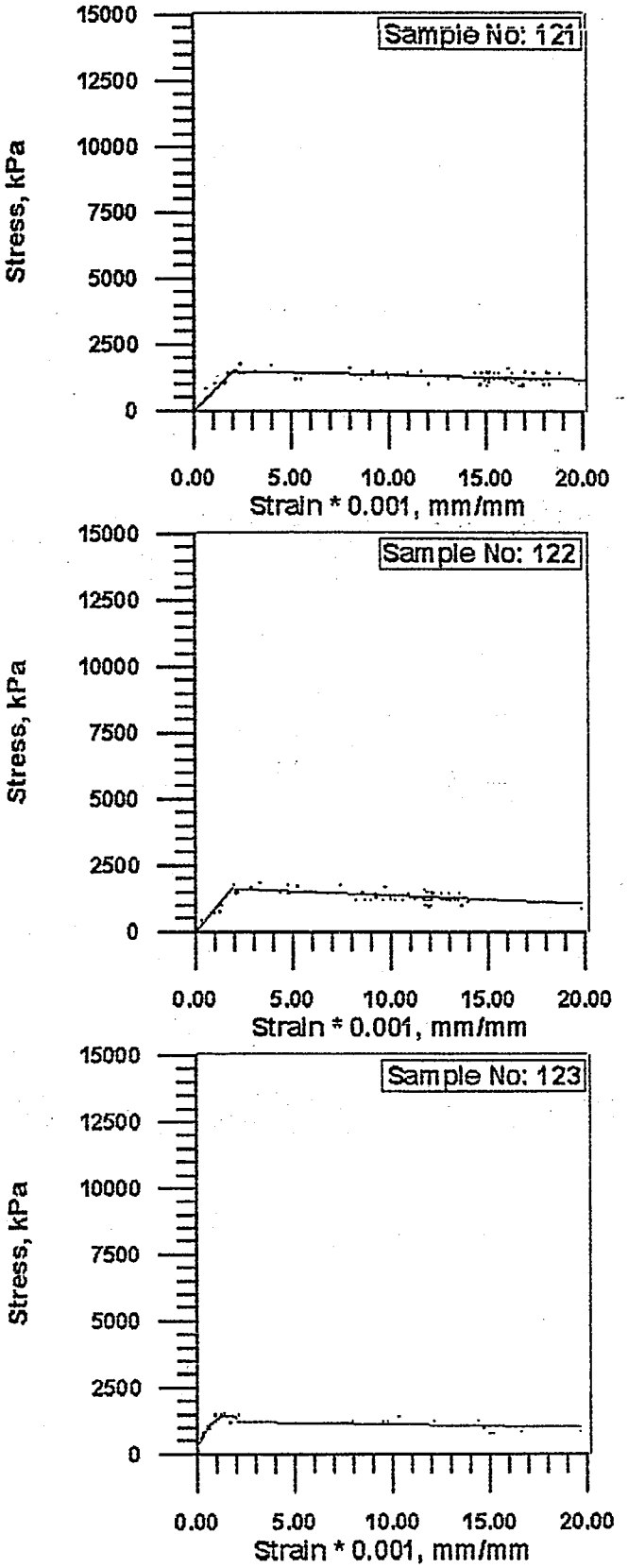

FIGURE E.21. Stress-strain curves for 70 per cent fly ash and 30 per cent rubber with 10 per cent crushed ice.

APPENDIX F. COMPRESSIVE LOADING TEST RESULTS

TABLE F.1. Mechanical properties of the samples without ice, determined by compressive loading.

Per Cent Lime or Rubber	Sample Number	Water content (%)	Dry unit weight (kN/m^3)	Young's Modulus ($*10^3$ MPa)	Maximum compressive strength (MPa)	Energy absorbing capacity (kPa)
-	1	18.29	11.61	4.5	5.08	26.8
	2	17.96	11.63	4.65	4.74	49.7
	3	17.36	11.92	4.8	5.37	20.6
10 per cent lime	7	20.42	11.32	5.5	8.3	299.8
	8	21.16	11.19	5.33	8.87	114.4
	9	20.11	11.37	6	9.75	44.2
20 per cent lime	13	19.52	11.27	16.5	8.39	18.3
	14	19.08	11.45	9.5	7.85	128.3
	15	19.05	11.41	5.3	8.84	435.5
30 per cent lime	19	20.09	10.91	4.6	5.84	18.1
	20	20.51	11.00	4.33	6.82	51.8
	21	20.39	10.92	5.25	5.39	24.2
10 per cent rubber	25	20.75	12.58	2.24	4.86	187.2
	26	20.62	12.59	4.75	5.08	23.3
	27	20.48	12.64	2.8	4.29	45.5
20 per cent rubber	31	20.42	12.01	1.8	2.68	45.3
	32	19.73	12.13	1	2.37	36.7
	33	19.20	12.36	2.81	2.68	77.4
30 per cent rubber	37	20.15	11.60	2	1.45	139.4
	38	20.20	11.68	0.75	1.07	22.4
	39	19.86	11.71	1	1.29	34.5

TABLE F.2. Mechanical properties of the samples with 10 per cent spherical ice, determined by compressive loading.

Per Cent Lime or Rubber	Sample Number	Water content (%)	Dry unit weight (kN/m^3)	Young's Modulus ($*10^3$ MPa)	Maximum compressive strength (MPa)	Energy absorbing capacity (kPa)
	43	27.78	11.30	3.2	6.82	64.2
-	44	29.61	11.07	1	5.15	21.66
	45	29.59	11.08	3.75	3.95	67.6
10 per	49	29.09	11.32	5	8.59	19.71
cent	50	30.25	10.86	4.2	8.71	44.9
lime	51	30.25	11.05	5.33	8.79	17.95
20 per	55	27.72	11.18	4.6	11.78	168.6
cent	56	28.23	11.08	7.4	8.87	58.5
lime	57	27.67	11.34	7.4	10.2	738.9
30 per	61	30.48	10.19	2.8	8.96	26.9
cent	62	30.68	10.38	6.9	9.32	29.2
lime	63	29.54	10.32	6.75	8.3	13.6
10 per	67	26.94	11.14	4.5	2.55	80.05
cent	68	27.14	11.12	2.7	3.32	50.5
rubber	69	27.88	10.82	1.75	3.36	50.6
20 per	73	25.29	10.87	6	2.99	64.6
cent	74	24.29	11.07	4	2.47	102.1
rubber	75	26.94	10.46	1.4	1.95	29.5
30 per	79	22.36	11.03	0.8	1.29	57.8
cent	80	18.30	11.62	0.9	1.18	289.5
rubber	81	21.95	11.08	1	0.77	16.9

TABLE F.3. Mechanical properties of the samples with 10 per cent crushed ice, determined by compressive loading.

Per Cent Lime or Rubber	Sample Number	Water content (%)	Dry unit weight (kN/m^3)	Young's Modulus ($*10^3$ MPa)	Maximum compressive strength (MPa)	Energy absorbing capacity (kPa)
-	85	24.90	12.19	4.9	5.65	72.5
	86	25.99	11.99	5	4.77	46.3
	87	26.58	11.97	5	6.57	109.3
10 per cent lime	91	27.36	11.84	5	12.04	54.9
	92	27.67	11.48	7.3	12.97	64.3
	93	27.36	11.50	2.4	15.07	49.3
20 per cent lime	97	26.67	11.93	5.7	7.7	168.5
	98	27.83	11.58	6.5	7.92	101.7
	99	26.66	11.74	4	7.67	30.7
30 per cent lime	103	28.64	11.32	3	10.02	149.5
	104	27.00	11.46	7	7.9	169.1
	105	28.73	11.17	4.7	8.23	260.9
10 per cent rubber	109	26.16	11.38	4.5	5.88	87.4
	110	28.79	10.76	6	4.09	20.9
	111	24.69	11.53	5	4.17	52.6
20 per cent rubber	115	26.88	10.84	2.5	3.44	55.3
	116	27.21	10.60	5.6	2.84	43.5
	117	26.93	10.65	2.8	3.44	35.8
30 per cent rubber	121	24.76	10.60	0.75	1.78	69.2
	122	24.87	10.53	0.85	2.11	44.1
	123	23.98	10.71	2	1.62	64.2

APPENDIX G. DOUBLE PUNCH TEST RESULTS

TABLE G.1. Double punch test results for samples without ice.

Per Cent Lime or Rubber	Sample Number	Water content (%)	Dry unit weight (kN/m^3)	Maximum tensile load (kg)	Maximum tensile stress (kPa)
-	4	18.4	12.1	1907.3	1031.5
	5	17.5	11.7	1572.6	850.5
	6	17.6	11.9	1673	904.8
10 per cent lime	10	19.9	11.5	2174.9	1176.2
	11	19.4	12.3	2375.7	1284.8
	12	20.1	11.5	2342.2	1266.7
20 per cent lime	16	19.1	11.3	1673	904.8
	17	19.5	11.2	2174.9	1176.2
	18	19.7	11.1	1940.7	1049.5
30 per cent lime	22	19.2	10.9	1873.8	1013.3
	23	19.2	11.1	1773.3	959
	24	19.6	11.2	1873.8	1013.3
10 per cent rubber	28	19.9	12.7	1840.3	995.2
	29	20.0	12.8	1673	904.75
	30	20.4	12.6	1706.5	922.9
20 per cent rubber	34	18.8	12.1	1472.2	796.2
	35	19.4	12.3	1271.5	687.6
	36	18.4	12.3	1037.3	560.9
30 per cent rubber	40	16.5	12.0	769.6	416.2
	41	18.0	11.9	903.5	488.6
	42	16.9	11.9	1104.1	597.1

TABLE G.2. Double punch test results for samples with 10 per cent spherical ice.

Per Cent Lime or Rubber	Sample Number	Water content (%)	Dry unit weight (kN/m^3)	Maximum tensile load (kg)	Maximum tensile stress (kPa)
-	46	27.3	11.4	1740	941
	47	27.1	11.5	1673	904.8
	48	28.8	11.3	1840.3	995.2
10 per cent lime	52	28.0	11.3	2576.4	1393.3
	53	27.1	11.4	3078.3	1664.7
	54	28.2	11.4	2308.7	1248.5
20 per cent lime	58	28.2	11.3	2476.1	1339.1
	59	27.6	11.1	2476.1	1339.1
	60	28.8	10.9	2308.7	1248.5
30 per cent lime	64	27.9	10.5	2141.4	1158.1
	65	29.5	10.6	1204.6	651.4
	66	28.5	10.5	2108	1140
10 per cent rubber	70	27.2	11.1	1171.1	633.3
	71	28.3	10.9	1137.6	615.2
	72	25.6	11.4	1171.1	633.3
20 per cent rubber	76	25.0	10.9	936.8	506.6
	77	27.7	10.5	1171.1	633.3
	78	25.6	11.2	870	470.5
30 per cent rubber	82	19.7	11.2	769.6	416.2
	83	19.9	11.3	836.5	452.4
	84	19.4	11.4	736.1	398.1

TABLE G.3. Double punch test results for samples with 10 per cent crushed ice.

Per Cent Lime or Rubber	Sample Number	Water content (%)	Dry unit weight (kN/m^3)	Maximum tensile load (kg)	Maximum tensile stress (kPa)
-	88	23.0	12.6	2275.3	1230.5
	89	24.0	12.4	2041	1103.8
	90	23.8	12.4	2543	1375.2
10 per cent lime	94	28.1	11.4	2476	1339
	95	27.4	11.5	1873.8	1013.3
	96	27.0	11.5	3145.2	1700.9
20 per cent lime	100	27.6	11.5	2944.5	1592.4
	101	28.5	11.6	2676.8	1447.6
	102	28.1	11.6	1505.7	814.3
30 per cent lime	106	29.2	11.2	2241.8	1212.4
	107	28.8	11.3	1438.8	778.1
	108	29.2	11.1	2542.9	1375.2
10 per cent rubber	112	27.5	11.0	1639.5	886.6
	113	28.6	10.9	1673	904.8
	114	25.9	11.3	1673	904.8
20 per cent rubber	118	25.3	11.0	1104.2	597.1
	119	25.3	11.0	1003.8	542.9
	120	25.9	10.9	1003.8	542.9
30 per cent rubber	124	23.8	10.7	1037.3	560.9
	125	24.0	10.7	903.4	488.6
	126	24.2	10.5	1037.2	560.9

REFERENCES

1. ASTM, "ASTM C618-80 - Standard Specification for Fly Ash and Raw or Calcined Natural Pozzolan for Use as a Mineral Admixture in Portland Cement Concrete," in *ASTM Standards in Building Codes*, Vol.II, pp. 329-332, Baltimore M.D., USA, 1983.

2. McMANIS, Kenneth L., Laboratory Evaluation of Fly Ash Treated Embankment and Base Materials, TRB Record No. 1031, Nov. 1987.

3. MEYERS, R. A., *Coal Structure*, New York: Academic Press, 1982.

4. DAMBERGER, H. H., R. D. HARVEY, R. R. RUCH and J. JR. THOMAS, "Coal Characterization," in B. R. Cooper and W. A. Ellinson (editors), *The Science and Technology of Coal and Coal Utilization*, pp. 7-45, New York: Plenum Press, 1984.

5. SMOOT, L. D. and P. J. SMITH, *Coal combustion and Gasification*, New York: Plenum Press, 1985.

6. SERDAROĞLU, Nami, *Türk Kömürlerinin Sınıflama Esasları*, Istanbul: Kutulmuş Matbaası, 1956.

7. MEHTA, P. Kumar, "Pozzolanic and Cementitious Byproducts as Mineral Admixtures for Concrete - A Critical Review," in American Concrete Institute Publication SP-79, *Fly Ash, Silica Fume, Slag and Other Mineral By-Products in Concrete*, Vol. 1, pp. 1-46, ACI, 1983.

8. KOST, Patricia J. (editor), "Use of Fly Ash in Concrete," *ACI Manual of Concrete Practice - Part 1 - Materials and General Properties of Concrete*, pp. 226.3R.1-226.3R.29, ACI, 1991.

9. ASTM, "ASTM C593-66T - Tentative Specifications for Fly Ash and other Pozzolans for Use with Lime," in *1968 Book of ASTM Standards with Related Materials - Cement, Gypsum, Lime*, Part 9, pp.428-433, Baltimore, USA, June 1968.

10. GRAY, Donald H. and Yen-Kuang LIN, "Engineering Properties of Compacted Fly Ash," Journal of the Soil Mechanics and Foundations Division - Proceedings of the American Society of Civil Engineers, Vol.98, pp.361-380, April 1972.

11. ALLEN, P. W. and D.PHIL, *Natural Rubber and the Synthetics*, London: Crosby Lockwood, 1972.

12. BRYDSON, J. A., *Rubbery Materials and their Compounds*, Elsevier Applied Science Publishers Ltd., 1988.

13. MAKAROV, V. M. and V. F. DROZDOVSKI, *Reprocessing of Tyres and Rubber Wastes - Recycling from the Rubber Products Industry*, Ellis Horwood Series in Applied Science and Industrial Technology, West Sussex, England, 1991.

14. RANKIN, Woodrow W. and Ronald D. LIPPS, "Highway Safety," in Robert F. Baker (editor), *Handbook of Highway Engineering*, pp. 165-183, Litton Educational Publishing, Inc., 1975

15. WRIGHT, Paul H. and Radnor J. PAQUETTE, *Traffic Engineering and Safety*, New York: John Wiley, 1987.

16. Bayındırlık Bakanlığı Karayolları Genel Müdürlüğü, *Otokorkuluk El Kitabı*, Ankara: TCK Matbaası, 1983.

17. Transportation and Road Research Laboratory Overseas Development Administration, *Towards Safer Roads in Developing Countries - A Guide for Planner and Engineers*, Ross Silcock Partnership, New Castle, England, 1991.

18. MICHIE, J. D. and M. E. BRONSTAD, Location, Selection and Maintenance of Highway Traffic Barriers, National Cooperative Highway Research Program Report No. 118, Washington D.C., 1971.

19. American Association of State Highway and Transportation Officials, *Guide Specifications for Bridge Railings*, AASHTO, Washington D.C., 1989.

20. Türk Standardları Enstitüsü, *T.S. 4022 - Kireçler-Söndürülmüş-Yapilarda Kullanılan*, T.S.E., Ankara, Nisan 1993.

21. VAN VLACK, Lawrence H., *Elements of Materials Science - An Introductory Text for Engineering Students*, Addison-Wesley Publishing Company, USA, August 1960.

22. POPOV, E. P., *Mechanics of Materials*, Prentice Hall, USA, September 1958.

23. ASTM, "ASTM D854-58 (Reapproved 1965) - Standard Method of Test for Specific Gravity of Soils," in *1968 Book of ASTM Standards with Related Materials - Bituminous Materials for Highway Construction; Water Proofing and Roofing; Soils; Skid Resistance*, Part 11, pp. 326-328, Baltimore, USA, March 1968.

24. ASTM, "ASTM D422-63 - Standard Method for Grain Size Analysis of Soils," in *1968 Book of ASTM Standards with Related Materials - Bituminous Materials for Highway Construction; Water Proofing and Roofing; Soils; Skid Resistance*, Part 11, pp. 205-216, Baltimore, USA, March 1968.

25. ASTM, "ASTM D698-66T - Tentative Methods of Test for Moisture-Dry Density Relations of Soils Using 5.5 lb. Rammer and 12-in. Drop," in *1968 Book of ASTM Standards with Related Materials - Bituminous Materials for Highway Construction; Water Proofing and Roofing; Soils;*

Skid Resistance, Part 11, pp. 311-316, Baltimore, USA, March 1968.

26. FANG H. Y. and W. F. CHEN, "New Method for Determination of Tensile Strength of Soils", *Highway Research Record No. 345*, pp. 62-68, 1971.

27. NILSON, Arthur H. and George WINTER, *Design of Concrete Structures*, Singapore: McGraw-Hill, 1987.

28. Bayındırlık Bakanlığı Karayolları Genel Müdürlüğü, *Yollar Fenni Şartnamesi*, Ankara: TCK Matbaası, Aralık 1992.

29. Türk Standardları Enstitüsü, *TS 500 - Betonarme Yapıların Hesap ve Yapım Kuralları*, T.S.E., Ankara, Nisan 1984.

REFERENCES NOT CITED

OGLESBY, Clarkson H. and R. Gary HICKS. *Highway Engineering.* 4 th ed., New York: John Wiley, 1982.

BOWLES, Joseph E. *Foundation Analysis and Design.* 4 th ed., Singapore: McGraw-Hill, 1988.

BOWLES, Joseph E. *Engineering Properties of Soils and Their Measurement.* 3 rd ed., New York: McGraw-Hill, 1986.